# SURFICIAL BEHAVIOR OF LAVA EXTRUDED BY SANTIAGUITO DOME, GUATEMALA, DURING JANUARY 2007 AND JANUARY 2009

by

Christina C. Forbes

Advisor: Jeffrey B. Johnson

Independent Study Submitted in Partial Fulfillment
of the Requirements for the Degree of

Master of Science in Geology

New Mexico Institute of Mining and Technology
Department of Earth and Environmental Science

Socorro, New Mexico

June 2010

## ABSTRACT

From 1-4 January 2009 a field team recorded 32 hours of high resolution video (3.7 megapixels, or 0.08 $m^2$ pixels) of explosive and extrusive activity of Santiaguito dome from the summit of Santa María volcano. We outline a method to determine time-averaged velocities and discharge rates of the lava flow field on the dome surface from oblique ground-based images by orthorectifying temporally differing image pairs from the same camera. This method is applicable to the measurement of lava dome deformation and lava lake surface evolution, but it is largely untested at Santiaguito for the lengths of time investigated in this study. A study period (days to weeks) would be expected to reveal short-term fluctuations not seen in long-term measurements (months to years) because behavior is averaged over time in longer measurements. Spatial resolution is also much higher (with pixels of about 10 $cm^2$) when using ground-based images, while satellite-based images are confined to 30 $m^2$, 60 $m^2$, and 120 $m^2$ pixel resolutions. The technique used in this study also differs from previous studies by focusing on one local portion of the lava flow to find short-term flux variations proximal to the flow source.

Lava block displacement and surface flow velocities were determined based on surficial behavior from January 2009, and were compared with measurements from images taken by a field team in January 2007. Santiaguito changed between these years with respect to flow velocity, flow direction, and vent geometry. Average flow field velocities in 2007 ranged

between 0.25 to 0.34 meters per hour, while flow field velocities in 2009 ranged between 0.22 to 0.24 meters per hour. Lava in 2007 clearly originated from a single (~20 m diameter) location and radiated from this point to in a southwestern and southern direction, while lava in 2009 originated from a fissure (~50 m length) oriented northwest-southeast and flowed southwest. Flow field velocities increase to about 0.79 to 5.17 meters per hour during explosions.

Limited extrusion rates are extrapolated from flow field velocities using estimated flow thicknesses. They range from 0.21 to 0.28 $m^3s^{-1}$ in 2007 using an area of 2200 $m^2$ orthogonal to the flow surface with a flow thickness of 20 meters, and from 0.24 to 0.26 $m^3s^{-1}$ in 2009 using an area of 3000 $m^2$ orthogonal to the flow surface.

**Keywords**: Santiaguito; lava extrusion; photogrammetry; lava domes.

## ACKNOWLEDGEMENTS

# TABLE OF CONTENTS

# LIST OF FIGURES

# LIST OF TABLES

This thesis is accepted on behalf of the
Faculty of the Institute by the following committee:

Jeffrey B. Johnson, Advisor Date

Philip R. Kyle, Committee Member Date

Nick R. Varley, Committee Member Date

I release this document to the New Mexico Institute of Mining and Technology.

Christina C. Forbes Date

# 1. INTRODUCTION

Lava domes are considered to be one of the most hazardous types of volcanic feature due to their potential for flank and lava flow collapse (Fink and Anderson, 2000). At Santiaguito, pyroclastic flows caused by partial dome collapse were responsible for an unknown number of fatalities at El Palmar (10 km southwest of the volcano) in 1929 (Sapper and Termer, 1930, *in* Rose, 1970). Though nearly or completely unpredictable, these events may be better understood by studying the lava dome's previous activity and current eruptive behavior. Of particular importance, accelerated lava extrusion rates have been linked to increased pyroclastic flow occurrences (Rose, 1987; Fink and Griffiths, 1998; Harris et al., 2003), fed by lava flow growth and collapse. Lava flow fronts, defined in this study as the farthest part of the lava flow from its source, release block and ash flows by explosive decompression of oversteepened slopes that collapse due to gravity (Harris et al., 2002).

From 1922 to 1925, Santiaguito, Guatemala, extruded at a peak rate of 2.06 $m^3s^{-1}$ (Harris et al., 2003), the highest rate of any cycle yet recorded at the dome. This vigorous period was accompanied by a high number of pyroclastic flows. The devastating pyroclastic flows in 1929 travelled ~10 km (Rose, 1987) when Santiaguito extruded ~0.57 $m^3s^{-1}$ (Harris et al., 2003) at the beginning of a 5-year-long high extrusion rate period. 4-kilometer-long pyroclastic flows caused by collapsing lava flow fronts occurred in 1973 during a three-year period of high extrusion rates (0.95 $m^3\ s^{-1}$). Lava extrusion rates seem to affect the morphology of a dome (Fink and Griffiths, 1998; Lyman et al., 2004) and its resulting behavior. Santiaguito, classified in the past as a spiny dome (its current activity does not exhibit signs of spine

formation), extrudes at a relatively slow rate compared with other domes worldwide. Spiny domes, often steep-sided, quite high and conical in profile, tend to grow spines which frequently collapse. Their steep flanks and thick lava flows are also both susceptible to collapse.

Measuring the volume of erupted lava over a given time is a way to determine the mass balance of the extruding system (Dzurisin et al., 1984; Dvorak and Dzurisin, 1993; Denlinger, 1997; Harris et al., 2007), thus leading to a better understanding of magma replenishment in the shallow reservoir (Francis et al. 1993; Allard, 1997; Harris and Stevenson, 1997; Oppenheimer and Francis, 1998; Harris et al., 2000; Lautze et al., 2004), the source depth of the magma (Harris et al. 2007), and the dome's conduit geometry.

Studying lava extrusion rates is essential for hazards analysis and modeling efforts, but practical and standardized methods for measurement are still being developed. Frequent measurements have so far been limited to less viscous lava flows such as those at Mount Etna, Kilauea, and Krafla volcanoes (Guest et al., 1987; Lipman and Banks, 1987; Harris et al., 2000; Calvari et al., 2002; Lautze et al., 2004; Bailey et al., 2006; James et al., 2006). The method outlined in this study has been applied to the long-lasting phonolite lava lake of Erebus volcano, located on Ross Island, Antarctica (Oppenheimer et al., 2009). Oppenheimer et al. (2009) orthorectified a time-series of thermal infrared images of the Erebus lava lake, mapped the surface motions which ranged from 0.05 to 0.15 m $s^{-1}$, and unexpectedly revealed lava movement oscillations that were matched and compared with gas ratios. A similar study (Spampinato et al., 2008) used thermal infrared images to map the surface motions of Erte 'Ale volcano, a lava lake located in Ethiopia. As in the Oppenheimer et al. (2009) study, velocities of

incandescent cracks ranged from 0.01 to 0.15 m $s^{-1}$. Both of these studies have many similarities to the methods used in this study, but will vary considerably from the behavior of the very viscous lava extrusion at Santiaguito. Furthermore, an awareness of a dome's extrusion rates allows for a basic estimation of how far a flow might travel before it cools (Walker, 1973; Wright et al., 2001). Higher extrusion rates, in general, permit lava to travel further before cooling. Thus, knowing a flow's extrusion rates and composition is important in order to estimate the potential extent it may travel in a given amount of time.

Extrusion rate measurements at Santiaguito are somewhat sporadic and are sometimes incomparable due to their differences in temporal and spatial definitions. Extrusion rates from 1922 to 1986 were determined by Rose et al. (1970), Rose (1987), and Harris et al. (2003), and rely on measuring the post-emplacement volume of each flow unit over the time it took to completely extrude (defined as the 'time-averaged discharge rate' by Harris et al. (2007)). These rates are all underestimated by about 5-25%, lacking the volume of eroded material and mobile ejecta (Harris et al., 2003). From 1986 to 2000, rates were measured by Harris et al. (2003) from Landsat Thematic Mapper (TM) and Enhanced Thematic Mapper Plus (ETM+) imagery. Satellite-based monitoring gives the advantage of consistent coverage with 18 useable images (of 29) over 13 years. Nearly all of the images used in their study were taken during the dry season when meteorological clouds are less of a problem.

Remaining studies at Santiaguito have been both satellite- and field-based (i.e. Harris et al., 2002; Bluth and Rose, 2004). Satellite monitoring has the advantage of fairly consistent coverage of remote locations. Unfortunately, passover times may or may not be ideal. For example, images may be saturated by volcanic or meteorological cloud cover. Ground-based

imaging is virtually continuous for the observation time period, and is capable of detecting change during less than a second. Satellite imagery is also limited by spatial resolution, usually having pixels of 30 or 60 square meters that increase (60, 90, 120 square meters) in thermal infrared bands. Some meteorological satellite imagery have pixels representing at least one kilometer. These resolutions yield pixels much larger than the thermal and spatial variations on a flow's surface (James et al., 2006). Often, satellite images usually either have high spatial resolution with a low temporal resolution, or a low spatial resolution with a high temporal resolution. Ground-based remote sensing yields much higher resolution images (tens of centimeters and less), though it has its own disadvantages to consider. Images are often strongly oblique requiring careful orthorectification before quantitative data can be extracted (James et al., 2006; James et al., 2007). This technique is, of course, dependent on infrequent (often yearly at best in the case of Santiaguito) field campaigns whose goals may or may not include photogrammetric observations.

The addition of one or more consumer-grade cameras to a team's instrument array is a relatively cheap way to effectively measure lava extrusion rates (Yamashima et al., 1999; Thompson and Schilling, 2007). Using a 'point and shoot' or digital single lens reflex (DSLR) camera instead of a film camera eliminates error caused by film-plane instability (Thompson and Schilling, 2007), and allows for high definition, high frequency shooting. Major camera companies including Canon, Nikon, Pentax and Panasonic are beginning to standardize high definition filming in consumer-grade DSLRs, which currently shoot between 24 and 60 frames per second (fps) with resolutions up to 1920x1080 pixels. DSLRs offer incredible flexibility with

interchangeable lenses. While typical consumer videocamera picture quality degrades in low light, a fast lens (bigger aperture) on a DSLR can potentially outcompete a camcorder.

Harris et al. (2007) summarized and standardized extrusion rate spatial and temporal definitions to avoid confusion and incorrect variation between studies. It is crucial to define experimental constraints in a lava extrusion study. Without clear definitions and similar measurement methods, compared studies may yield incorrect results (Tanguy et al., 1996; Harris et al., 2007). While previous extrusion rate estimations at Santiaguito were measured from a long-term output of lava, this study focuses on a short time period (four days). According to Harris et al. (2007), the time period in this study would reveal a time-averaged discharge rate. An extrusion rate measurement made from a longer period would smooth out and average short-term variations that may be revealed in a time period of four days at Santiaguito. Thus a study like this one is useful in evaluating short-term variations in magma supply, but may not be comparable with previous extrusion rate estimations.

Spatially, the majority of previous studies at Santiaguito derive extrusion rate estimations from the entire lava flow, or from distal regions of the flow, while this study focuses entirely on the vent location. Distal regions of the lava flow would be expected to smooth out short-term flux variations, while locations proximal to the vent would more likely reveal any short-term changes in flow rate.

# 2. BACKGROUND

## 2.1 Eruption history and extrusive cyclicity

Santa María volcano, located in western Guatemala (Figure 2.1), erupted in October 1902 with a Volcanic Explosivity Index (VEI) of about 6-7 (Simpkin and Siebert, 2000). The blast left a crater in the southwest slope (Figure 2.2) with a volume of 0.5 $km^3$ (Rose, 1972a), much smaller than the estimated eruption debris volume of 8.5 $km^3$ (Stoiber and Rose, 1969).

Lava extrusion in the center of the crater began in 1922 to create the Santiaguito dome complex (Rose, 1972b). This first vent, called Caliente, extruded at a peak rate of ~2.06 $m^3 s^{-1}$ which lasted until about 1925 and continued until 1929 at the less vigorous rate of around 0.19 $m^3 s^{-1}$ (Harris et al., 2003). Initial extrusion rates were the highest of any other following cycle up to present time and emplaced about 0.2 $km^3$ of lava in three years (Rose, 1972b; Harris et al., 2003). Activity probably shifted from endogenous processes to exogenous processes after 1929 (Rose, 1972b). This change is often attributed to changes in the magma supply and to collapse events (Hale and Wage, 2008).

In 1939, activity migrated 700 meters to the west of Caliente where La Mitad vent began extruding (Harris et al., 2003). La Mitad ceased extruding in 1949 when activity migrated further west to create El Monje vent. After a second El Monje dome unit was extruded, activity shifted further west in 1958 where El Brujo formed (Harris et al., 2003). Caliente began erupting concurrently with El Brujo in 1968 until El Brujo ceased activity in 1977. The Caliente vent has been regularly extruding until present time.


**Figure 2.1: Location map of Santiaguito dome, Guatemala. Inset photo by David A. G. Wilson, used with permission. Inset photo views Santiaguito and Santa María from the south. Map from Google Earth.**

Santiaguito has always extruded in cycles that begin with a relatively high extrusion rate and end with a relatively low extrusion rate (Rose, 1972b; Rose, 1987). Each cycle lasts 3-14 years as defined by Rose (1972b; 1987) and Harris et al. (2003), and about nine cycles have been identified between 1922 and 2000 (Figure 2.3). From 1922 to 1984, Rose (1972c; 1987) have determined the 'high' (0.6-2.1$m^3s^{-1}$) extrusion rate periods last around 3-5 years, and the 'low' (~0.2 $m^3s^{-1}$) extrusion rate periods last around 10-12 years.

Cyclical behavior in lava dome extrusion is somewhat common (Barmin et al., 2002) and may even be characteristic of these features (for example: Mount St. Helens, U.S.A., from 1980-1986; Mount Unzen, Japan, from 1991-1995; Soufrière Hills volcano, Montserrat, from 1995 to 1998 and 1999 to present; Shiveluch volcano, Kamchatka, from 1963 to 1964, 1971 to 1972, 1983 to 1984, 1993 to 2001). Why lava domes extrude in cycles is much less understood, though Barmin et al. (2002) have successfully developed a simplified model to reproduce periodic behavior. Their results suggest that the cycle period depends mostly on the size of the magma chamber, and that a longer period implies a larger source. They determined Santiaguito's magma chamber size is ~65 $km^3$, attributed to the dome's large eruptive volume and longer period.

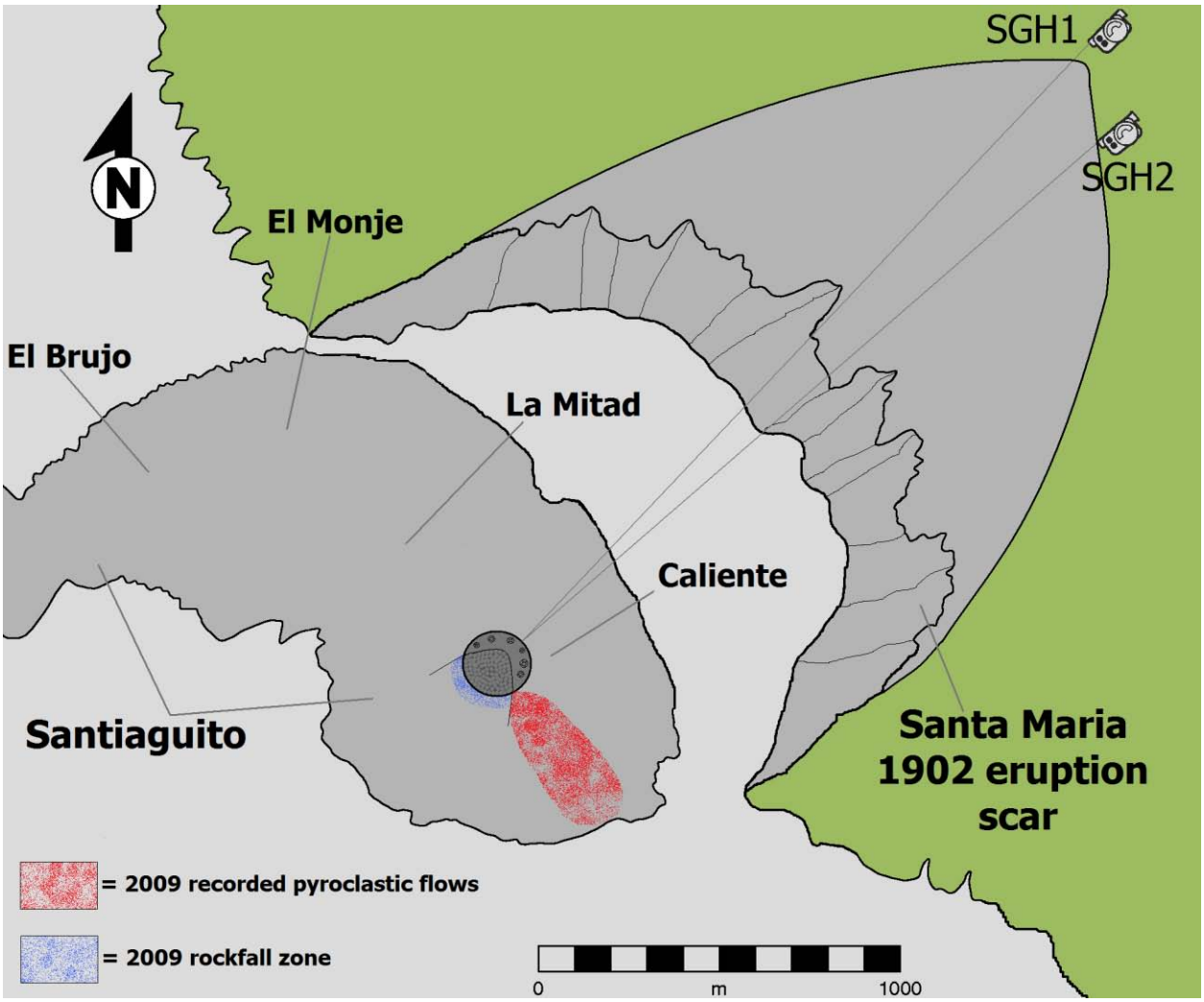


**Figure 2.2: Schematic map of Santiaguito dome in relation to Santa María (green) and cameras located on the summit. See Figure 2.4 for detail on the active Caliente vent. Figure based on a DEM (Estudio del establecimiento de los mapas básicos y mapas de amenaza para el sistema de información geográfica de la República de Guatemala) and Figure 3.3 (Dr. Jonathan Lees, University of North Carolina at Chapel Hill).**

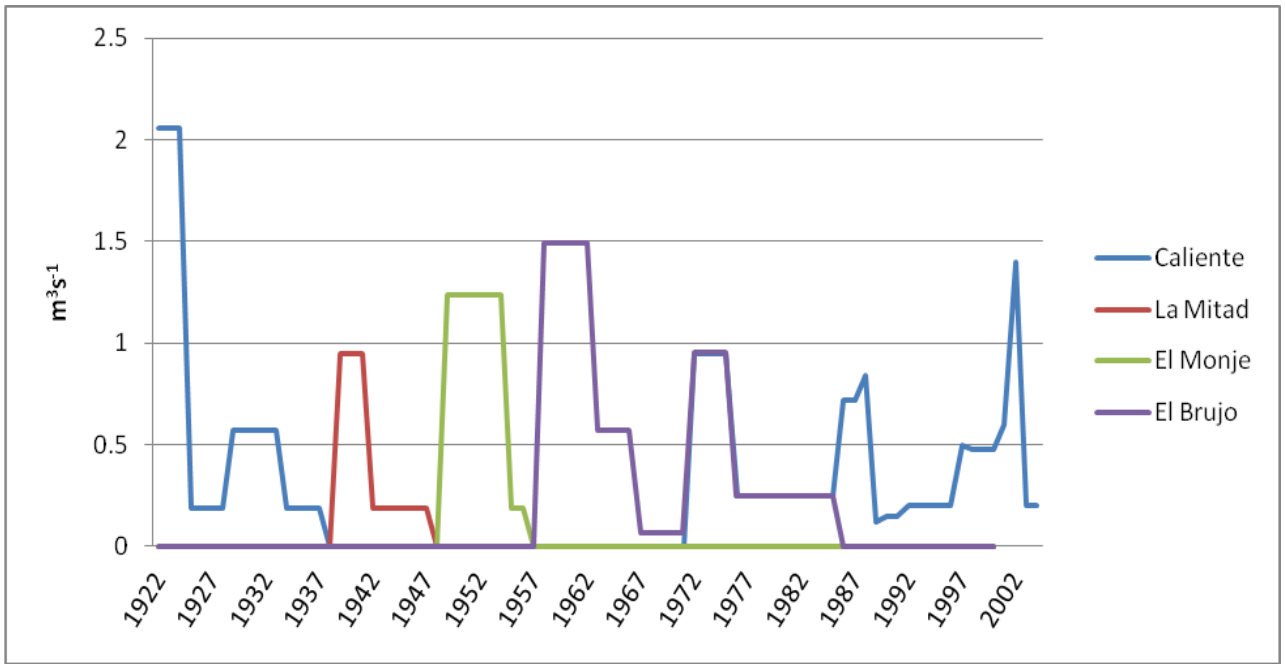


**Figure 2.3: Extrusion rates measured at Santiaguito from 1922-2004 (Constructed from data found in: Rose, 1972c; Rose, 1987; Harris et al., 2003; Bluth and Rose, 2004; Harris et al., 2004).**

## 2.2 January 2009 activity and general observations

In January 2009, Santiaguito dome was extruding a block lava flow from the Caliente vent that spilled over the southwestern dome edge. The crater surface was approximately 200 meters in diameter (Figure 2.2). Incandescence on the dome surface was visible from our viewing location at night and was strongly visible from Caliente's neighboring El Monje dome as seen by our dome team at night. Events (explosions, degassing episodes, and rockfalls) recorded during the field campaign in January 2009 are catalogued in Appendices C and D.

The center of the dome surface was covered in subrounded to subangular grayish-tan blocks (~1-10 meters diameter), and a gray semi-circle of ash partially surrounded the active flow. This material was pocketed with pit craters (~20 meters in diameter) that frequently changed locations and size, often noticed to change after explosions. Lava flows, such as the one Santiaguito is extruding, typically advance by flow front oversteepening and subsequent rockfalling (Rose, 1972b). Ashy plumes generated by rockfalls were visible in the videos about every few minutes and originated below the dome edge out of the field of view. Harris et al. (2002) determined these rockfalls in January 2000 exposed hot core material (up to 805°C), but argue these small events were unable to cause explosive depressurization and subsequent block and ash flows. At least 110 of these rockfall plumes were recorded by the cameras (Figure 2.4). Most rockfall plumes were very small, though several were long-lived and obscured distal portions (relative to the cameras) of the dome surface.

**Figure 2.4: A large plume formed from a rockfall on the active lava flow, southwestern slope, seen from near the summit of Santa Maria (1132 meters above the dome surface, and 2428 meters horizontally away from the dome surface). The crater diameter is approximately 200 meters.**

About seven degassing events were recorded, and these are described as ash-poor, typically less vigorous and less impulsive than explosions. These events would originate from several locations around the dome surface and would occasionally form from weakly ring-shaped vents. Vortices frequently formed from degassing events or from loose ash already present.

Thirteen individual explosions were recorded, and many of them developed from ring-shaped vents. Explosions created ashy plumes that occasionally reached as high as or higher than the cameras on Santa María (a vertical difference of 1132 meters or more) due to thermal buoyancy. Several explosions formed small pyroclastic flows (see Figure 2.6) which commonly travelled down the south to southeastern dome flanks. Some reached as far as the base of the dome. Most explosions were accompanied by rumbling and/or whoosing audible from the Santa María summit.

**Figure 2.6: A typical explosion with a pyroclastic flow and vigorous fumarolic activity outside the crater. Image was taken with a personal camera from the location of camera SGH2.**

# 3. METHODS

## 3.1 Field methods and equipment used

From 1 January to 4 January 2009, two high resolution (3.7 megapixels, or ~0.08 $cm^2$ pixels) Casio Exilim EX-F1 cameras recorded FHD (full high definition) videos at 60 fps (frames per second) with a maximum focal length of 87.6 mm, equivalent to 432 mm in a 35 mm format camera. The exact specifications are in Table 3.2. One camera (SGH1) was located just below the Santa María summit (3660 meters a.s.l., NAD83 655824.64E 163168.93N, Zone 15, Figure 3.1), and the other camera (SGH2) was located further south along the 1902 blast scar (3465 m a.s.l., NAD83 655851.66E 1631402.77N) (see Figure 3.2, Table 3.1). The two cameras are separated horizontally by 285 meters, and vertically by 195 meters. SGH1 began recording at the first light of each morning; SGH2 began recording shortly after. Both stopped recording an hour or so before noon local time when meteorological conditions would regularly deteriorate and make recording impossible. The cameras recorded over 30 combined hours of video, all of which are documented in Appendices C and D.

**Figure 3.1: View from camera SGH1 on the Santa María summit looking southwest at the Santiaguito dome complex. Caliente vent is the far left. Photo by Dr. Nick Varley, Universidad de Colima (2007).**

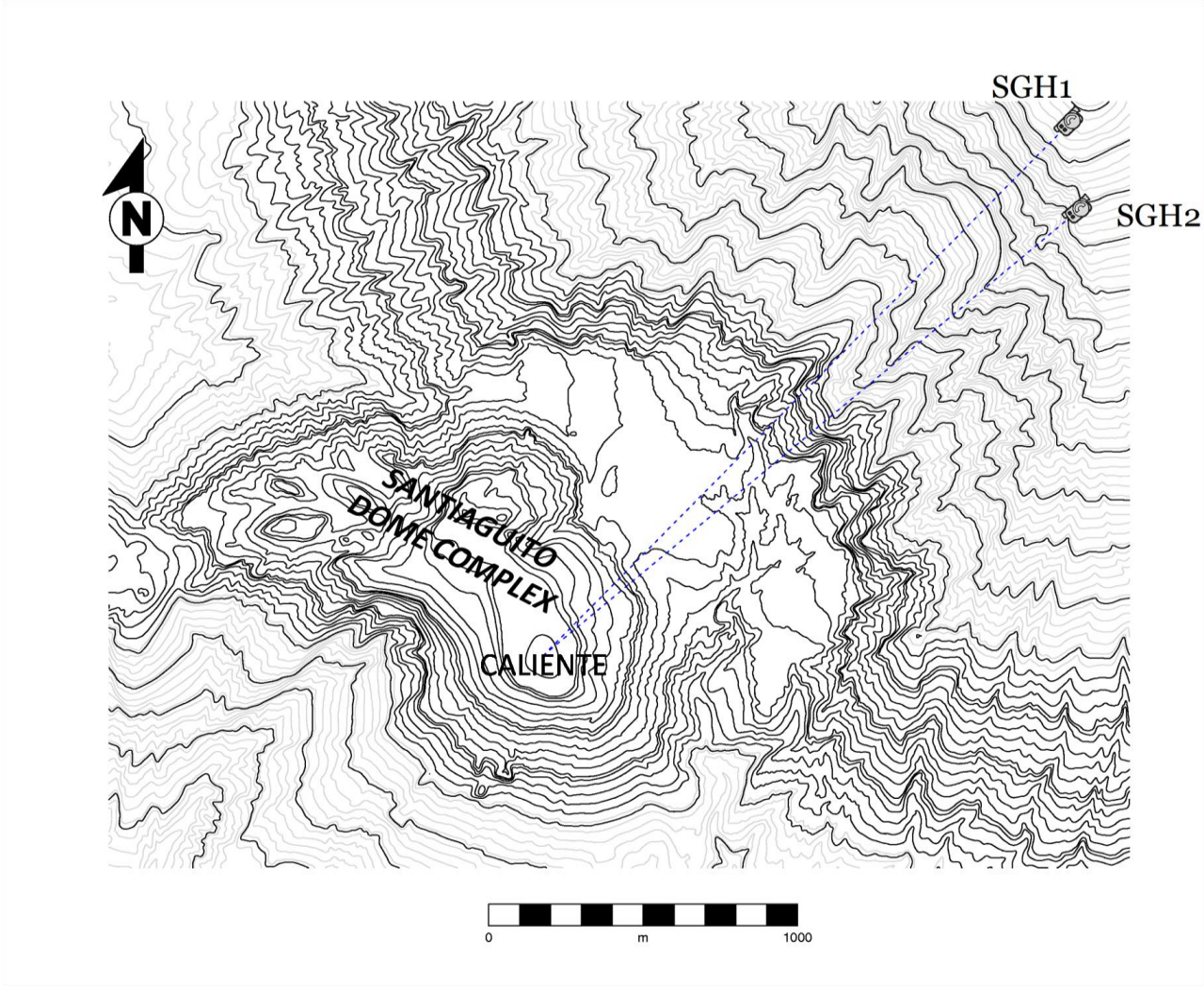


**Figure 3.2: Locations for cameras SGH1 (3660 m a.s.l.) and SGH2 (3465 m a.s.l.) on a topographic map relative to the Santiaguito dome complex where the two blue lines intersect. Contour interval is 20 m. Figure by Dr. Jonathan Lees, University of North Carolina at Chapel Hill (Estudio del establecimiento de los mapas básicos y mapas de amenaza para el sistema de información geográfica de la República de Guatemala).**

| | DOME | SGH1 | SGH2 |
|---|---|---|---|
| **Easting (m)** | 654118 | 655825 | 655852 |
| **Northing (m)** | 1629960 | 1631687 | 1631403 |
| **Elevation (m)** | 2505.5 | 3637 | 3444 |

**Table 3.1: UTM locations (NAD83, Zone 15) used for the dome edge and cameras SGH1, SGH2.**

## 3.2 Camera calibration

The manufacturer's focal length for any camera lens is only a generic measurement for that product model. No individual product undergoes tests by the manufacturer. As a result, camera lenses may have unique imperfections which have the potential to introduce error into any photogrammetric measurements. Both cameras used in this study were tested using geometric relationships (Figure 3.3) to determine if their lenses caused a deviation from the manufacturer's focal length.

A camera (SGH1 and SGH2) was set up parallel to a target with a known object horizontal distance (A) a measured distance away (H). Using the CMOS (complementary metal oxide semiconductor) image sensor horizontal distance (W = 7.176 mm), the focal length was calculated and compared with the manufacturer's maximum focal length (f = 87.6 mm) to estimate the error. The ratio f/H should equal W/A.

$$\frac{f}{H} = \frac{W}{A} \qquad \textit{Eq. 1}$$

The calculated focal lengths for both of the cameras approached the manufacturer's focal length as the object distance (H) was increased (Tables 3.3 and 3.4), and so we assume the focal length will be 87.6 mm at the significantly longer H values between the cameras and Santiaguito dome. We decided to use 87.6 mm as the actual maximum focal length for calculations involving both cameras.

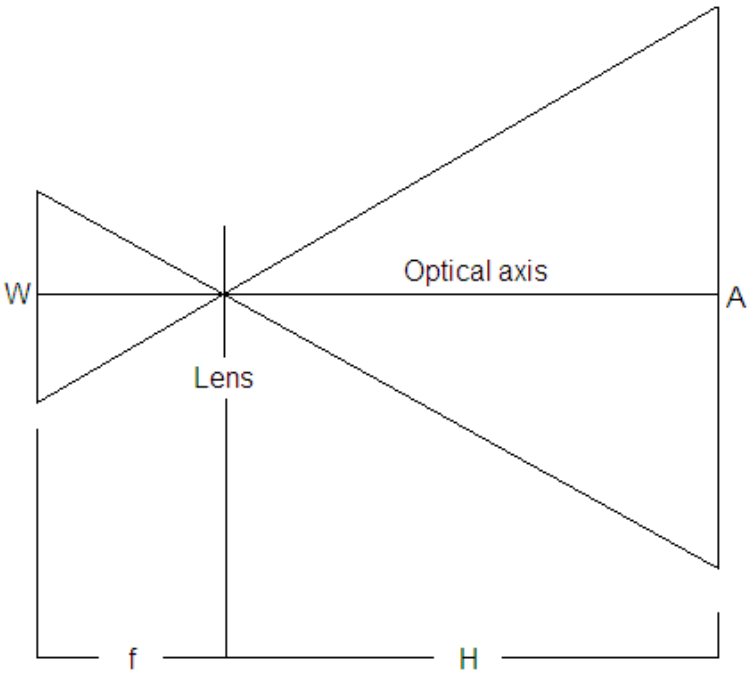


**Figure 3.3: Camera lens geometry.**

**Table 3.2: Casio Exilim EX-F1 specifications and settings used in the field.**

| | | |
|---|---|---|
| **Sensor type** | 1/1.8" CMOS | http://www.exilim.com/intl/ex_f1/spec.html |
| **Aspect ratio** | 4:3 | http://www.dpreview.com/news/0210/02100402sensorsizes.asp |
| **Sensor width (W)** | 7.176 mm | http://www.dpreview.com/news/0210/02100402sensorsizes.asp |
| **Sensor height** | 5.319 mm | http://www.dpreview.com/news/0210/02100402sensorsizes.asp |
| **Sensor diagonal** | 8.932 mm | http://www.dpreview.com/news/0210/02100402sensorsizes.asp |
| **Sensor area** | 38.169mm$^2$ | http://www.dpreview.com/news/0210/02100402sensorsizes.asp |
| **Focal length equiv. to 35 mm camera** | 432 mm | http://www.exilim.com/intl/ex_f1/spec.html |
| **Focal length** | 87.6 mm | http://www.exilim.com/intl/ex_f1/spec.html |
| **Focus** | Infinite | |
| **Video definition** | FHD | |
| **Pixels** | 1920 x 1080 | http://www.exilim.com/intl/ex_f1/spec.html |
| **FPS** | 60 | http://www.exilim.com/intl/ex_f1/spec.html |

**Table 3.3: Calibration data for camera SGH1.**

| | **H** | **A** | **Calculated f** | **Difference between calculated f and manufacturer's f** |
|---|---|---|---|---|
| **Test 1** | 16383 mm | 1371.6 mm | 85.713 mm | 0.022% |
| **Test 2** | 6207.76 mm | 533.4 mm | 83.515 mm | 4.7% |
| **Test 3** | 1745 mm | 167 mm | 74.983 mm | 14.4% |
| **Test 4** | 1323 mm | 132 mm | 71.923 mm | 18% |
| **Test 5** | 887 mm | 94 mm | 67.714 mm | 22.7% |

**Table 3.4: Calibration data for camera SGH2.**

| | **H** | **A** | **Calculated f** | **Difference between calculated f and manufacturer's f** |
|---|---|---|---|---|
| **Test 1** | 16383 mm | 1330.96 mm | 88.331 mm | 0.008% |
| **Test 2** | 1323 mm | 126 mm | 75.348 mm | 14% |
| **Test 3** | 887 mm | 90 mm | 70.723 mm | 19.3% |

## 3.3 Photogrammetry and orthorectification of images

Images were selected based on clarity and timing, and were exported from video sequences using Quicktime Pro. The cameras in the field, though held in place by tripods, were susceptible to movement created by wind, daily setup, and human error (accidental bumping, nudging from battery/card replacement, etc.). A reference point was designated as the Cartesian coordinate system origin to allow comparison between unlimited images. The reference point in the 2009 images was a large block on the northeast flank of the dome (Figure 3.4) that does not move over four days of observation.

Image pairs were then matched together by aligning long-lasting shared features (blocks on flanks, slope contours, crater outline, etc.). Blocks within the lava flow were tracked by hand because of the evolving appearance of the flow surface. Over time, blocks topple, rotate, shatter, are pushed up through the flow, and are covered by ash. Furthermore, the angle of sunlight changes over the time periods in this study and would confuse automated particle tracking computer programs. Tracking these blocks visually by hand rather than by computer programs is more effective, and potentially the only option, in this situation. Very short term (minutes to an hour) periods are better suited for automatic processing. Tracking blocks in the lava flow is always limited temporally by resolution. Movements less than the size of a pixel (0.08 $m^2$ for SGH1 and SGH2) are not detectable.

Blocks in the first image of a chronological sequence are marked with a vertical crosshair, and the same blocks in the next chronological image are marked with an inclined crosshair. Every effort was made to mark the same part of the block in both images, which

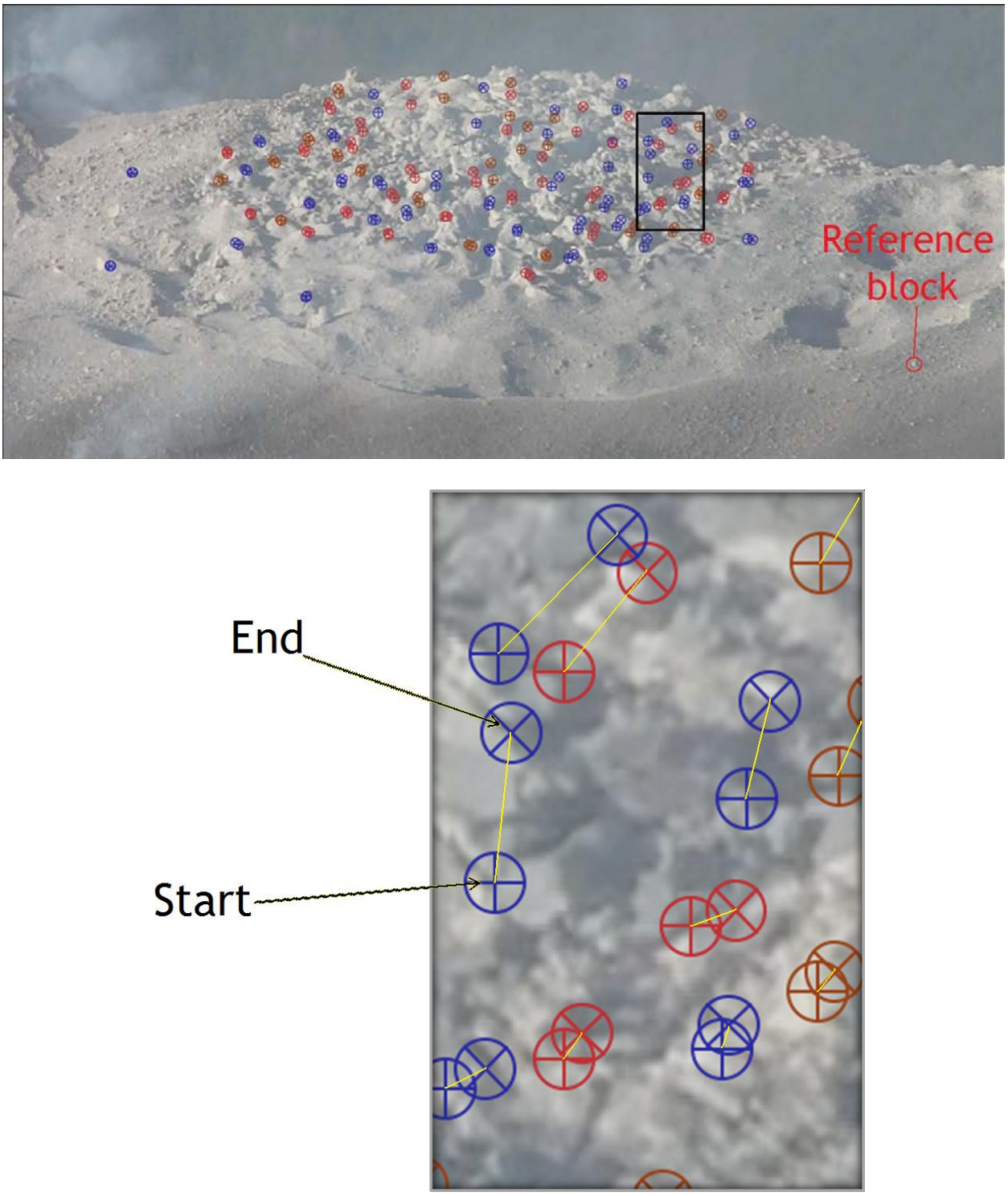


**Figure 3.4: An example of an unorthorectified displacement map (above) and a magnified section (below) showing the displacement between two images spaced temporally viewed from SGH1. Colors were only used to differentiate between closely-spaced blocks. The reference point was located on the lower right side of the top image. Yellow lines indicate tie lines that connect the starting and ending locations of a block.**

were frequently the edges of blocks. In some images, crosshair pairs are different colors. Crosshair colors were random and were only used to discern between different block paths. As many blocks as possible were identified to get a representation of the entire flow area. The result is an unorthorectified displacement map (Figure 3.4), a map which shows displacement vectors before orthorectification as viewed from SGH1 or SGH2. All the starting and ending locations of blocks are recorded as positive or negative x and y positions in pixels relative to the reference point.

Each block location must then be adjusted to a map-view plane, accomplished by orthorectification. We chose to fit the displacement vectors to a plane rather than a curved dome surface to simplify the solution. We acknowledge that the dome surface is not perfectly flat, but a plane is a reasonable approximation of the dome surface because the precise dome surface topography is not known.

A DEM (Estudio del establecimiento de los mapas básicos y mapas de amenaza para el sistema de información geográfica de la República de Guatemala) was used to determine the horizontal distance from the Santa María summit to the dome (D), and the elevation difference between the two (E) (Figure 3.5). The slant distances from the cameras to the dome (H) were calculated using the Pythagorean Theorem, Equation 2. The slant angle ($\ominus$, inverse tangent of E/D) is calculated in Equation 3. Variables for SGH1 and SGH2 are listed in Table 3.5.

$$H = \sqrt{E^2 + D^2} \qquad \textit{Eq. 2}$$

$$\ominus = \tan^{-1}\left(\frac{E}{D}\right) \qquad \textit{Eq. 3}$$

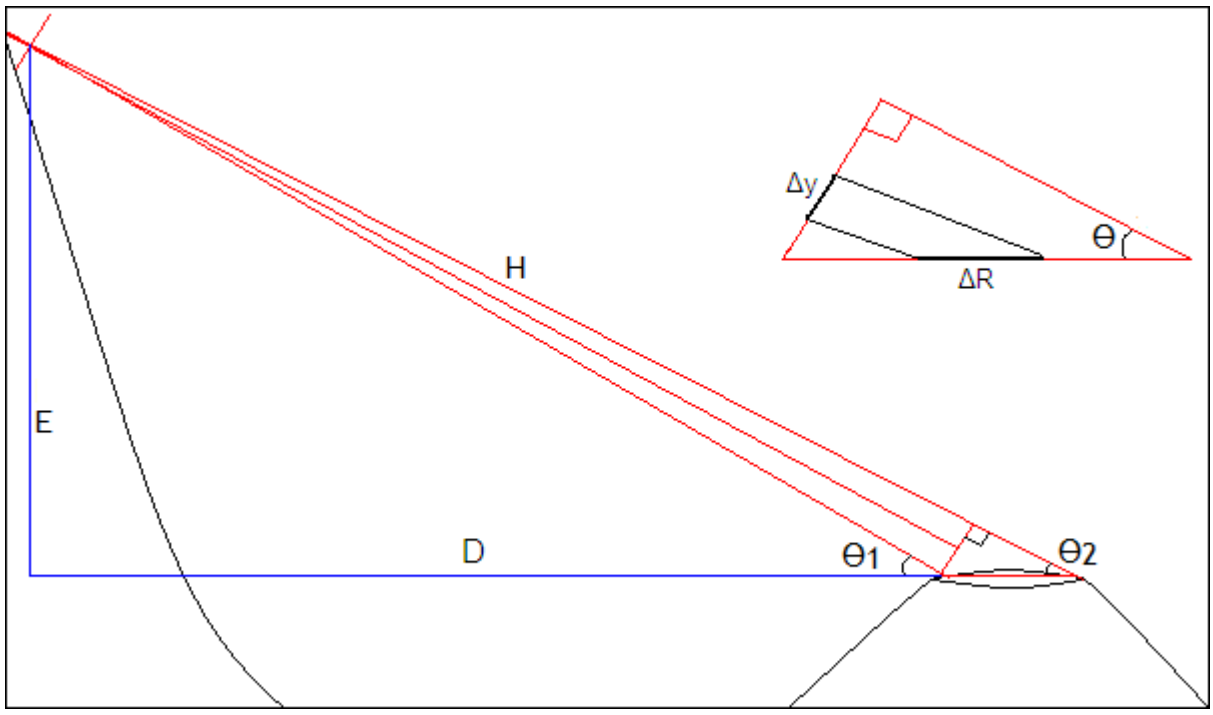


**Figure 3.5: Viewing geometry from the Santa María summit to Santiaguito showing the locations of the different slant angles ($\Theta_1$ and $\Theta_2$).**

| | SGH1 | SGH2 |
|---|---|---|
| **A** | 220 m | 203 m |
| **H** | 2679 m | 2482 m |
| **D** | 2428 m | 2297 m |
| **E** | 1132 m | 939 m |
| **ɵ** | 25° | 22° |

**Table 3.5: Viewing geometry variables of the cameras SGH1 and SGH2 with respect to the dome.**

Images in 2007 had a slant angle of 25°, images in 2009 taken by camera SGH1 had a slant angle of 25°, and images in 2009 taken by camera SGH2 had a slant angle of 22.2°. Most images were taken from SGH2 footage with the exception of three intervals (from the beginning of the day to the end of the day on 1 January, 2 January, and 4 January 2009). The slant angle ($\ominus$) will change across the dome surface, therefore the transformation of the block locations to a map plane is dependent upon the horizontal distance from the camera to the dome surface (D). The slant angle ($\ominus$) was calculated for two locations on the dome surface to determine its variability. The first location on the northeast side of Caliente along the 2500 meter contour yields a slant angle of 25.5° for SGH1, and 22.9° for SGH2. The second location on the southwest side of Caliente along the 2500 meter contour yielded a slant angle of 24.7° for SGH1 and 21.5° for SGH2. The average angle of the near and far slant angles of SGH1 is 25°, a 1.6% difference between $\ominus_1$ and $\ominus_2$. The average angle of the near and far slant angles of SGH2 is 22.2°, a 3.1% difference between $\ominus_1$ and $\ominus_2$. Even though the near and far sides of the dome surface do not have the same slant angle, the assumption is made that $\ominus$ is the same for the entire dome surface.

To find the horizontal field of view (A) from Equation 1, the image sensor width (W) is multiplied by the slant distance (H), and WH is divided by the camera's focal length (f, Equation 4). The horizontal field of view (A) is divided by the number of pixels in the x-direction to determine meters per pixel in the x-direction. Subsequently, the x-location of a pixel in meters is determined by multiplying the number of pixels from the reference point by meters per pixel in the x-direction.

$$A = \frac{WH}{f} \qquad \textit{Eq. 4}$$

Dividing the horizontal field of view (A) in meters by the aspect ratio (obtained by dividing an image's width in pixels by height in pixels) yields the vertical field of view in meters. This is then divided by the number of pixels in the y-direction to determine meters per pixel in the y-direction. The y-location of a pixel in meters is determined by multiplying the number of pixels from the reference point by the meters per pixel in y-direction.

Since the images in this study are oblique, they must be orthorectified to fit a map-view plane. Conversion is only necessary in the y-direction because there is little distortion in the x-direction. The y-location of a pixel (number of pixels from the reference point) is multiplied by meters per pixel and the result (y) is entered into Equation 5. The location on the map plane in the y-direction (away from the viewing direction) is 'R', and $\ominus$ is the slant angle.

$$R = \frac{y}{\sin\theta} \qquad \textit{Eq. 5}$$

Once the horizontal and vertical dimensions of each point are orthorectified to the map plane, vectors may be calculated from starting and ending locations of lava blocks. This is done by finding the difference between the starting and ending x-locations in meters of each block, and then the same for the y-locations in meters. Displacement (T) is found by taking the square root of the summation of $\Delta x^2$ and $\Delta y^2$ (Equation 6).

$$T = \sqrt{\Delta x^2 + \Delta y^2} \qquad \textit{Eq. 6}$$

The azimuth of a displacement vector, relative to the reference point, can be rotated with respect to north on a map plane. Camera SGH1 has a look angle of 44.7° from north to Caliente, and camera SGH2 has a look angle of 50.2°. When these angles are subtracted from 180°, 135.3° is the resulting angle for SGH1 and 129.8° is the resulting angle for SGH2. Either of these angles, depending on the camera, may then be subtracted from the azimuth of a displacement vector to yield the azimuth of the displacement vector on a map plane with respect to north. If the original azimuth is less than 135.3° for SGH1 or 129.8° for SGH2, 360° must be added to the result.

Camera focal lengths were unknown and variable throughout the 2007 data, so displacement vectors were calculated by relating the diameter of the dome in 2009 to the diameter of the dome in 2007.

## 3.4 Example calculation

First, the horizontal field of view (A) is found using information in Table 3.1, solved with Equation 1. The slant distance (H) for SGH1 is 2679 meters, and the slant distance for SGH2 is 2481.5 meters. Camera SGH2 is used for the following example.

$$\frac{0.0876\ m}{2481.5\ m} = \frac{0.007176\ m}{A}$$

A = 203.3 meters (x-direction)

Images taken in January 2009 have 2562x1442 pixels, which is an aspect ratio of 1.78. Dividing A by the number of pixels in the x-direction yields the length of a pixel in the x-direction. Dividing A by the aspect ratio yields the length of the vertical field of view, and dividing this number by 1442 pixels yields the length of a pixel in the y-direction.

$$\frac{203.3\ m}{2562\ pixels} = 0.08 \text{ meters per pixel (x-direction)}$$

$$\frac{203.3\ m}{1.78} = 114.2 \text{ meters (y-direction)}$$

$$\frac{114.2\ m}{1442\ pixels} = 0.08 \text{ meters per pixel (y-direction)}$$

Next, the slant angle ($\ominus$) is determined by using the trigonometric identity $\tan\ominus$. The inverse tangent of E/D solves for $\ominus$.

$$\tan\Theta = \frac{opposite}{adjacent}$$

$$\Theta = \tan^{-1}\left(\frac{938.5\ m}{2297.2\ m}\right) = 22.2°$$

The slant angle is used to transform pixel y-locations from the image to the dome surface. Using the trigonometric identity of sinΘ, Equation 5 can be solved.

$$\sin\Theta = \frac{opposite}{hypotenuse}$$

$$\sin(22.2°) = \frac{y}{R}$$

$$R = \frac{y}{0.38}$$

From a theoretical image, two pixels are picked as the starting and ending locations of a lava block traveling over some time. The starting pixel is (495, 612) and the ending pixel is (487, 614). The reference pixel is (2386, 292), which transforms the starting pixel to (-1891, 320) and the ending pixel to (-1899, 322) with respect to the reference pixel. The starting pixel's x-location is multiplied by the meters per pixel in the x-direction (0.08 m/pixel). The starting pixel's y-location is also multiplied by the meters per pixel length in the y-direction (0.08 m/pixel), but then this number, 'y', is divided by 0.38 (sinΘ) to determine R, the actual location of the pixel in the y-direction as applied to the dome surface.

*Starting pixel:*

-1891 pixels x 0.08 m/pixel = -151.28 meters (x-direction)

320 pixels x 0.08 m/pixel = 25.39 meters (y- direction)

$$\frac{25.39\ m}{0.38}$$ = 66.82 meters (R-direction)

(-151.28 m, 66.83 m) relative to the reference pixel

*Ending pixel:*

-1899 pixels x 0.08 m/pixel = -151.92 meters (x-direction)

322 pixels x 0.08 m/pixel = 25.76 meters (y-direction)

$$\frac{25.76\ m}{0.38}$$ = 67.79 meters ( R-direction)

(-151.92 m, 67.79 m) relative to the reference pixel

The differences of the x-locations and R-locations are applied in the Pythagorean Theorem to determine the displacement (T) of the pixels.

$\Delta x$ = -0.64 meters

$\Delta R$ = 0.97 meters

$$T = \sqrt{\Delta x^2 + \Delta y^2}$$

$$T = \sqrt{(0.64)^2 + (0.97)^2}$$

T = 1.2 meters

The block moves at 326.6° with respect to the reference point on the image. Subtract 129.8° from this angle since the camera used in this example is SGH2 (section 3.3), and this yields 196.8° as the true angle of block travel relative to north on the map plane.

# 4. RESULTS

Surface flow was quantified and compared using computation tools scripted in MATLAB (Appendix E). Each time period investigated has three corresponding figures. The first figure in each set (Figures 4.2-4a, 4.6-25a) is an orthorectified map of measured displacement (blue arrows), shown with the approximate crater rim (solid black) and the active lava flow boundary (solid black, bisecting the crater circle). The second figure in each set (Figures 4.2-4b, 4.6-25b) is a streamline map based on the trending block movements. Each line in the streamline map is tangent to the displacement vectors and shows the path a fluid element will travel during the time period specified. Because the data are sparse and irregular, they were interpolated to a grid space (5 $m^2$ spacing) using a cublic spline interpolation (blue arrows) as the third figure in each set (Figures 4.2-4c, 4.6-25c). Displacement contours (magenta) were applied to these vectors.

The mean and peak velocities of each set were calculated from the interpolated displacement vectors within the interpreted flow area (Tables 4.1a-b, 4.2a-d).

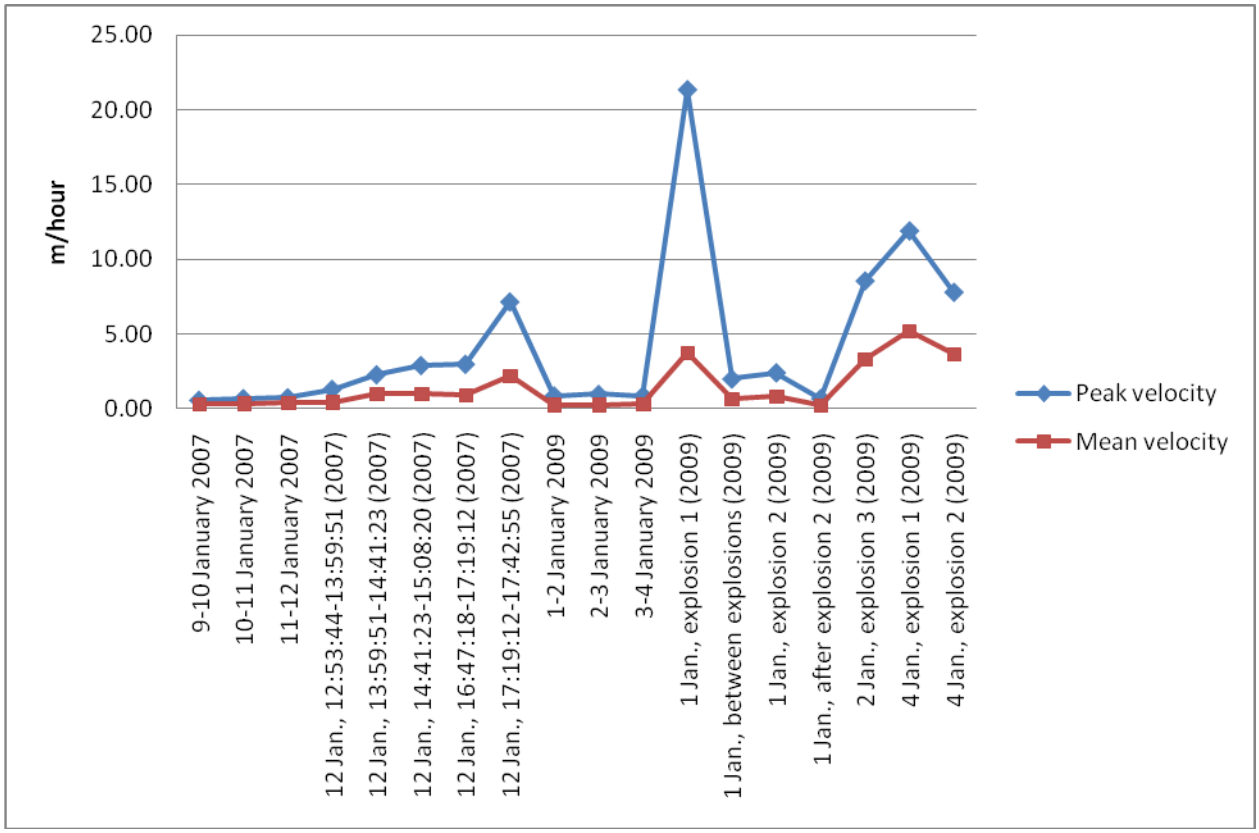


**Figure 4.1: Surface flow velocities during January 2007 and January 2009. Velocities are based on the interpolated grid space within the interpreted flow area. 9-10, 10-11, and 11-12 January 2007 and 1-2, 2-3, 3-4 January 2009 intervals cover a time of approximately 24 hours each. Individual time intervals on 12 January 2007 are in UTC. An explosion occurred from about 17:27-17:34 UTC on 12 January 2007.**

## 4.1 JANUARY 2007

Eight time periods during January 2007 were investigated. Three of these periods last approximately 24 hours each (Figures 4.2a-c; Figures 4.3a-c; Figures 4.4a-c) from 9-10 January, 10-11 January, 11-12 January. The remaining five periods focus on 12 January from 12:50 to 17:19 UTC (Figures 4.6a-c; Figures 4.7a-c; Figures 4.8a-c; Figures 4.9a-c; Figures 4.10a-c) lasting variably from 23 minutes to one hour each. The final interval on 12 January (17:19-17:42 UTC) encompasses an explosion that is followed by several 'pulsing' events (brief increases in dome surface temperatures) lasting from 17:27-17:34 UTC.

Displacement vectors during the day-to-day (~24 hours) 2007 intervals show lava exiting a small (~20 meter diameter) vent dominantly in a southerly direction. One image pair shows the radiating, 'blossoming' flow very well: 10-11 January 2007 (Figures 4.3a-c). The interpolated contour lines show two sustained regions of relatively large displacements, one to the west and one to the east. This pattern is present in all three of the day-to-day (~24 hour) intervals in 2007. Though three data points is a small spread, the three day-to-day intervals (9-10 January, 10-11 January, 11-12 January) show an increasing trend in velocity (Figure 4.1) starting at a mean of 0.25 meters per hour from 9-10 January, increasing to an average of 0.30 meters per hour from 11-12 January, and ending at 0.34 meters per hour from 11-12 January. The peak velocities for each day compliment the mean velocity trend. Figure 4.5 displays the oblique displacement vectors relative to the flow field. Surface flow velocities during 12 January appeared to increase somewhat dramatically relative to the day-to-day velocities (Figure 4.1).

**Table 4.1a: Surface flow velocities during 2007 based on the interpolated displacement vectors of the interpreted flow area. 'Peak velocity' and 'mean velocity' are designated for the elapsed time between the images.**

| Period | Time elapsed between images | Peak displacement | Peak velocity (m/second) | Peak velocity (m/day) | Peak velocity (m/hour) | Mean displacement | Mean velocity (m/second) | Mean velocity (m/day) | Mean velocity (m/hour) | Figures |
|---|---|---|---|---|---|---|---|---|---|---|
| 9-10 January | 27:22:00 | 14.64 | $1.49^{-4}$ | 12.84 | 0.54 | 6.75 | $6.85^{-5}$ | 5.92 | 0.25 | 4.2a-c |
| 10-11 January | 20:52:00 | 13.71 | $1.83^{-4}$ | 15.77 | 0.65 | 6.19 | $8.24^{-5}$ | 7.12 | 0.30 | 4.3a-c |
| 11-12 January | 23:51:00 | 16.87 | $1.96^{-4}$ | 16.98 | 0.71 | 8.03 | $9.35^{-5}$ | 8.08 | 0.34 | 4.4a-c |

**Table 4.1b: Surface flow velocities during 12 January 2007 based on the interpolated displacement vectors of the interpreted flow area. 'Peak velocity' and 'mean velocity' are designated for the elapsed time between the images. Period times are UTC. The fifth period, 17:19:12-17:42:55, encompasses one explosion and several thermal fluctuations.**

| Period | Time elapsed between images | Peak displacement | Peak velocity (m/second) | Peak velocity (m/day) | Peak velocity (m/hour) | Mean displacement | Mean velocity (m/second) | Mean velocity (m/day) | Mean velocity (m/hour) | Figures |
|---|---|---|---|---|---|---|---|---|---|---|
| 12:53:44-13:59:51 | 1:06:07 | 1.4 | $3.53^{-4}$ | 30.49 | 1.27 | 0.42 | $1.06^{-4}$ | 9.15 | 0.38 | 4.6a-c |
| 13:59:51-14:41:23 | 0:41:32 | 1.56 | $6.26^{-4}$ | 54.09 | 2.25 | 0.68 | $2.73^{-4}$ | 23.58 | 0.98 | 4.7a-c |
| 14:41:23-15:08:20 | 0:26:57 | 1.29 | $7.98^{-4}$ | 68.93 | 2.87 | 0.42 | $2.60^{-4}$ | 22.44 | 0.94 | 4.8a-c |
| 16:47:18-17:19:12 | 0:31:54 | 1.57 | $8.20^{-4}$ | 70.87 | 2.95 | 0.45 | $2.35^{-4}$ | 20.31 | 0.85 | 4.9a-c |
| 17:19:12-17:42:55 | 0:23:43 | 2.82 | $1.98^{-3}$ | 171.22 | 7.13 | 0.85 | $5.97^{-4}$ | 51.61 | 2.15 | 4.10a-c |

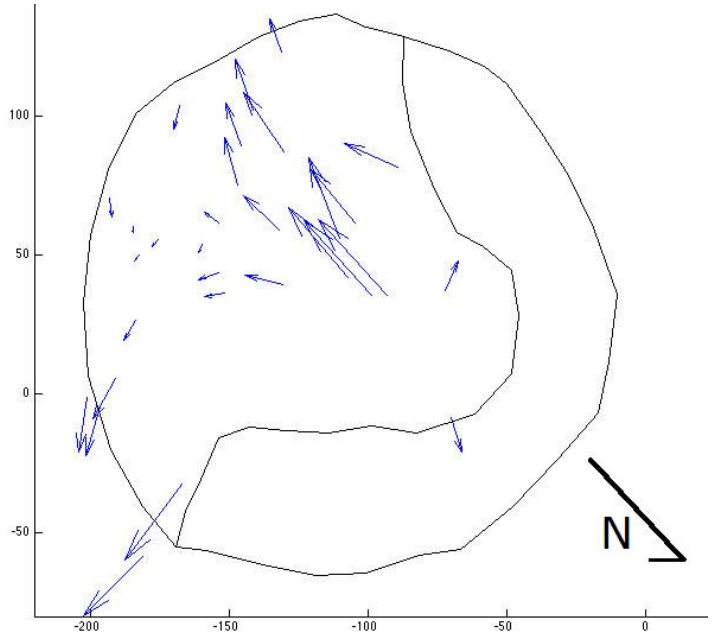


**Figure 4.2a: Block displacements from 13:54 (UTC) on 9 January 2007 to 17:16 (UTC) on 10 January 2007. The time difference is 27 h, 22 m. The farthest a block travelled was 14.14 meters.**

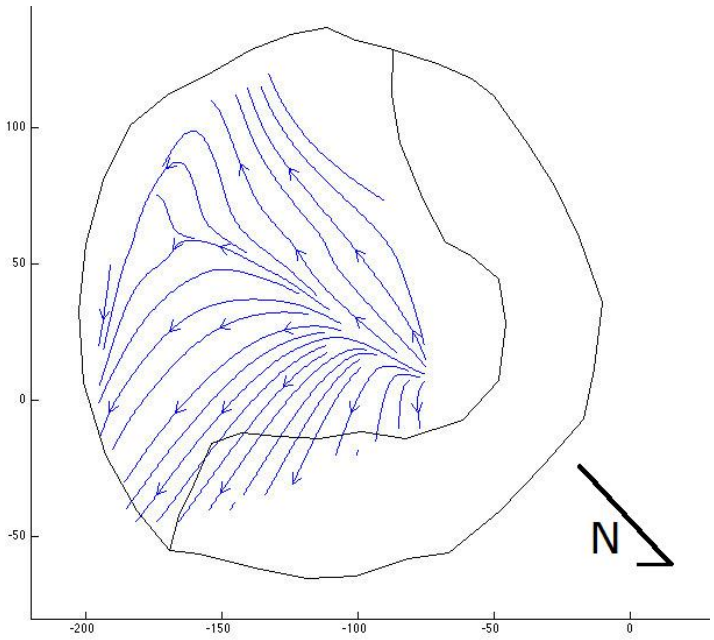


**Figure 4.2b: Streamlines from 13:54 (UTC) on 9 January 2007 to 17:16 (UTC) on 10 January 2007. The time difference is 27 h, 22 m.**

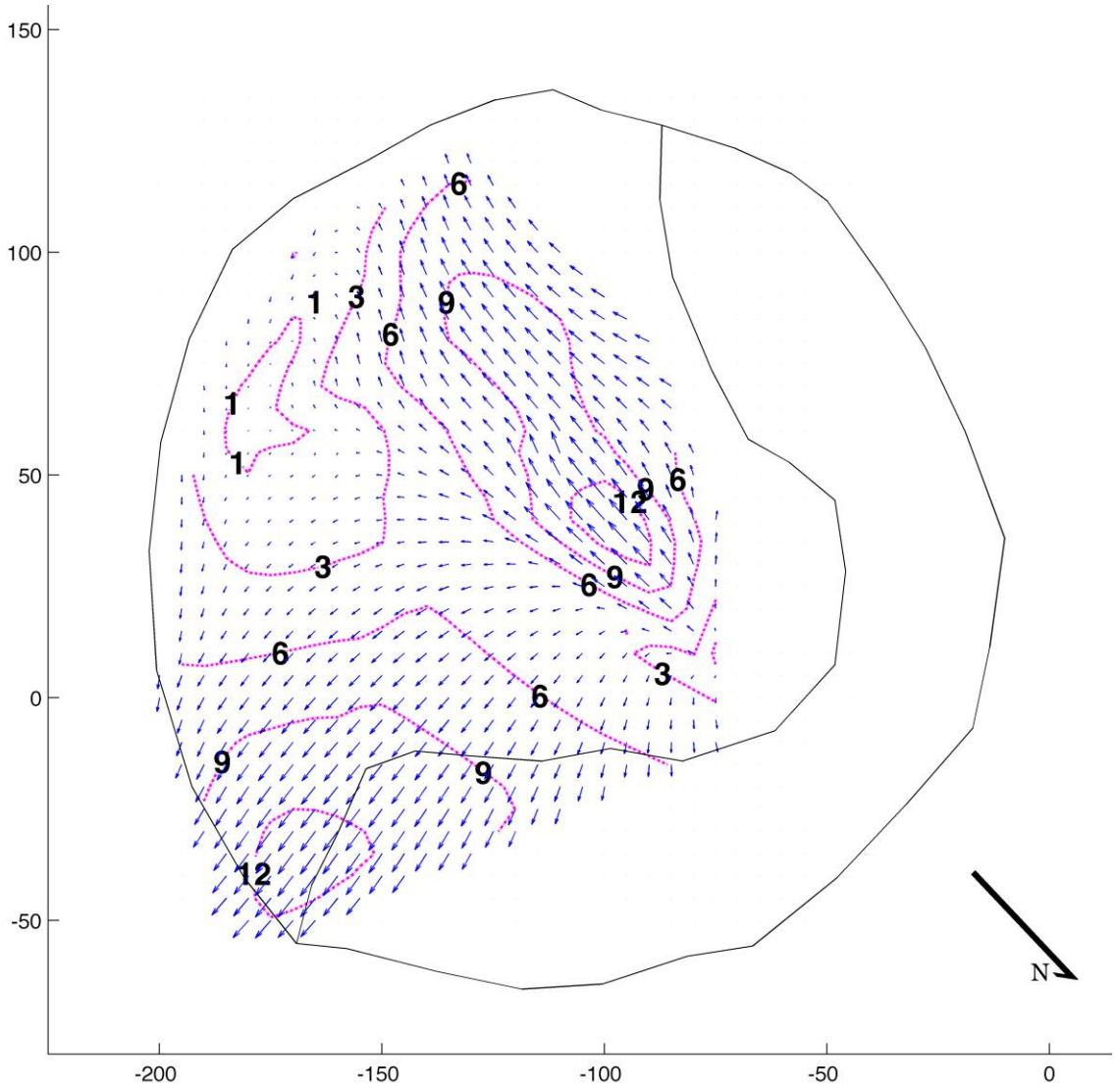


**Figure 4.2c: Interpolated block displacements from 13:54 (UTC) on 9 January 2007 to 17:16 (UTC) on 10 January 2007. The time difference is 27 h, 22 m. Black contour labels are in meters over time elapsed.**

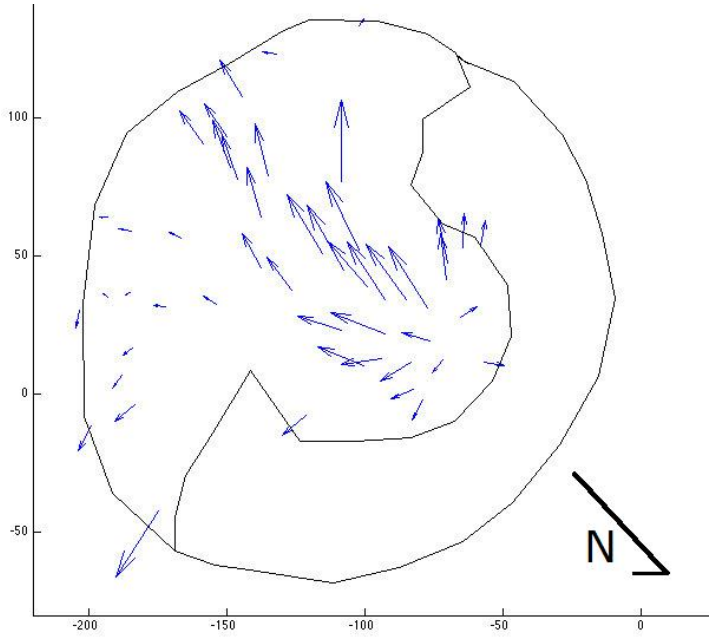


**Figure 4.3a: Block displacements from 17:54 (UTC) on 10 January 2007 to 14:08 on 11 January 2007. The time difference is 20 h, 52 m. The farthest a block travelled was 13.47 meters.**

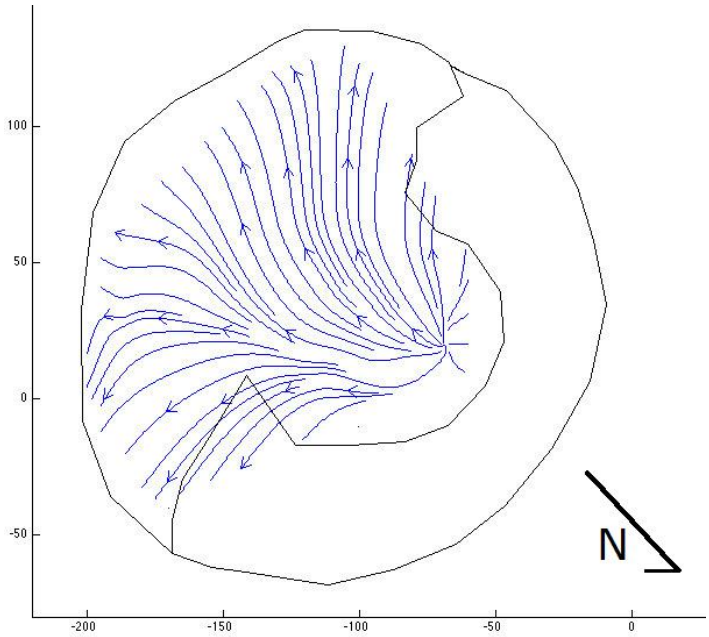


**Figure 4.3b: Streamlines from 17:54 (UTC) on 10 January 2007 to 14:08 on 11 January 2007. The time difference is 20 h, 52 m.**

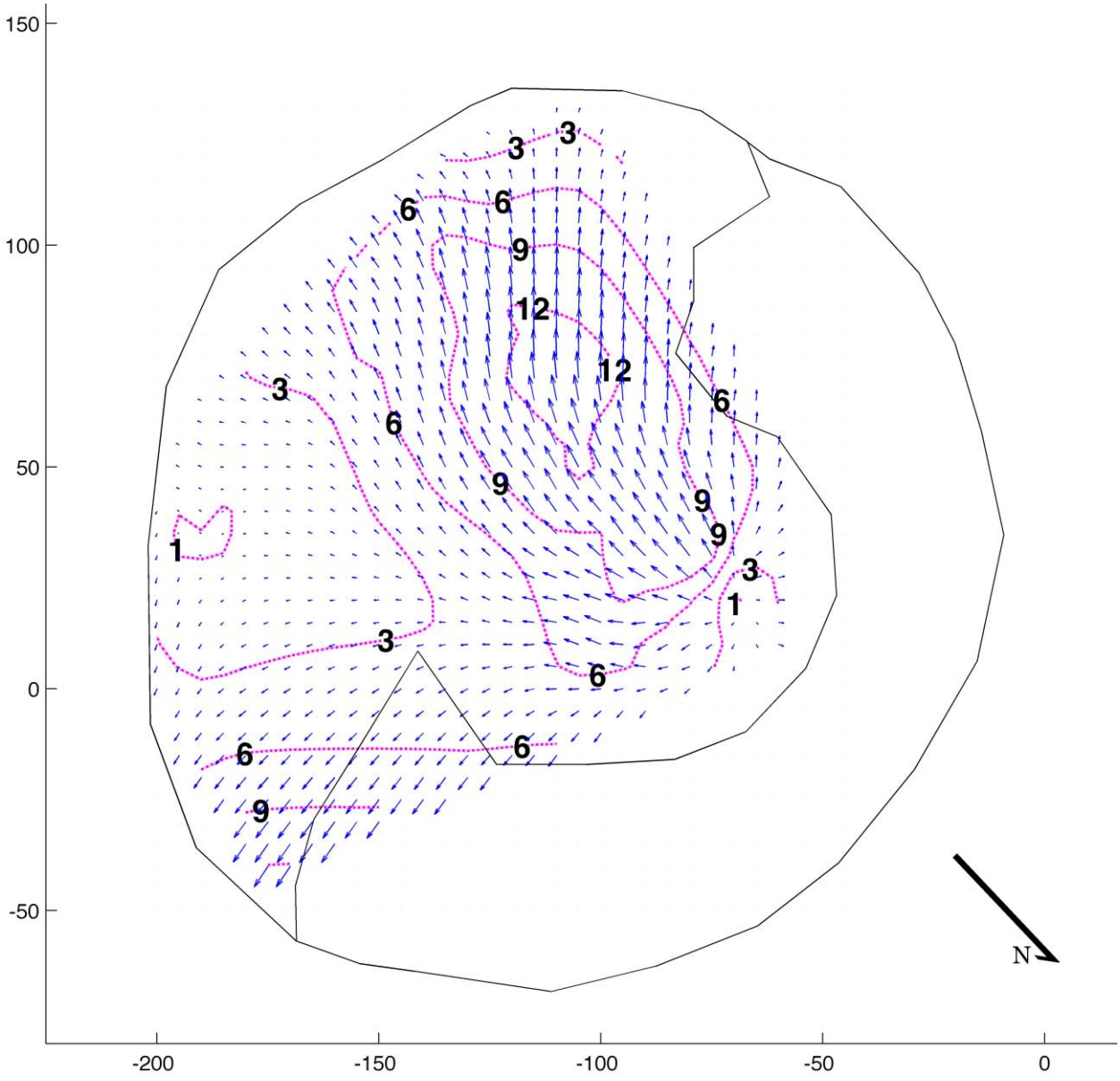


**Figure 4.3c: Interpolated block displacements from 17:54 (UTC) on 10 January 2007 to 14:08 on 11 January 2007. The time difference is 20 h, 52 m. Black contour labels are in meters over time elapsed.**

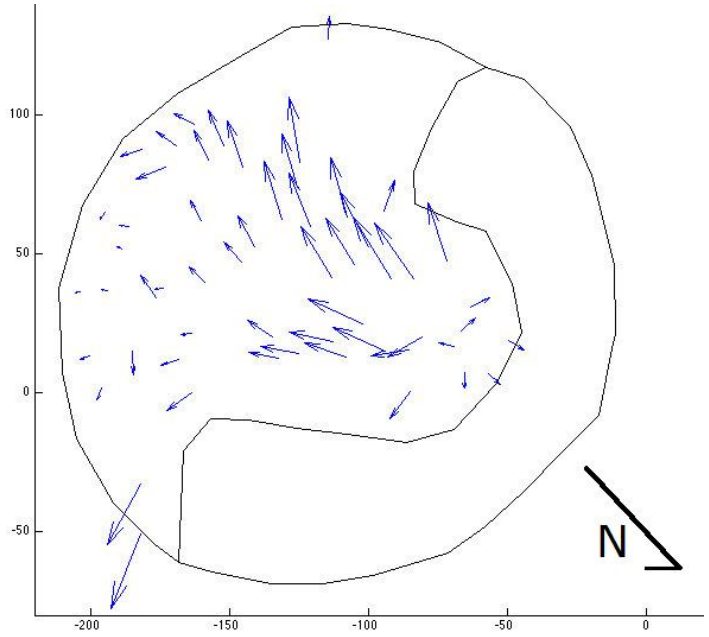


**Figure 4.4a: Block displacements from 14:08 (UTC) on 11 January 2007 to 13:59 (UTC) on 12 January 2007. The time difference is 23 h, 51 m. The farthest a block travelled was 17.35 meters.**

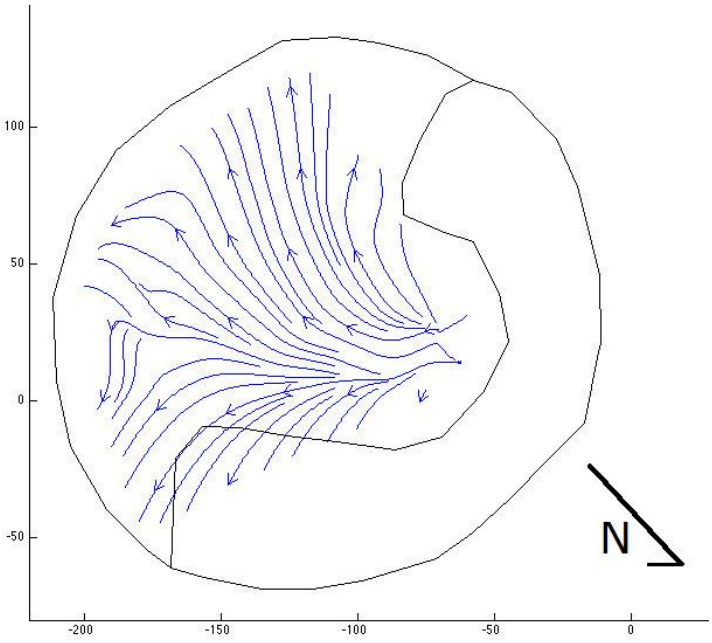


**Figure 4.4b: Streamlines from 14:08 (UTC) on 11 January 2007 to 13:59 (UTC) on 12 January 2007. The time difference is 23 h, 51 m.**

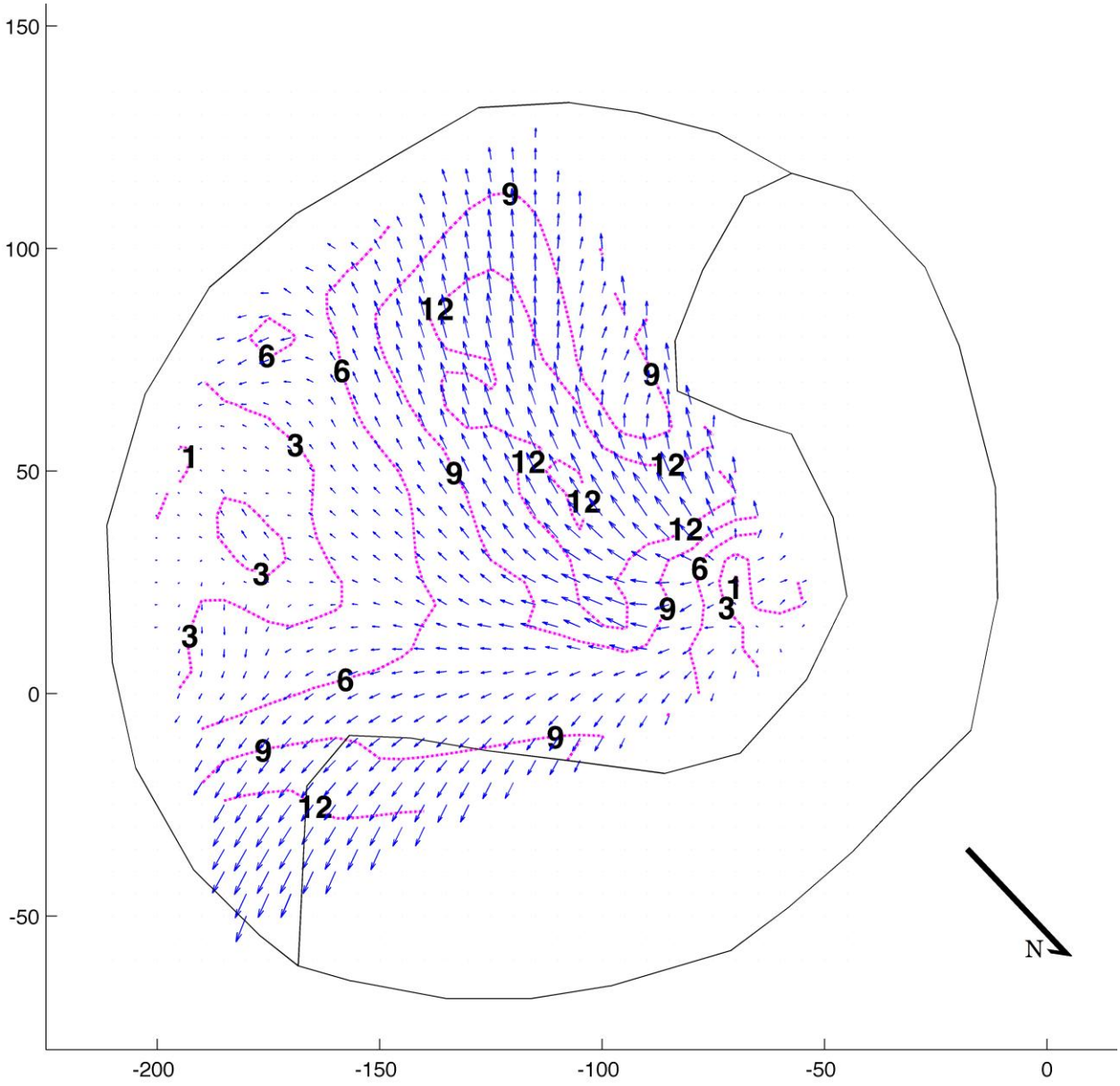


**Figure 4.4c: Interpolated block displacements from 14:08 (UTC) on 11 January 2007 to 13:59 (UTC) on 12 January 2007. The time difference is 23 h, 51 m. Black contour labels are in meters over time elapsed.**

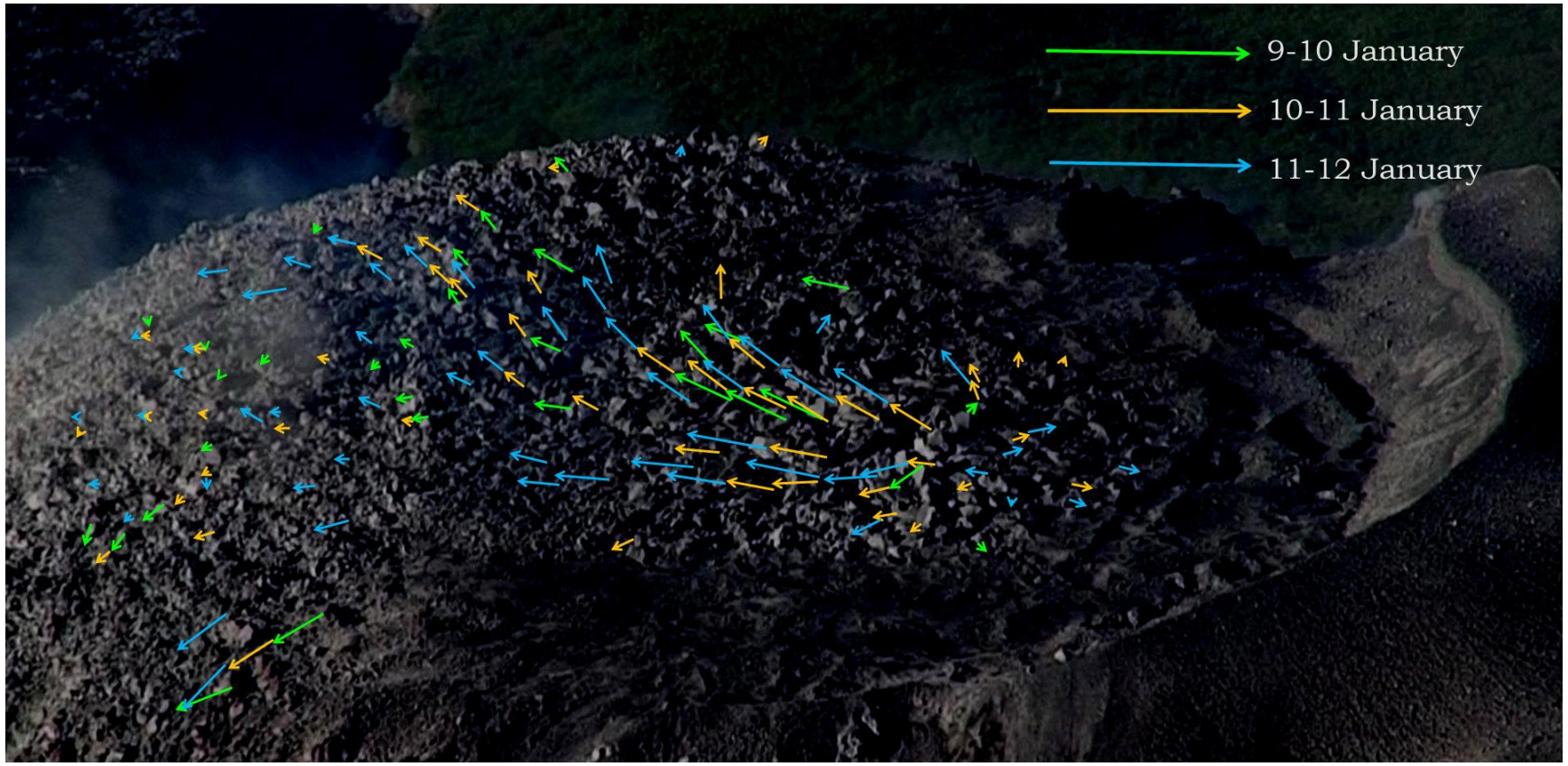


**Figure 4.5: Unorthorectified block displacements from 9-12 January 2007. Intervals are about 24 hours in duration. Crater is approximately 200 meters in diameter.**

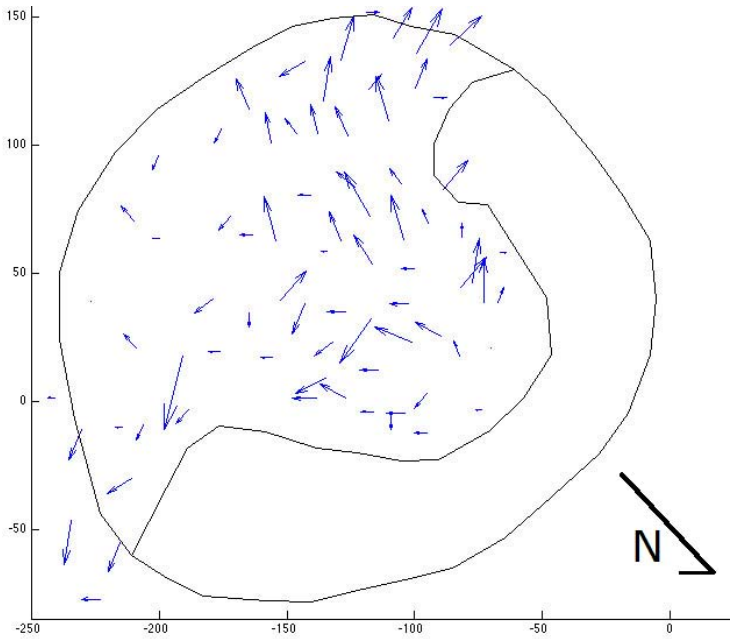


**Figure 4.6a: Block displacements from 12:53:44 to 13:59:51 (UTC) on 12 January 2007. The time difference is 1 h, 6 m, 7 s. The farthest a block travelled was 1.41 meters.**

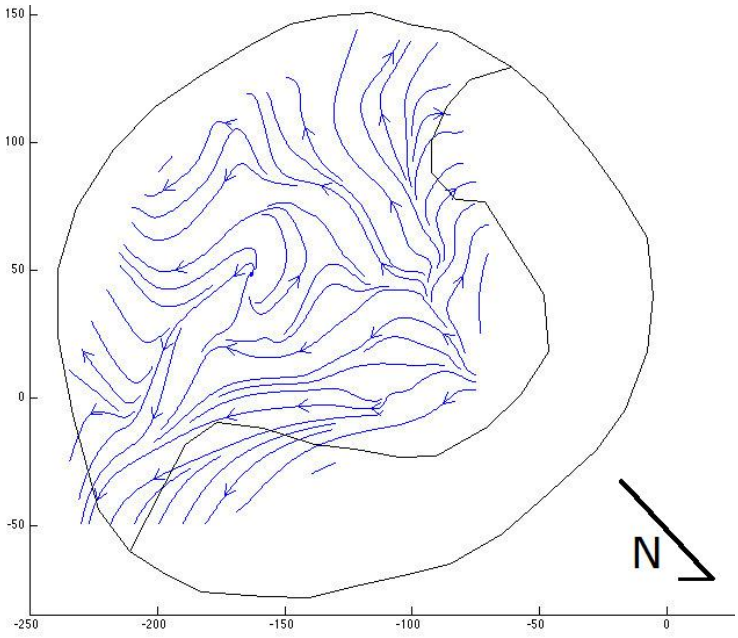


**Figure 4.6b: Streamlines from 12:53:44 to 13:59:51 (UTC) on 12 January 2007. The time difference is 1 h, 6 m, 7 s.**

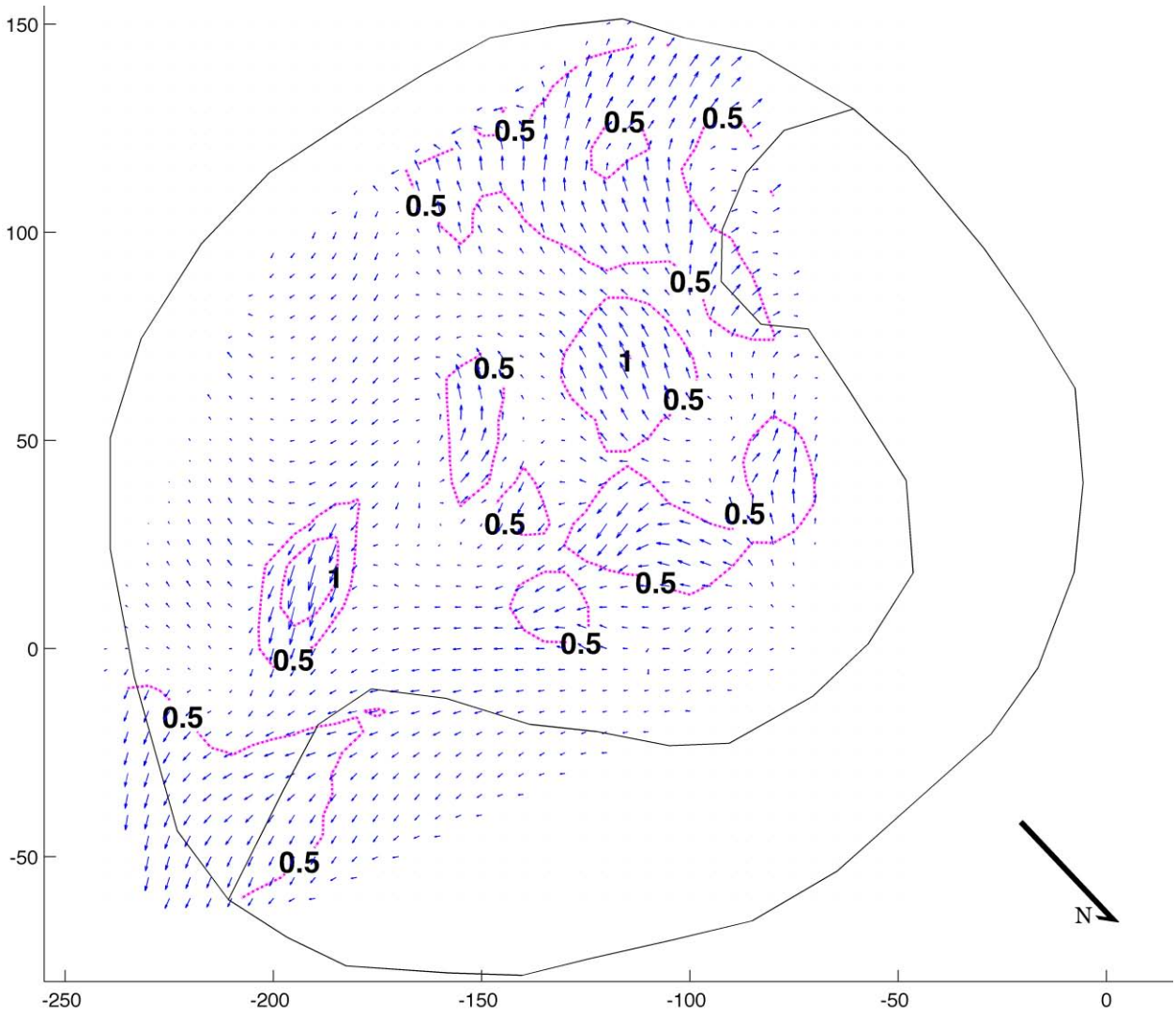


**Figure 4.6c: Interpolated block displacements from 12:53:44 to 13:59:51 (UTC) on 12 January 2007. The time difference is 1 hour, 6 minutes, 7 seconds. Black contour labels are in meters over time elapsed.**

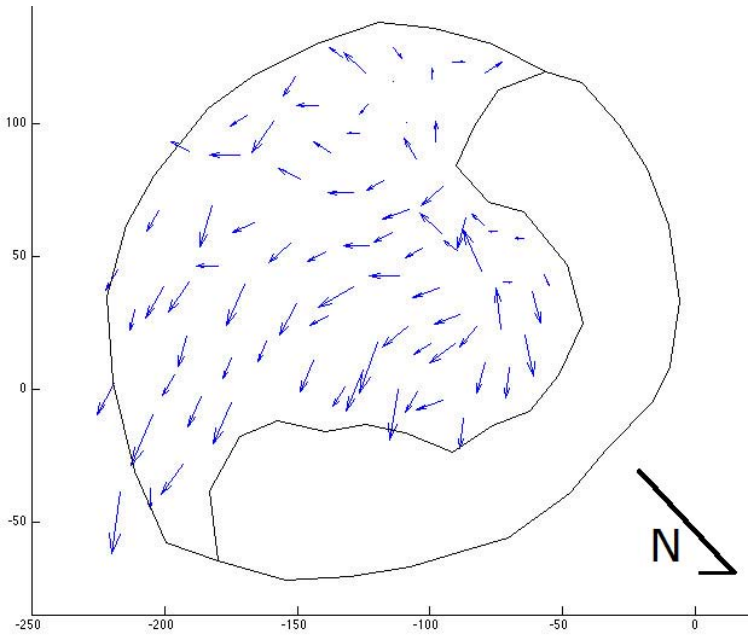


**Figure 4.7a: Block displacements from 13:59:51 to 14:41:23 (UTC) on 12 January 2007. The time difference is 41 m, 32 s. The farthest a block travelled was 1.57 meters.**

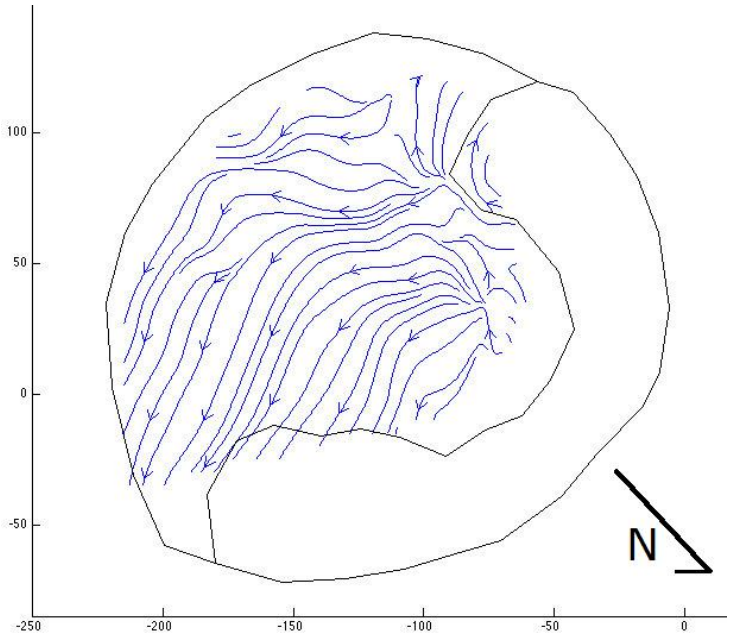


**Figure 4.7b: Streamlines from 13:59:51 to 14:41:23 (UTC) on 12 January 2007. The time difference is 41 m, 32 s.**

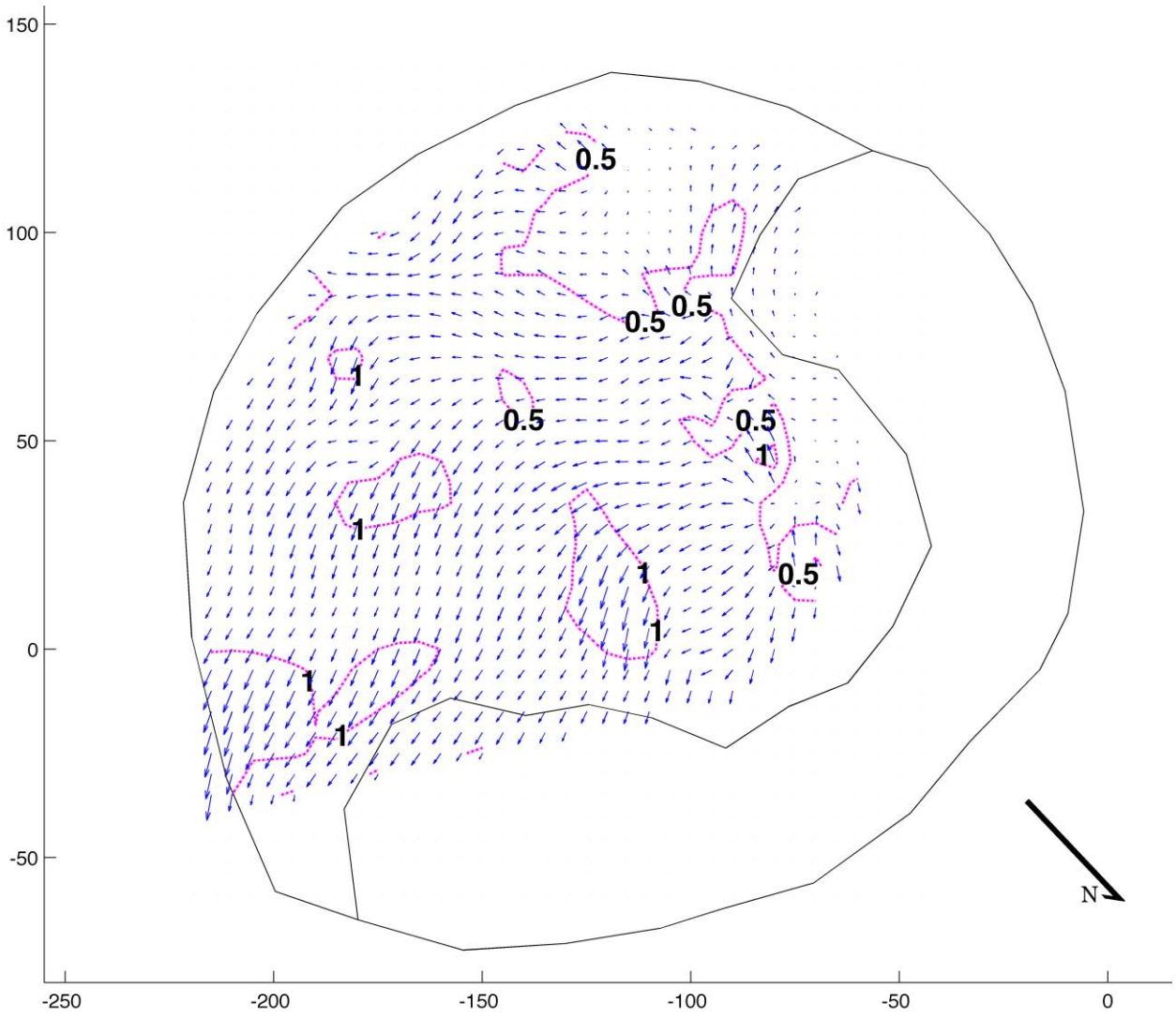


**Figure 4.7c: Interpolated block displacements from 13:59:51 to 14:41:23 (UTC) on 12 January 2007. The time difference is 41 m, 32 s. Black contour labels are in meters over time elapsed.**

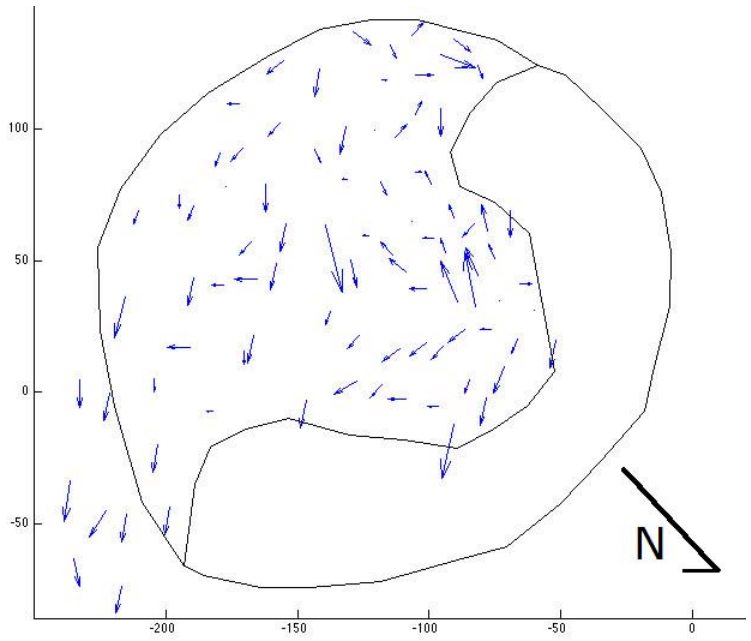


**Figure 4.8a: Block displacements from 14:41:23 to 15:08:20 (UTC) on 12 January 2007. The time difference is 26 m, 57 s. The farthest a block travelled was 1.31 meters.**

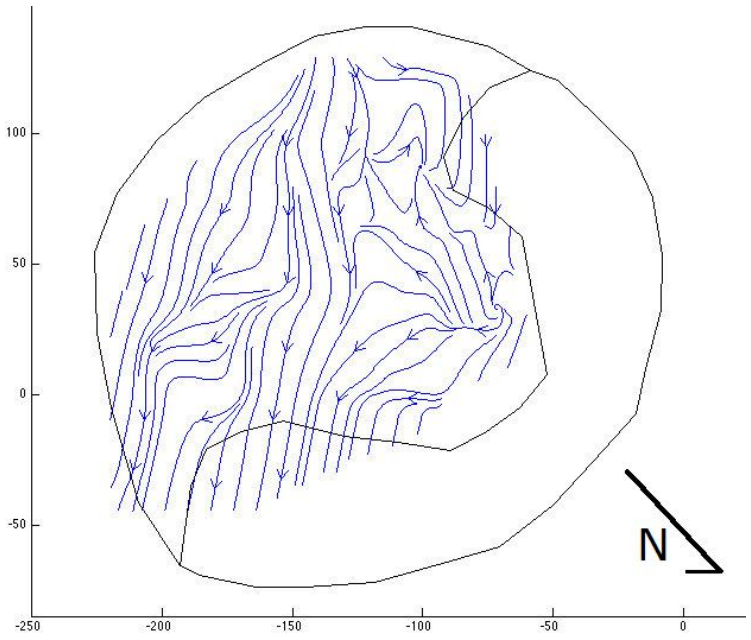


**Figure 4.8b: Streamlines from 14:41:23 to 15:08:20 (UTC) on 12 January 2007. The time difference is 26 m, 57 s.**

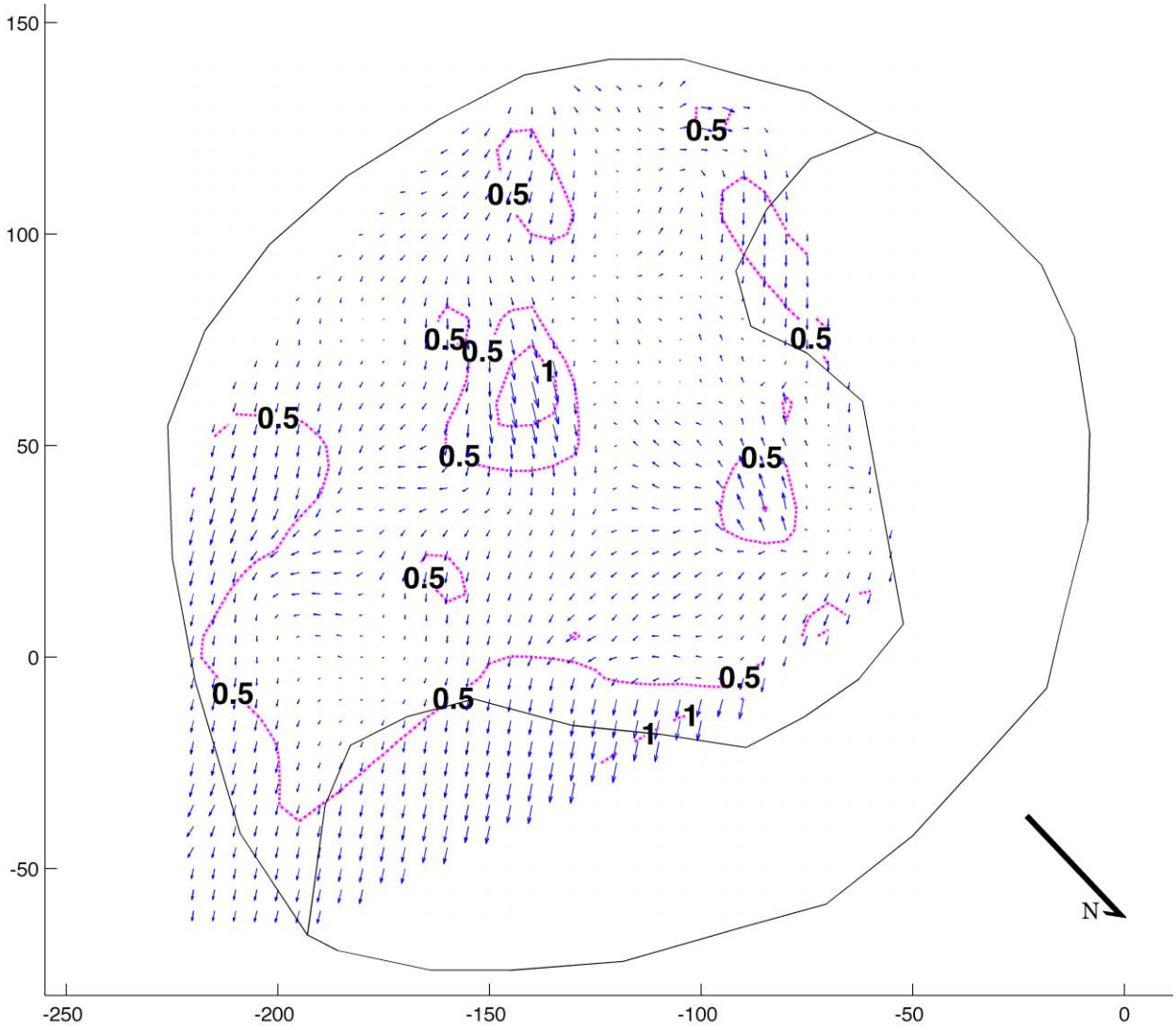


**Figure 4.8c: Interpolated block displacements from 14:41:23 to 15:08:20 (UTC) on 12 January 2007. The time difference is 26 m, 57 s. Black contour labels are in meters over time elapsed.**

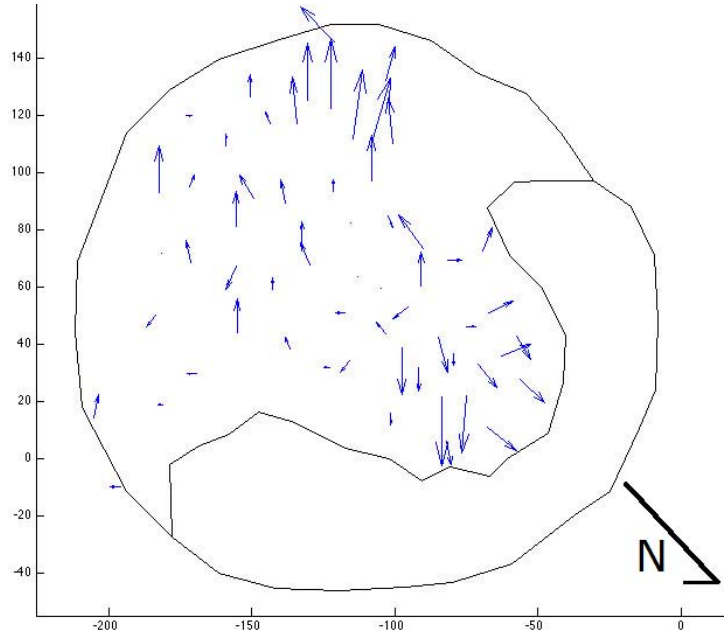


**Figure 4.9a: Block displacements from 16:47:18 to 17:19:12 (UTC) on 12 January 2007. The time difference is 31 m, 54 s. The farthest a block travelled was 1.59 meters.**

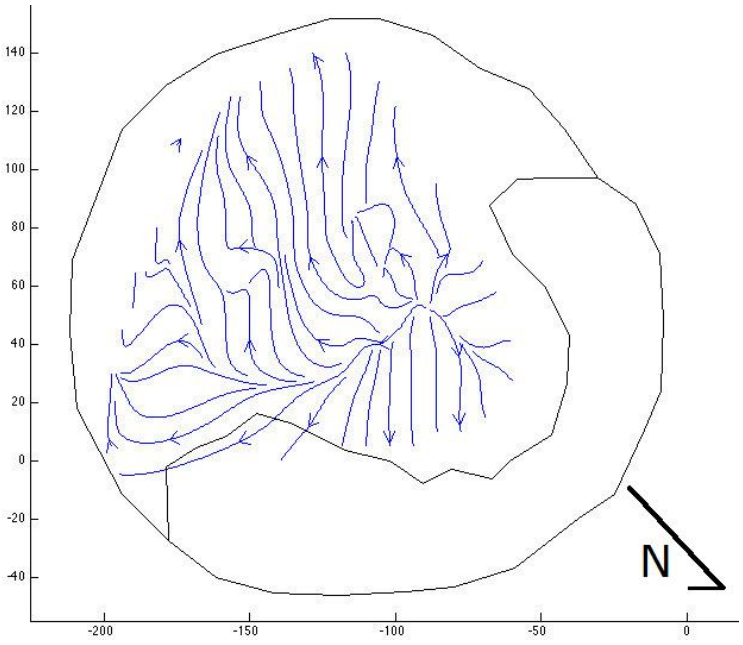


**Figure 4.9b: Streamlines from 16:47:18 to 17:19:12 (UTC) on 12 January 2007. The time difference is 31 m, 54 s.**

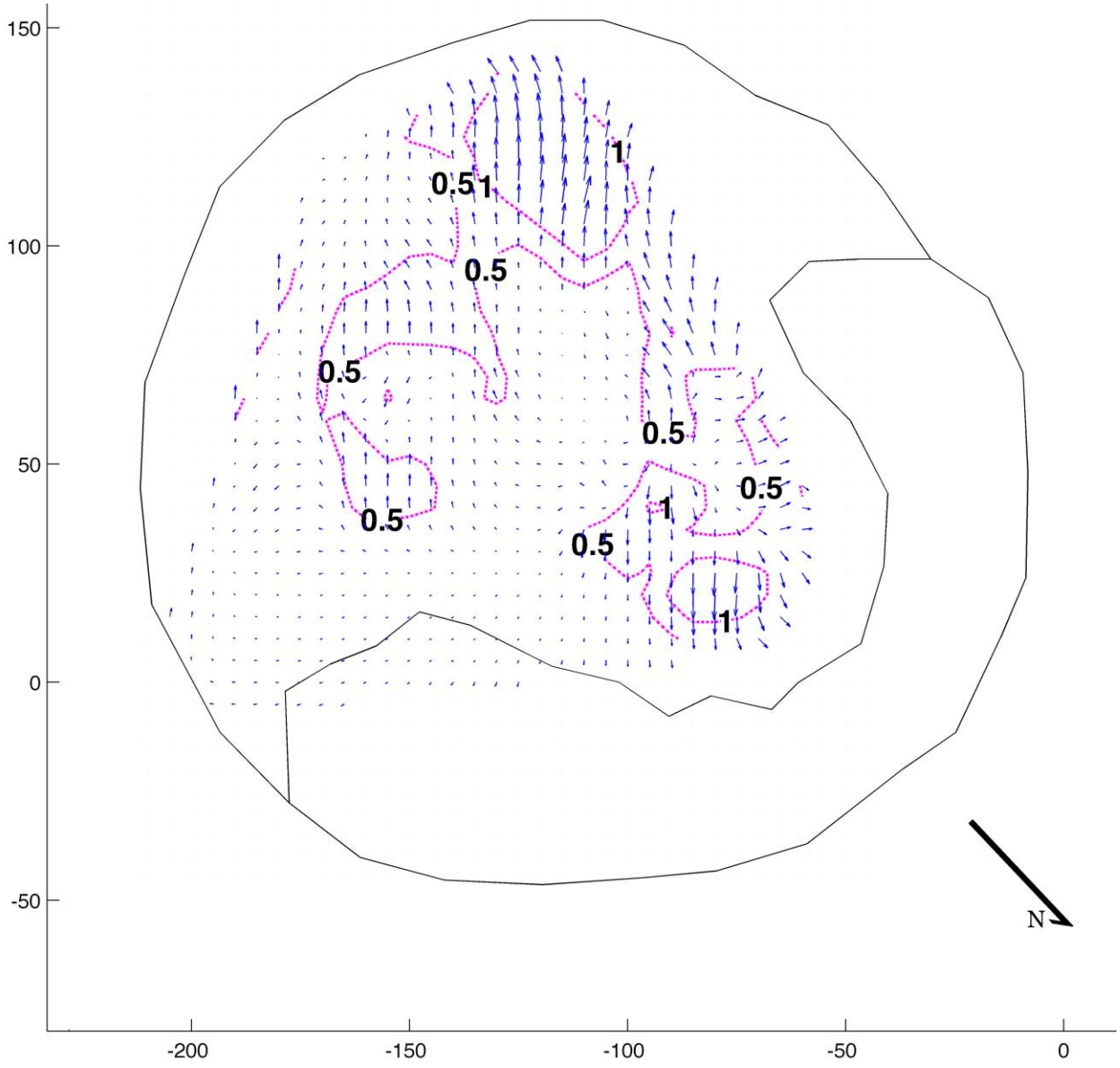


**Figure 4.9c: Interpolated block displacements from 16:47:18 to 17:19:12 (UTC) on 12 January 2007. The time difference is 31 m, 54 s. Black contour labels are in meters over time elapsed.**

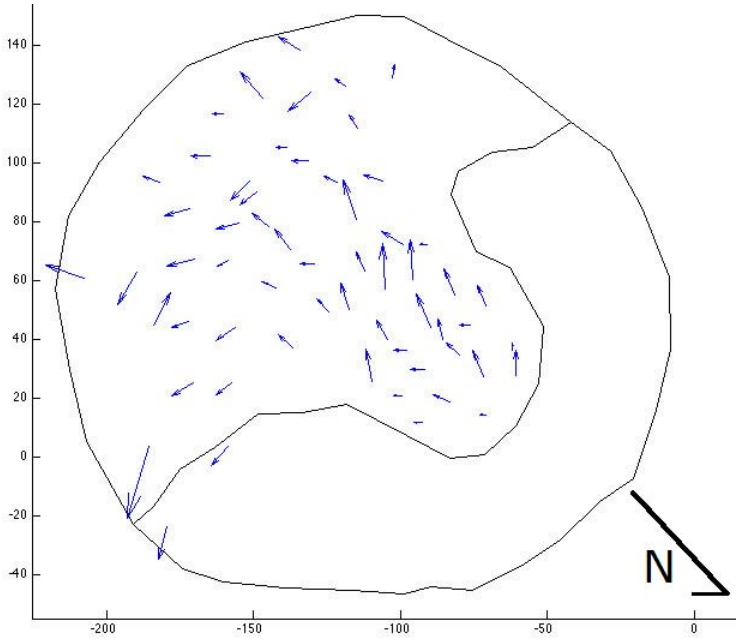


**Figure 4.10a: Block displacements from 17:19:12 to 17:42:55 (UTC) on 12 January 2007. The time difference is 23 m, 43 s. The farthest a block travelled was 2.8 meters.**

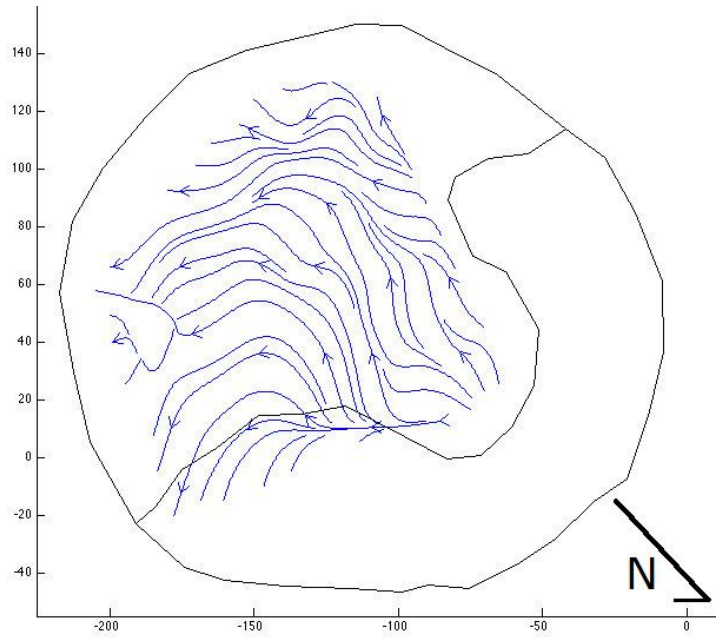


**Figure 4.10b: Streamlines from 17:19:12 to 17:42:55 (UTC) on 12 January 2007. The time difference is 23 m, 43 s.**

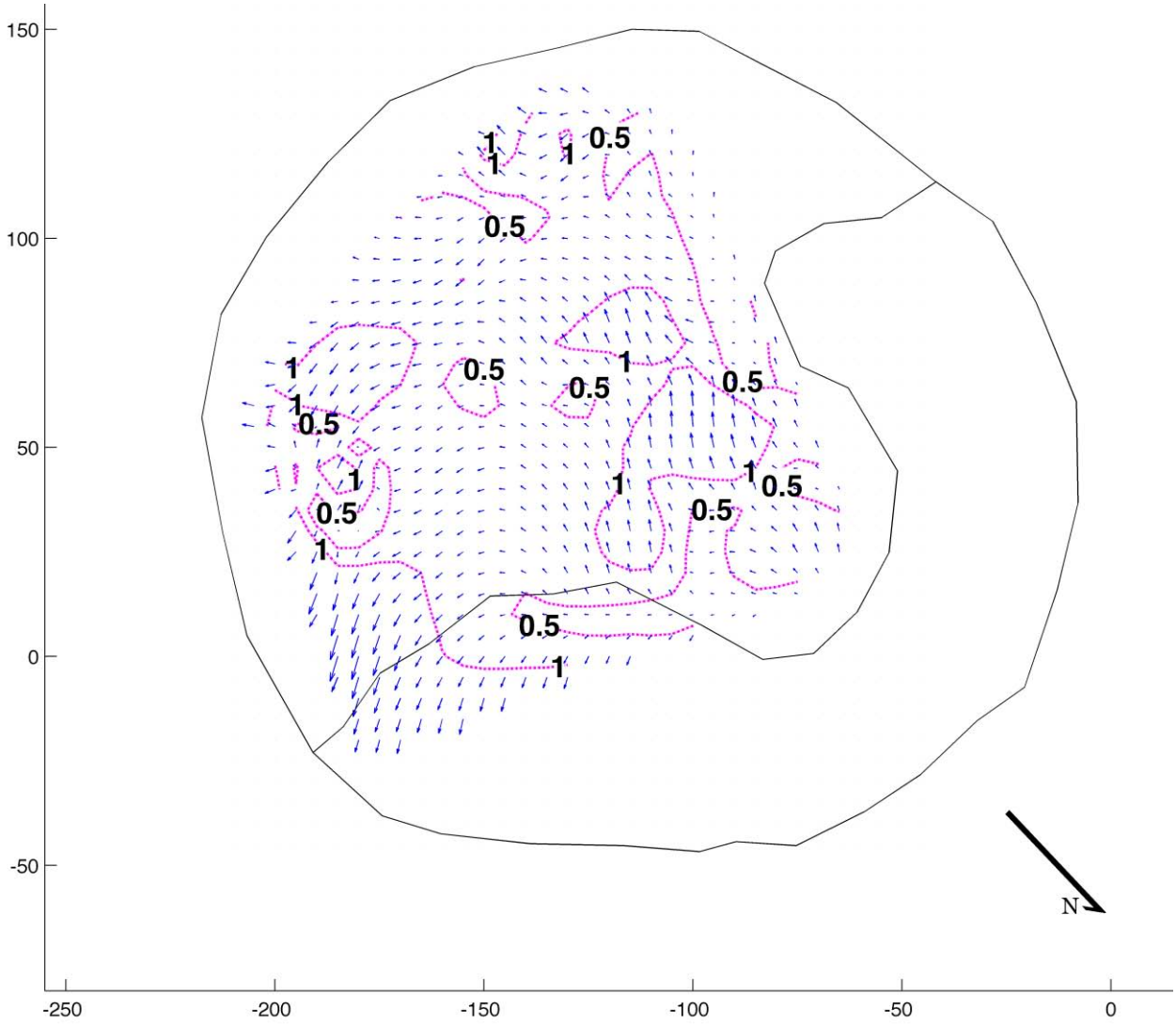


**Figure 4.10c: Interpolated block displacements from 17:19:12 to 17:42:55 (UTC) on 12 January 2007. The time difference is 23 m, 43 s. Black contour labels are in meters over time elapsed.**

## 4.2 JANUARY 2009

Ten time intervals were investigated during January 2009. Three were ~24-hour intervals from 1-2, 2-3, and 3-4 January (Figures 4.11a-c; Figures 4.12a-c; Figures 4.13a-c). The ~24-hour intervals begin on the first day in the morning at first recording, and end on the next day in the morning at the first recording. Each day was also individually analyzed from the beginning of the morning until the dome was obscured by meteorological clouds (Figures 4.14a-c; Figures 4.15a-c; Figures 4.16a-c; Figures 4.17a-c). These intervals each last about one hour 45 minutes to three hours 40 minutes. Finally, three explosions were selected and analyzed from just before the explosion onset to just after the explosion ended when visibility returned. The explosion on 2 January (Figures 4.18a-c) last about four minutes 30 seconds. The explosions on 4 January (Figures 4.19a-c; Figures 4.20a-c) last from five minutes 30 seconds, to six minutes 40 seconds.

The lava in 2009 flowed west-southwest over the crater edge, originating from a linear vent (~50 m) located on the eastern side of the crater. As in 2007, a distinct region of large displacement is visible in the ~24-hour interval image sets (Figures 4.11-4.13c).

More explosions were analyzed on 2 January and 4 January to compare with the two recorded explosions on 1 January. Poor meteorological conditions on 3 January did not allow for clear short-term images to be compared.

**Table 4.2a: Surface flow velocities during January 2009 based on the interpolated displacement vectors within the interpreted flow area. 'Peak velocity' and 'Mean velocity' are measured from the time elapsed between the images. The intervals are measured from the start of the first day to the approximate same time on the next day (~24 hours).**

| Period | Time elapsed between images | Peak displacement | Peak velocity (m/second) | Peak velocity (m/day) | Peak velocity (m/hour) | Mean displacement | Mean velocity (m/second) | Mean velocity (m/day) | Mean velocity (m/hour) | Figures |
|---|---|---|---|---|---|---|---|---|---|---|
| 1-2 January | 24:05:00 | 19.94 | $2.30^{-4}$ | 19.87 | 0.83 | 5.22 | $6.02^{-5}$ | 5.20 | 0.22 | 4.11a-c |
| 2-3 January | 25:35:26 | 23.77 | $2.58^{-4}$ | 22.29 | 0.93 | 5.81 | $6.31^{-5}$ | 5.45 | 0.23 | 4.12a-c |
| 3-4 January | 23:33:50 | 19.8 | $2.33^{-4}$ | 20.17 | 0.84 | 5.6 | $6.60^{-5}$ | 5.70 | 0.24 | 4.13a-c |

**Table 4.2b: Surface flow velocities during January 2009 based on the interpolated displacement vectors within the interpreted flow area. 'Peak velocity' and 'Mean velocity' are measured from the time elapsed between the images. The intervals are measured from the start of the day to the end of the same day.**

| Period | Time elapsed between images | Peak displacement | Peak velocity (m/second) | Peak velocity (m/day) | Peak velocity (m/hour) | Mean displacement | Mean velocity (m/second) | Mean velocity (m/day) | Mean velocity (m/hour) | Figures |
|---|---|---|---|---|---|---|---|---|---|---|
| 1-Jan | 01:45:32 | 1.83 | $2.89^{-4}$ | 24.97 | 1.04 | 0.75 | $1.19^{-4}$ | 10.23 | 0.43 | 4.14a-c |
| 2-Jan | 03:24:55 | 3.01 | $2.45^{-4}$ | 21.15 | 0.88 | 1.38 | $1.12^{-4}$ | 9.70 | 0.40 | 4.15a-c |
| 3-Jan | 02:25:18 | 2.05 | $2.35^{-4}$ | 20.32 | 0.85 | 0.95 | $1.09^{-4}$ | 9.42 | 0.39 | 4.16a-c |
| 4-Jan | 03:39:43 | 3.92 | $2.97^{-4}$ | 25.69 | 1.07 | 1.47 | $1.12^{-4}$ | 9.63 | 0.40 | 4.17a-c |

**Table 4.2c: Surface flow velocities during January 2009 based on the interpolated displacement vectors within the interpreted flow area. 'Peak velocity' and 'Mean velocity' are measured from the time elapsed between the images. The explosions were measured from just before the explosion onset to the next clear image after the explosion.**

| Period | Time elapsed between images | Peak displacement | Peak velocity (m/second) | Peak velocity (m/day) | Peak velocity (m/hour) | Mean displacement | Mean velocity (m/second) | Mean velocity (m/day) | Mean velocity (m/hour) | Figures |
|---|---|---|---|---|---|---|---|---|---|---|
| 2 Jan., explosion 3 | 00:04:34 | 0.65 | $2.37^{-3}$ | 204.96 | 8.54 | 0.25 | $9.12^{-4}$ | 78.83 | 3.28 | 4.18a-c |
| 4 Jan., explosion 1 | 00:05:27 | 1.08 | $3.30^{-3}$ | 285.36 | 11.89 | 0.47 | $1.44^{-3}$ | 124.18 | 5.17 | 4.19a-c |
| 4 Jan., explosion 2 | 00:06:38 | 0.86 | 2.16-3 | 186.69 | 7.78 | 0.4 | $1.00^{-3}$ | 86.83 | 3.62 | 4.20a-c |

**Table 4.2d: Surface flow velocities during 1 January 2009 based on the interpolated displacement vectors over the interpreted flow area. 'Peak velocity' and 'Mean velocity' refer to the period duration. The explosion intervals are measured from just before onset to the next clear image after the explosion. 'Between explosions' was measured from the end of the first explosion to the beginning of the second explosion. 'After explosion 2' was measured after the end of the second explosion until the very beginning of the next field day.**

| Period | Time elapsed between images | Peak displacement | Peak velocity (m/second) | Peak velocity (m/day) | Peak velocity (m/hour) | Mean displacement | Mean velocity (m/second) | Mean velocity (m/day) | Mean velocity (m/hour) | Figures |
|---|---|---|---|---|---|---|---|---|---|---|
| Explosion 1 | 00:04:33 | 1.62 | $5.93^{-3}$ | 512.70 | 21.36 | 0.28 | $1.03^{-3}$ | 88.62 | 3.69 | 4.21a-c |
| Between explosions | 00:50:36 | 1.65 | $5.43^{-4}$ | 46.96 | 1.96 | 0.51 | $1.68^{-4}$ | 14.51 | 0.60 | 4.22a-c |
| Explosion 2 | 00:24:57 | 0.99 | $6.61^{-4}$ | 57.14 | 2.38 | 0.33 | $2.20^{-4}$ | 19.05 | 0.79 | 4.23a-c |
| After explosion 2 | 21:11:26 | 13.97 | $1.82^{-4}$ | 15.82 | 0.66 | 4.06 | $5.32^{-5}$ | 4.60 | 0.19 | 4.24a-c |

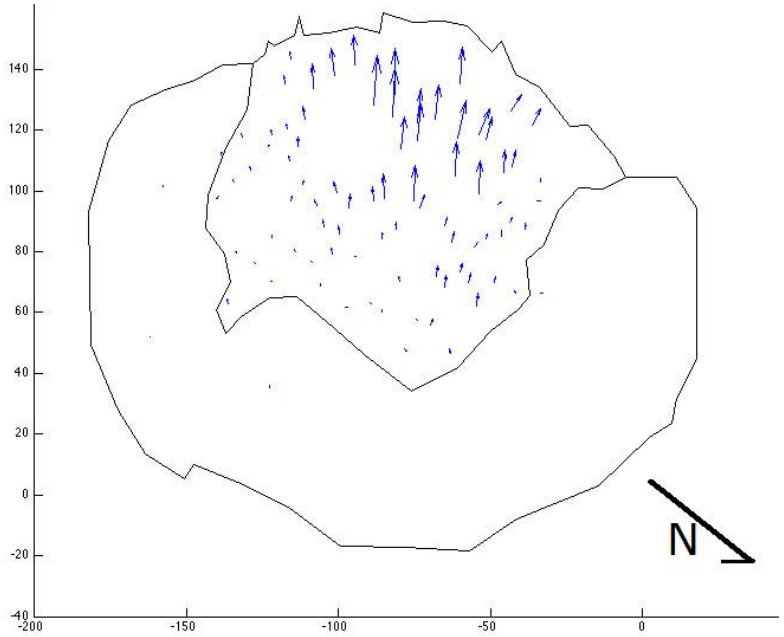


**Figure 4.11a: Block displacements from 14:03:38 UTC on 1 January to 14:08:38 UTC on 2 January 2009. The farthest a block travelled was 19.17 meters. Time elapsed was 24 h, 5 m. Camera: SGH2.**

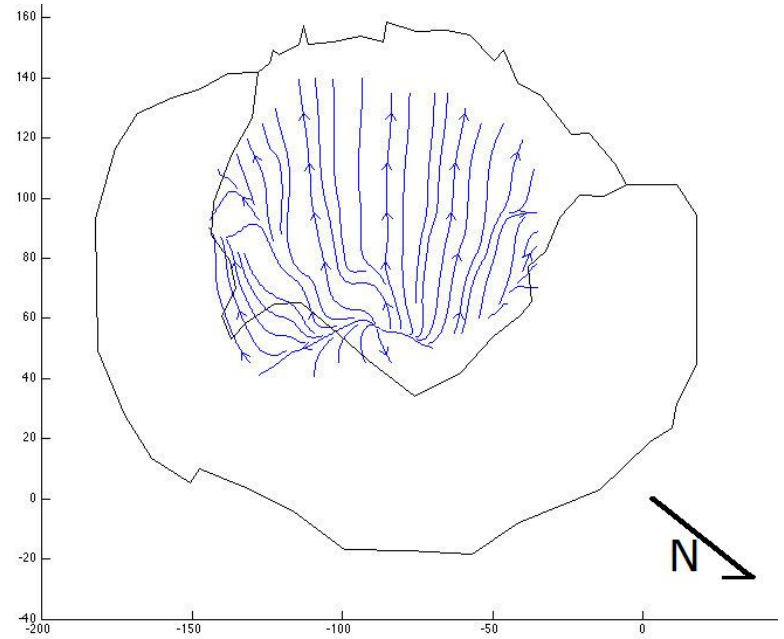


**Figure 4.11b: Streamlines from 14:03:38 UTC on 1 January to 14:08:38 UTC on 2 January 2009. Time elapsed was 24 h, 5 m. Camera: SGH2.**

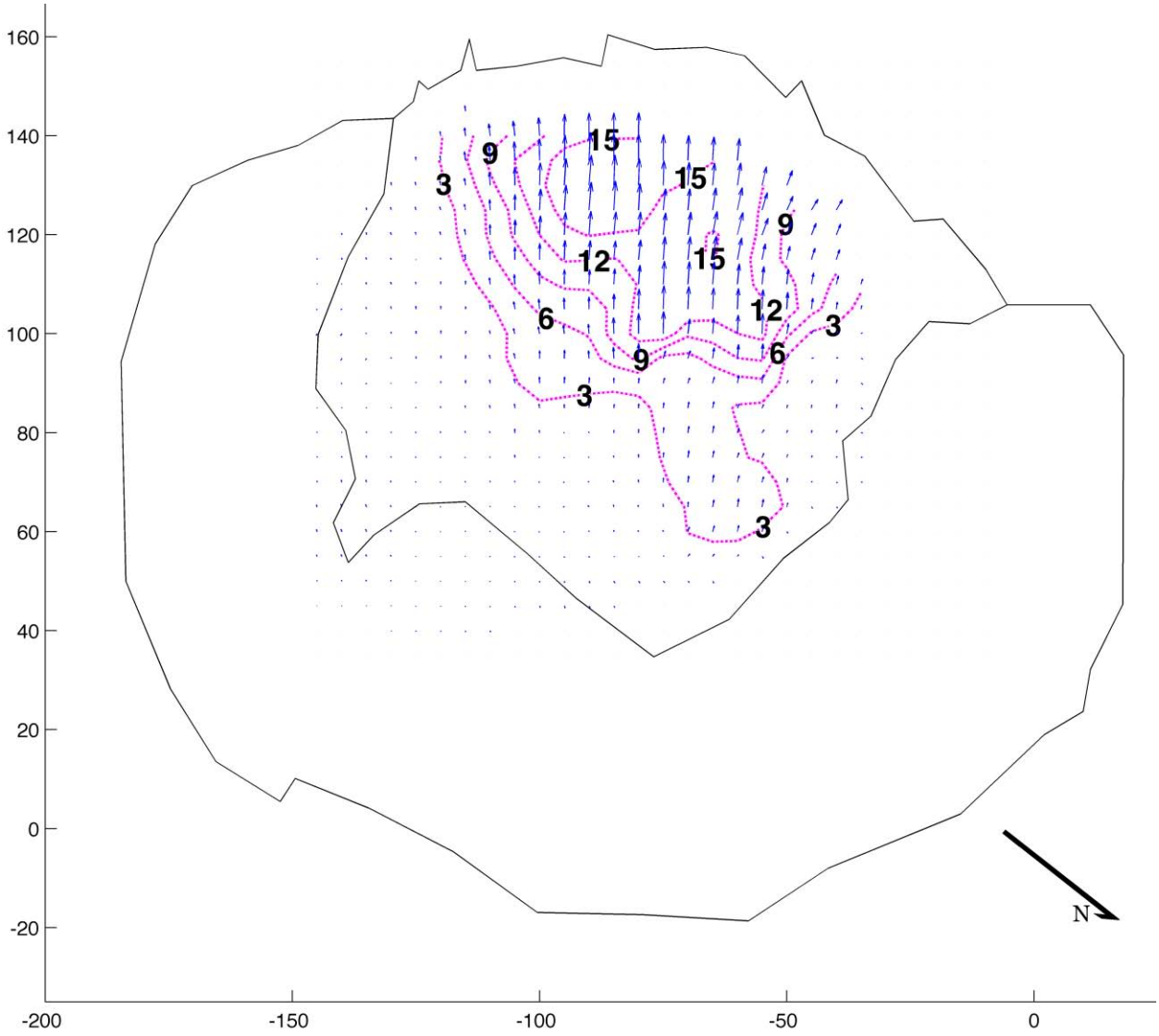


**Figure 4.11c: Interpolated block displacements from 14:03:38 on 1 January to 14:08:38 on 2 January 2009. Time elapsed was 24 h, 5 m. Camera: SGH2.**

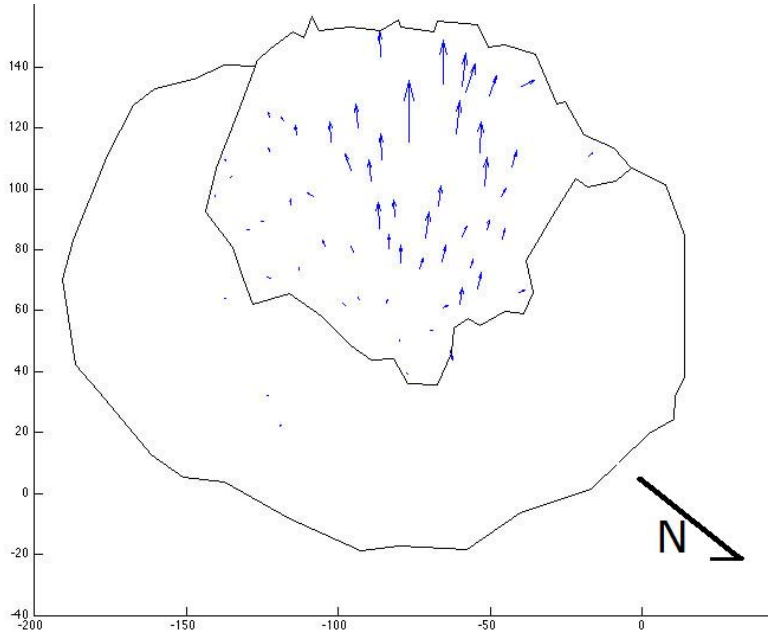


**Figure 4.12a: Block displacements from 14:08:38 UTC on 2 January to 15:44:04 UTC on 3 January 2009. The farthest a block travelled was 23.94 meters. Time elapsed was 25 h 35 m. Camera: SGH2.**

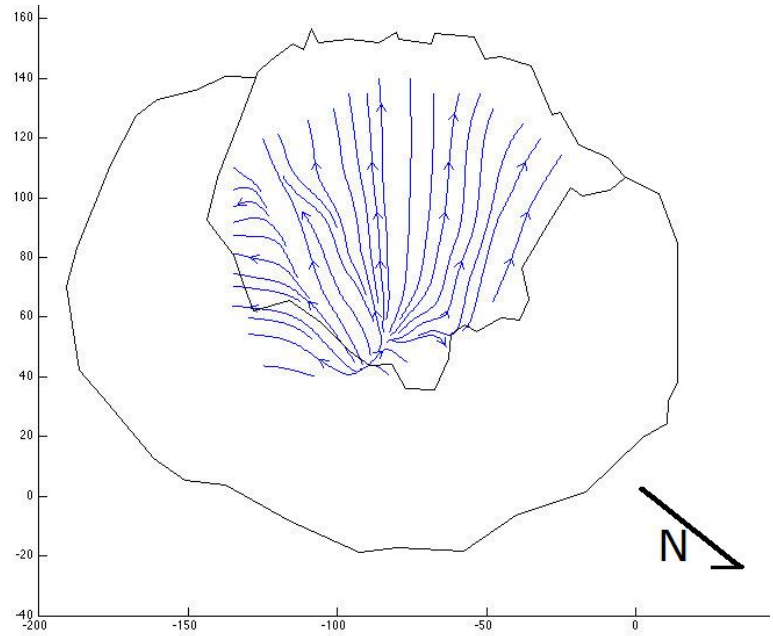


**Figure 4.12b: Streamlines from 14:08:38 UTC on 2 to 15:44:04 UTC on 3 January 2009. Time elapsed was 25 h 35 m. Camera: SGH2.**

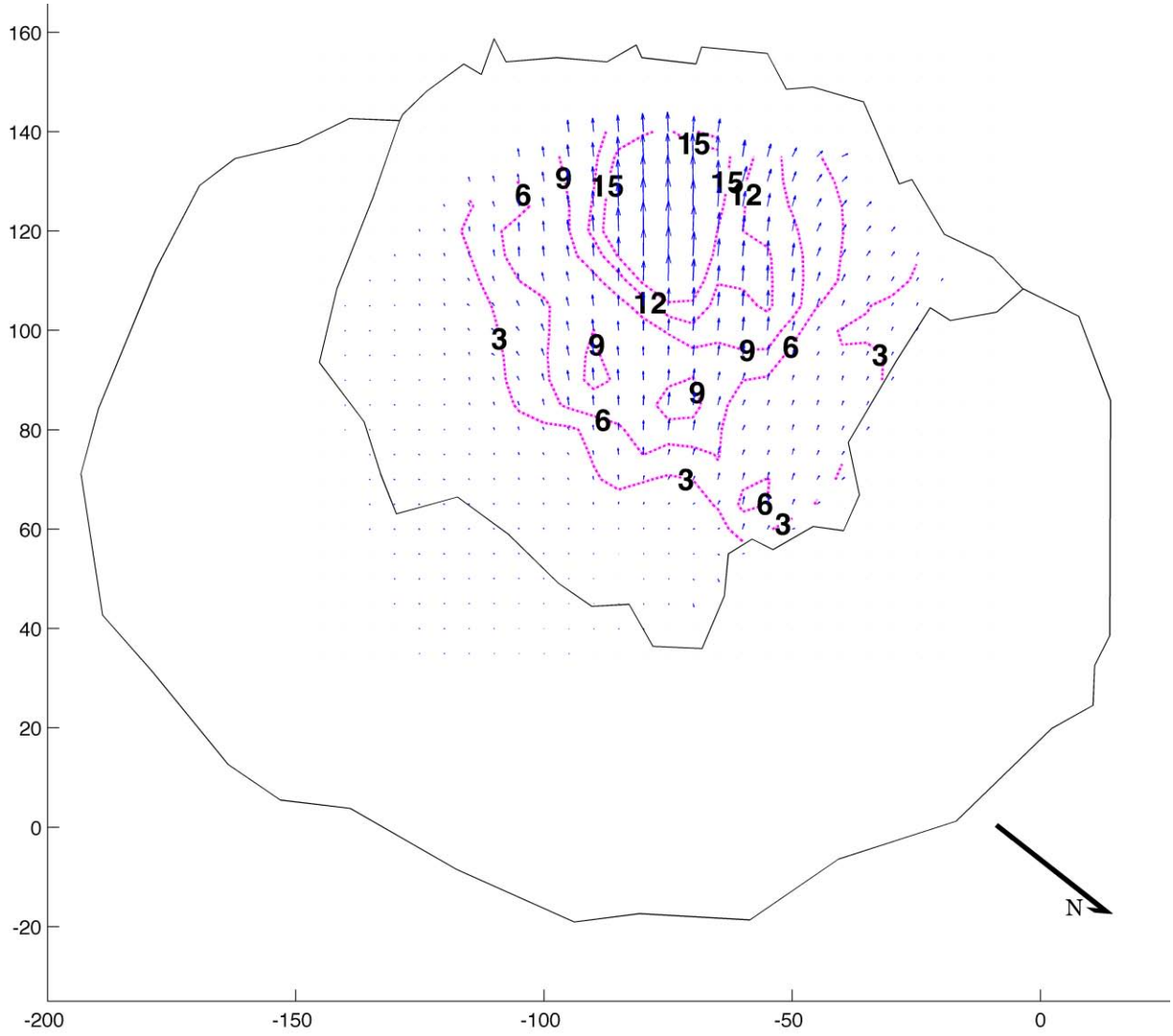


**Figure 4.12c: Interpolated block displacements from 14:08:38 UTC on 2 January to 15:44:04 UTC on 3 January 2009. Time elapsed was 25 h 35 m. Camera: SGH2.**

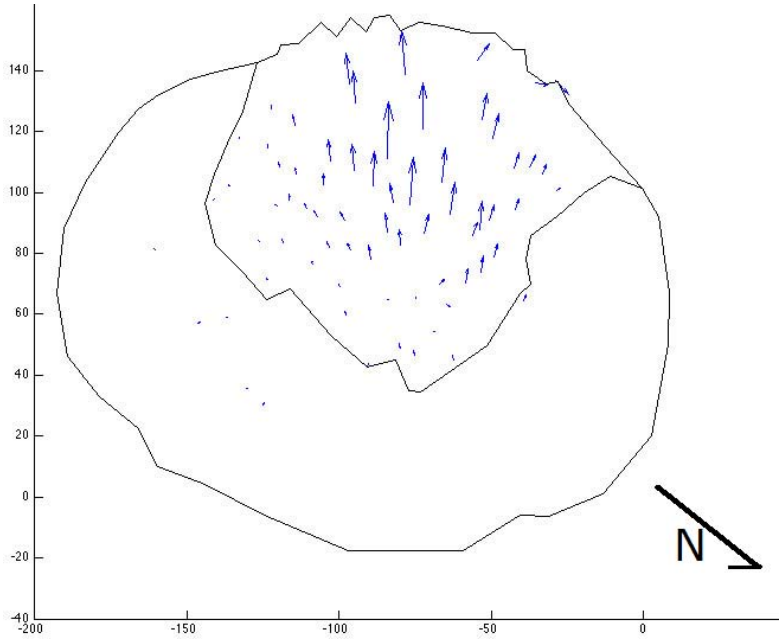


**Figure 4.13a: Block displacements from 15:44:04 UTC on 3 January to 15:17:54 UTC on 4 January 2009. The farthest a block travelled was 20.17 meters. Time elapsed was 23 h 33 m. Camera: SGH2.**

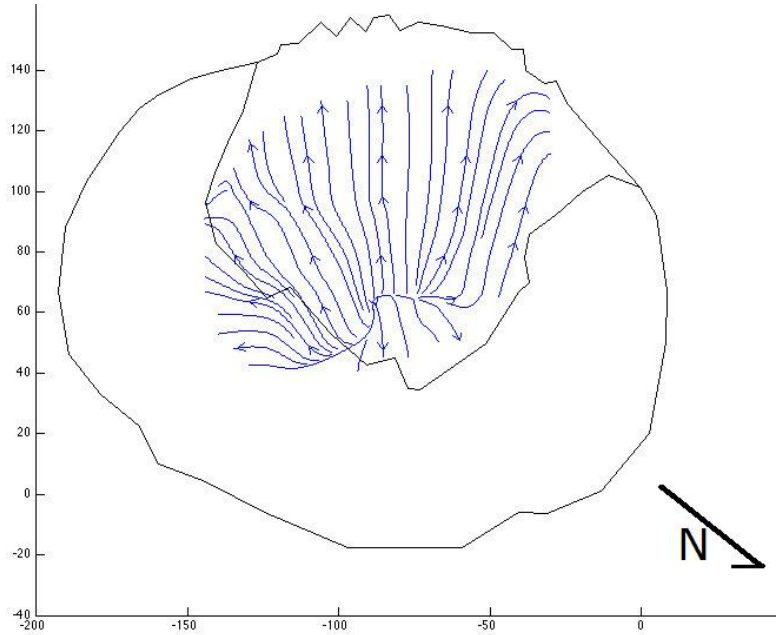


**Figure 4.13b: Streamlines from 15:44:04 UTC on 3 January to 15:17:54 UTC on 4 January 2009. Time elapsed was 23 h 33 m. Camera: SGH2.**

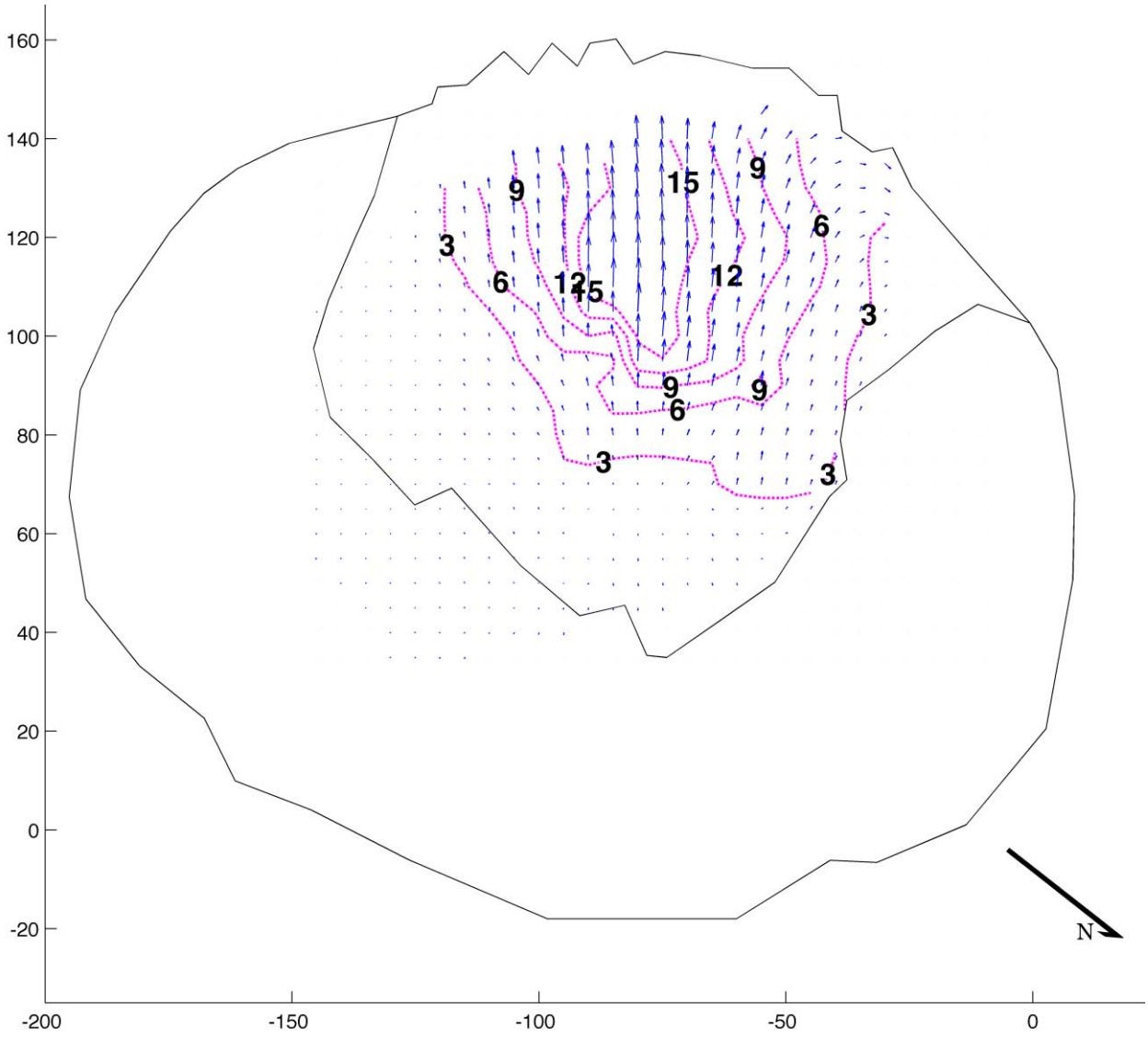


**Figure 4.13c: Interpolated block displacements from 15:55:04 UTC on 3 to 15:17:34 UTC on 4 January 2009. Time elapsed was 23 h 33 m. Camera: SGH2.**

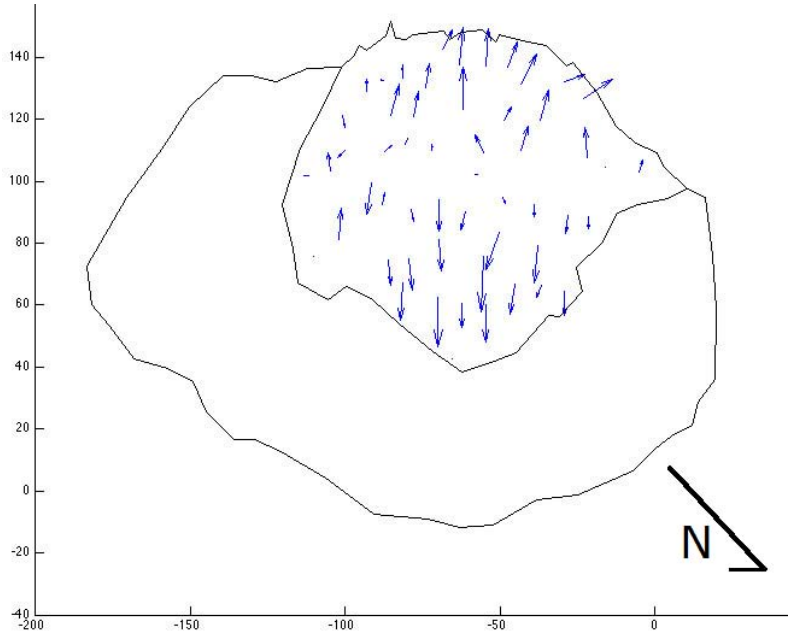


**Figure 4.14a: Block displacements from the beginning of the field day (13:42:44 UTC) to the end of the field day (15:28:17 UTC), 1 January 2009. The farthest a block travelled was 1.82 meters. Time elapsed was 1 h, 45 m. Camera: SGH1.**

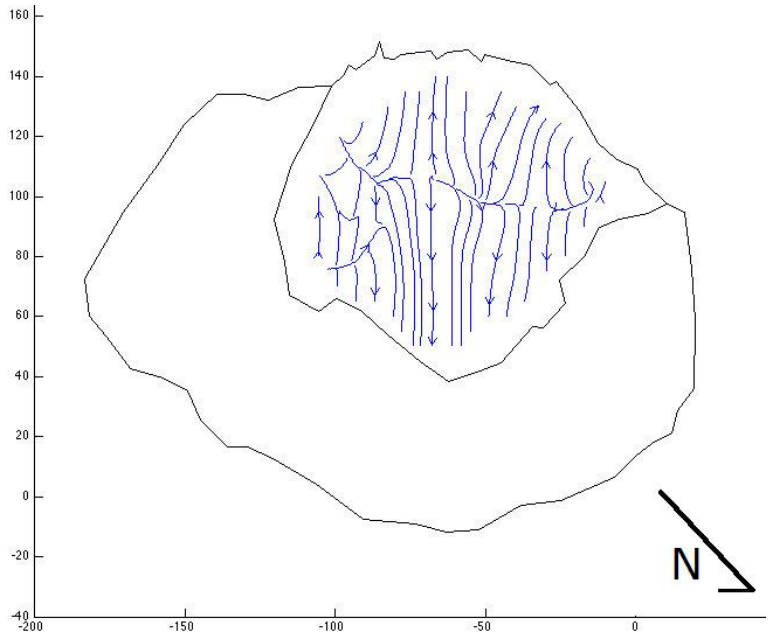


**Figure 4.14b: Streamlines from the beginning of the field day (13:42:44 UTC) to the end of the field day (15:28:17 UTC), 1 January 2009. Time elapsed was 1 h, 45 m. Camera: SGH1.**

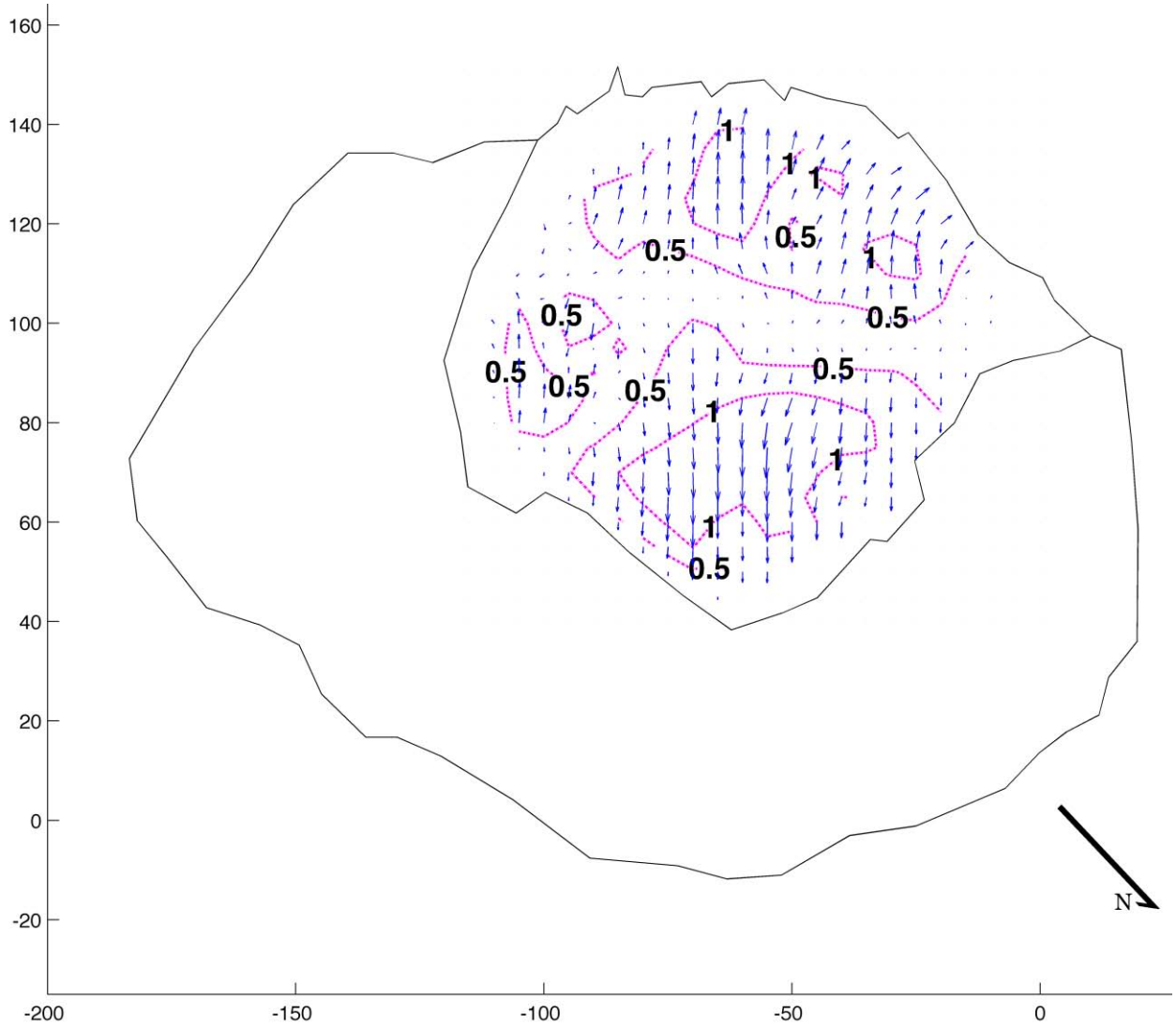


**Figure 4.14c: Interpolated block displacements from the beginning of the field day (13:42:44 UTC) to the end of the field day (15:28:17 UTC), 1 January 2009. Time elapsed was 1 h, 45 m. Camera: SGH1.**

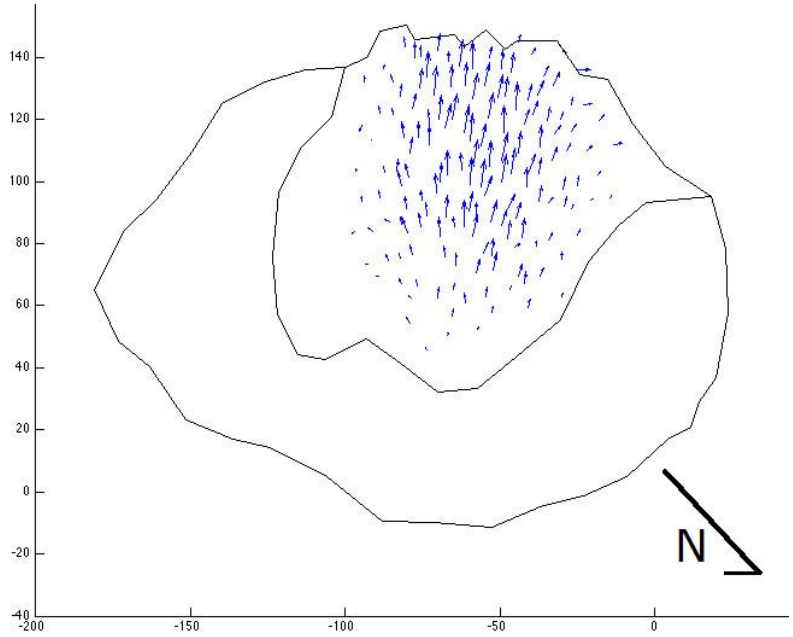


**Figure 4.15a: Block displacements from the beginning of the field day (12:21:45 UTC) to the end of the field day (15:46:40 UTC), 2 January 2009. The farthest a block travelled was 3.05 meters. Time elapsed was 3 h, 25 m. Camera: SGH1.**

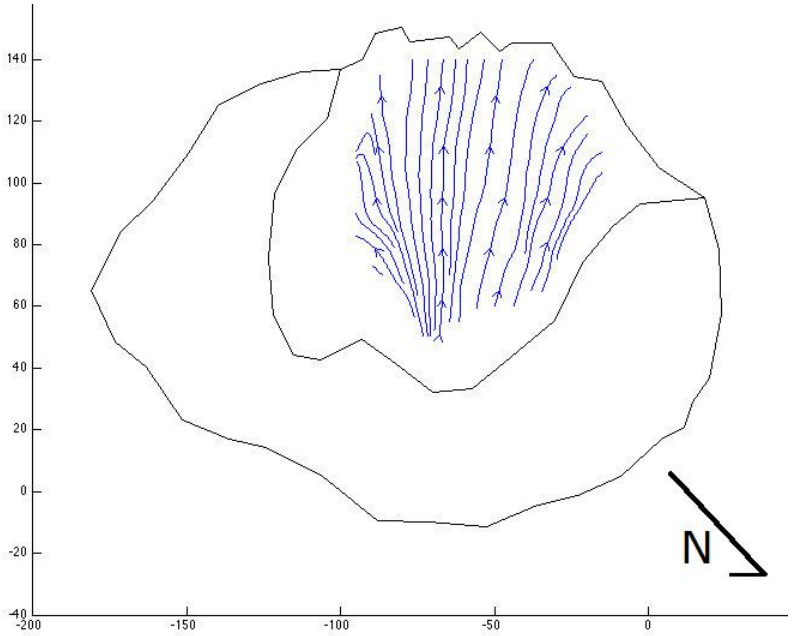


**Figure 4.15b: Streamlines from the beginning of the field day (12:21:45 UTC) to the end of the field day (15:46:40 UTC), 2 January 2009. Time elapsed was 3 h, 25 m. Camera: SGH1.**

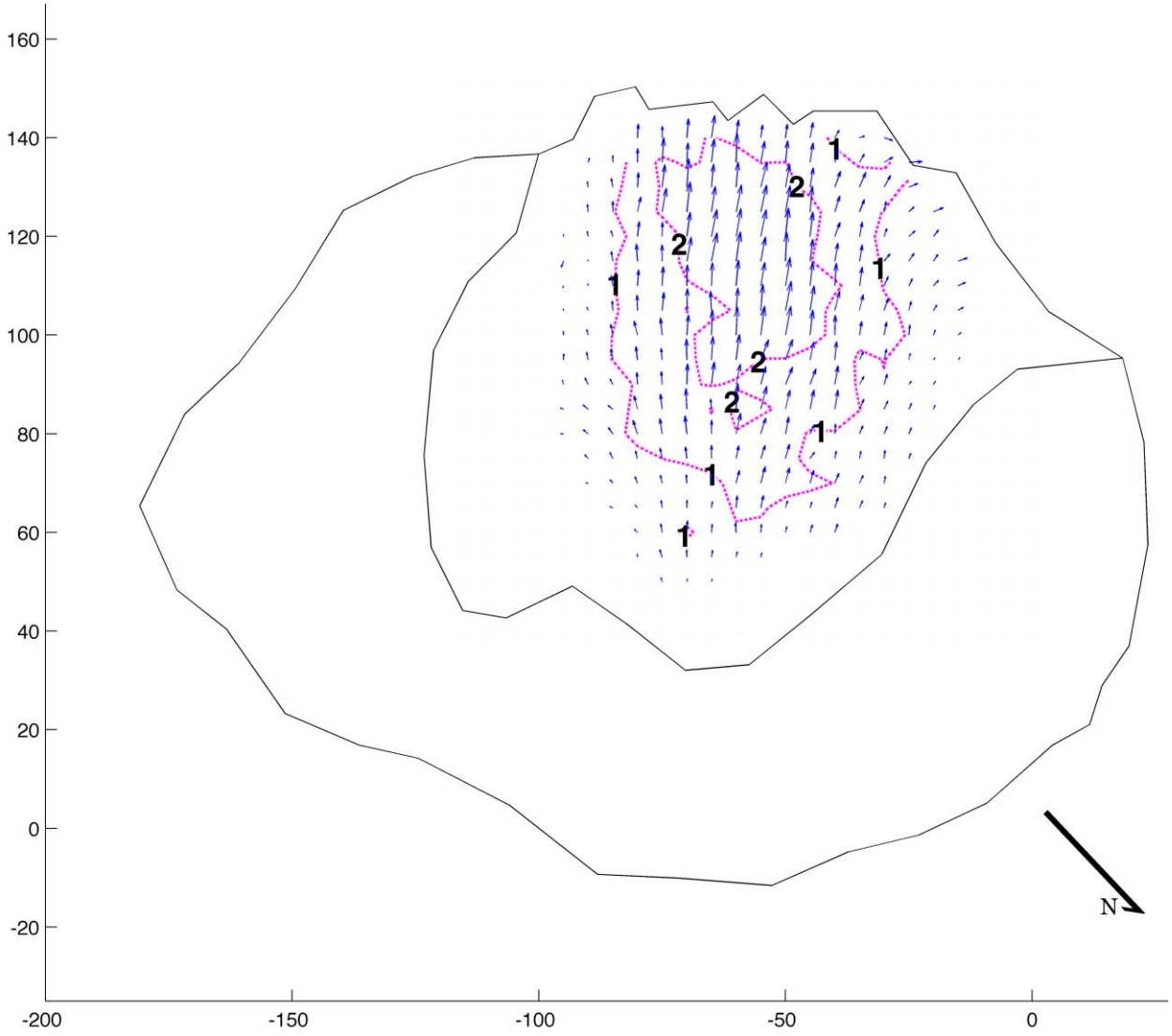


**Figure 4.15c: Interpolated block displacements from the beginning of the field day (12:21:45 UTC) to the end of the field day (15:46:40 UTC), 2 January 2009. Time elapsed was 3 h, 25 m. Camera: SGH1.**

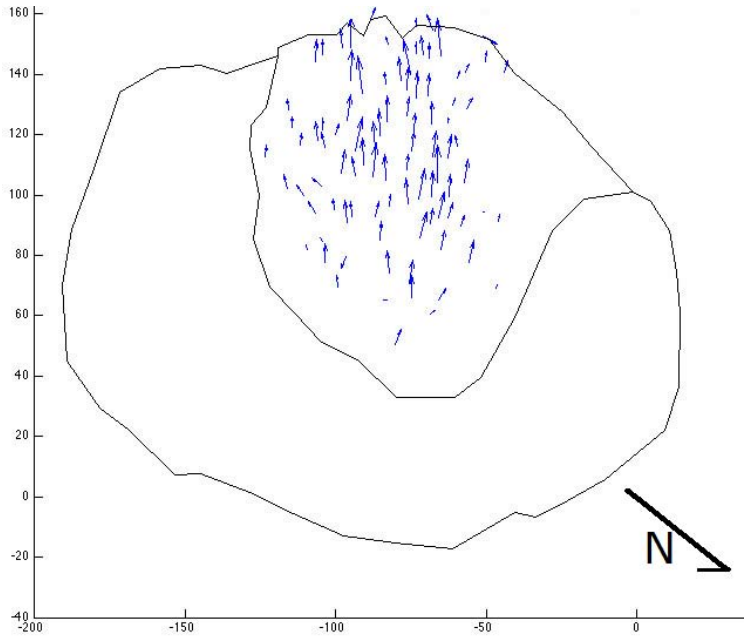


**Figure 4.16a: Block displacements from the beginning of the field day (13:23:41 UTC) to the end of the field day (16:01:42 UTC), 3 January 2009. The farthest a block travelled was 2.11 meters. Time elapsed was 25 m, 18 s. Camera: SGH2.**

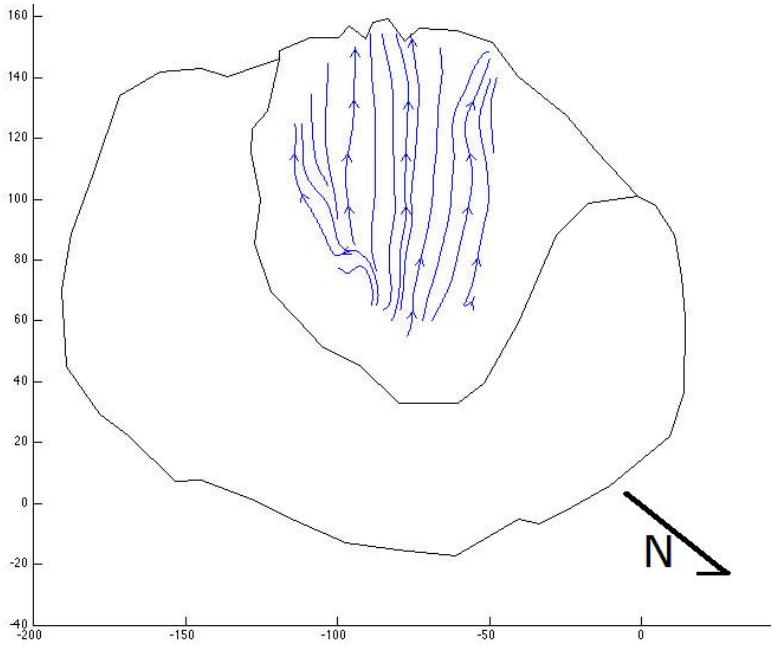


**Figure 4.16b: Streamlines from the beginning of the field day (13:23:41 UTC) to the end of the field day (16:01:42 UTC), 3 January 2009. Time elapsed was 25 m, 18 s. Camera: SGH2.**

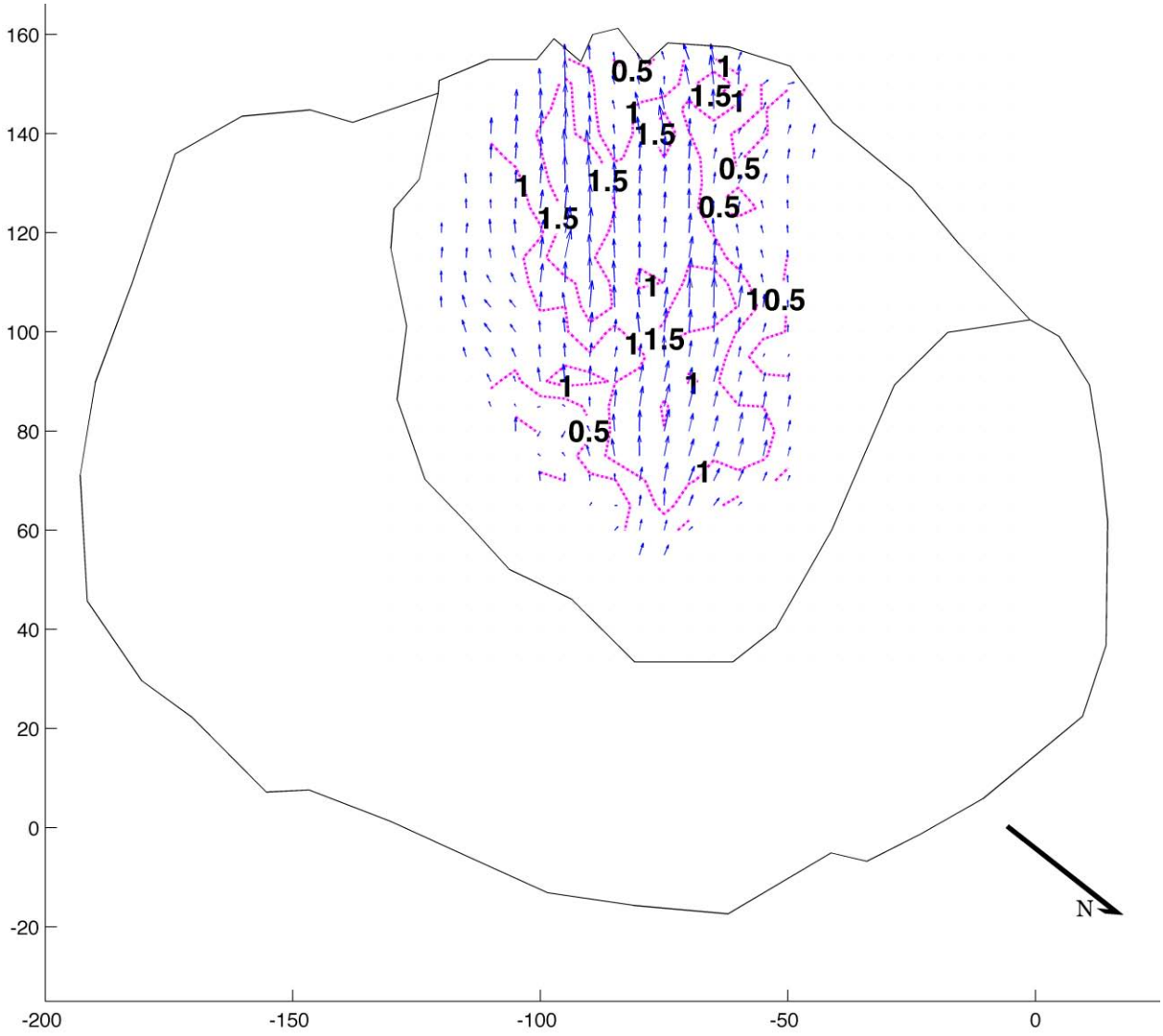


**Figure 4.16c: Interpolated block displacements from the beginning of the field day (13:23:41 UTC) to the end of the field day (16:01:42 UTC), 3 January 2009. Time elapsed was 25 m, 18 s. Camera: SGH2.**

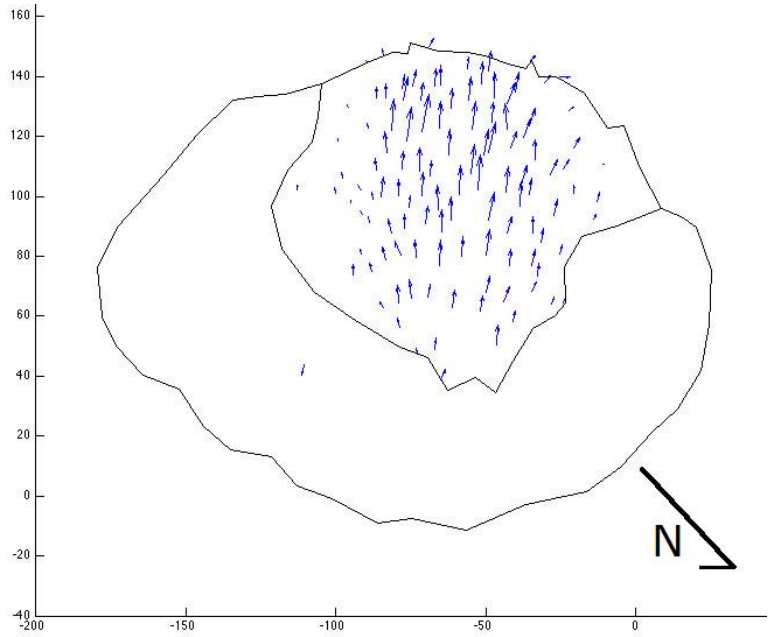


**Figure 4.17a: Block displacements from the beginning of the field day (12:38:14 UTC) to the end of the field day (16:21:41 UTC), 4 January 2009. The farthest a block travelled was 4.24 meters. Time elapsed was 3 h, 39 m. Camera: SGH1.**

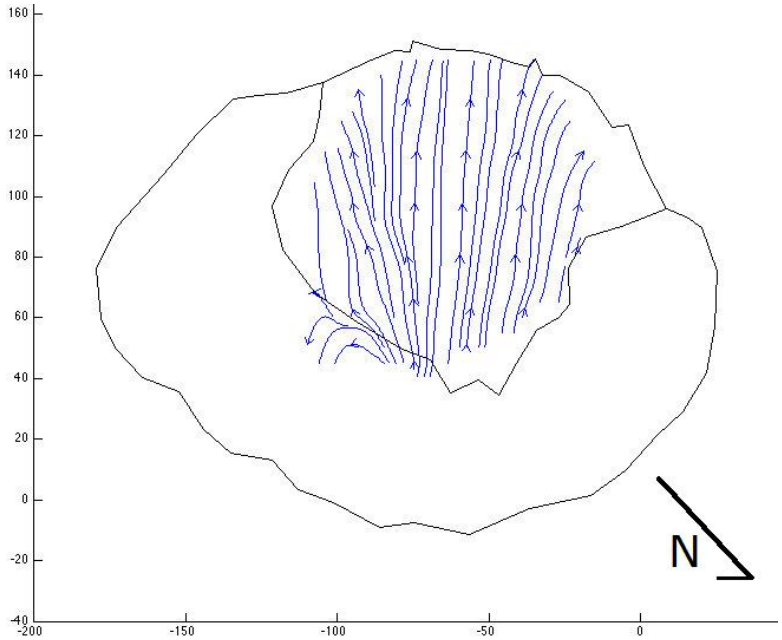


**Figure 4.17b: Streamlines from the beginning of the field day (12:38:14 UTC) to the end of the field day (16:21:41 UTC), 4 January 2009. Time elapsed was 3 h, 39 m. Camera: SGH1.**

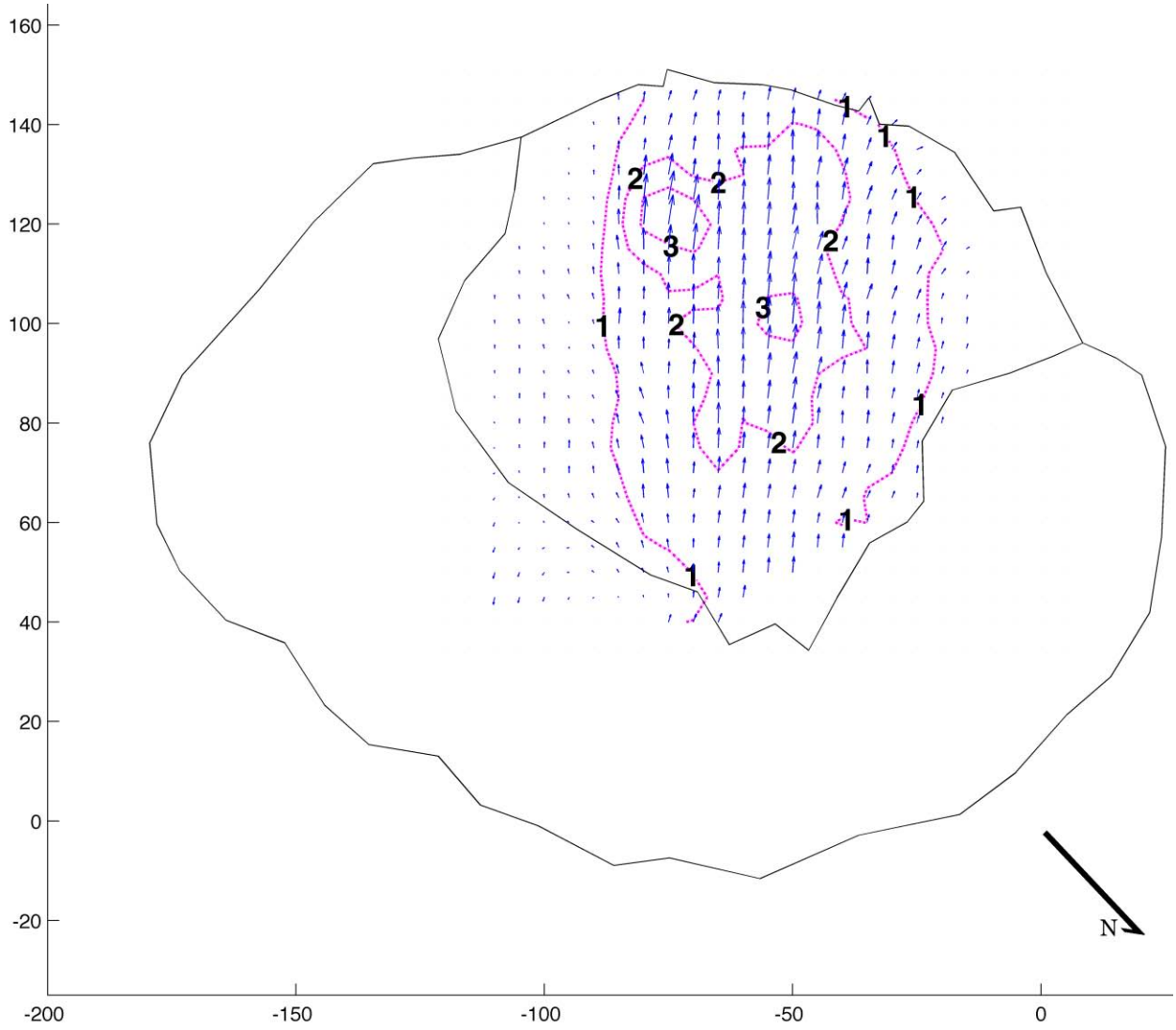


**Figure 4.17c: Interpolated block displacements from the beginning of the field day (12:38:14 UTC) to the end of the field day (16:21:41 UTC), 4 January 2009. Time elapsed was 3 h, 39 m. Camera: SGH1.**

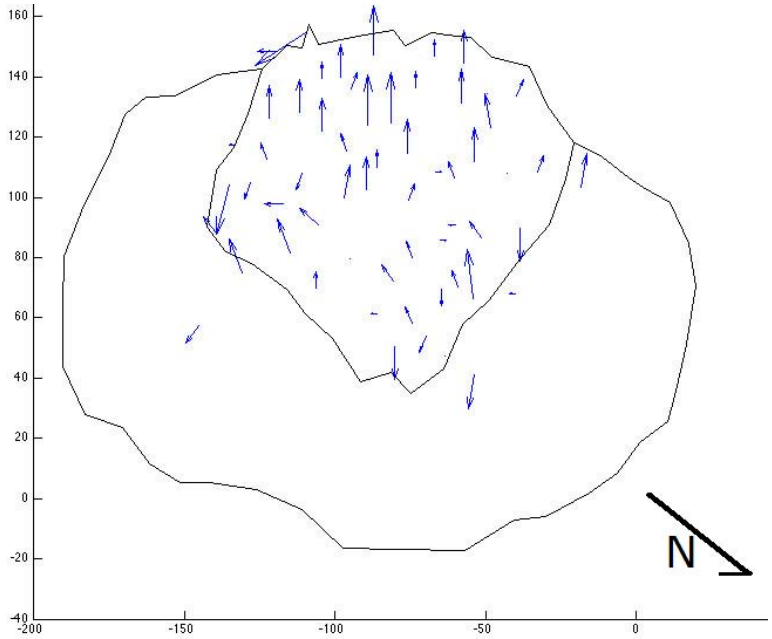


**Figure 4.18a: Block displacements from the beginning of the third explosion (14:16:30 UTC) to the end of the same explosion (14:21:19 UTC), 2 January 2009. The farthest a block travelled was 0.77 meters. Time elapsed was 4 m, 34 s. Camera: SGH2.**

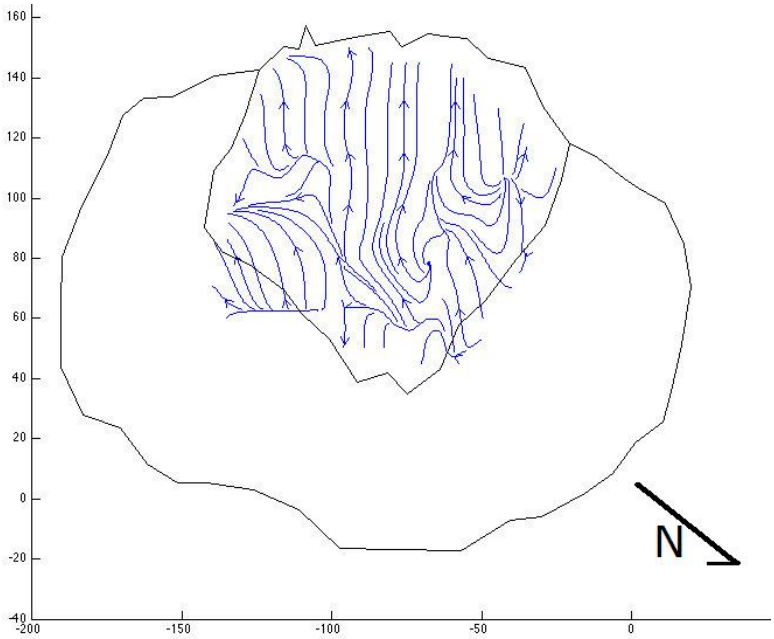


**Figure 4.18b: Streamlines from the beginning of the third explosion (14:16:30 UTC) to the end of the same explosion (14:21:19 UTC), 2 January 2009. Time elapsed was 4 m, 34 s. Camera: SGH2.**

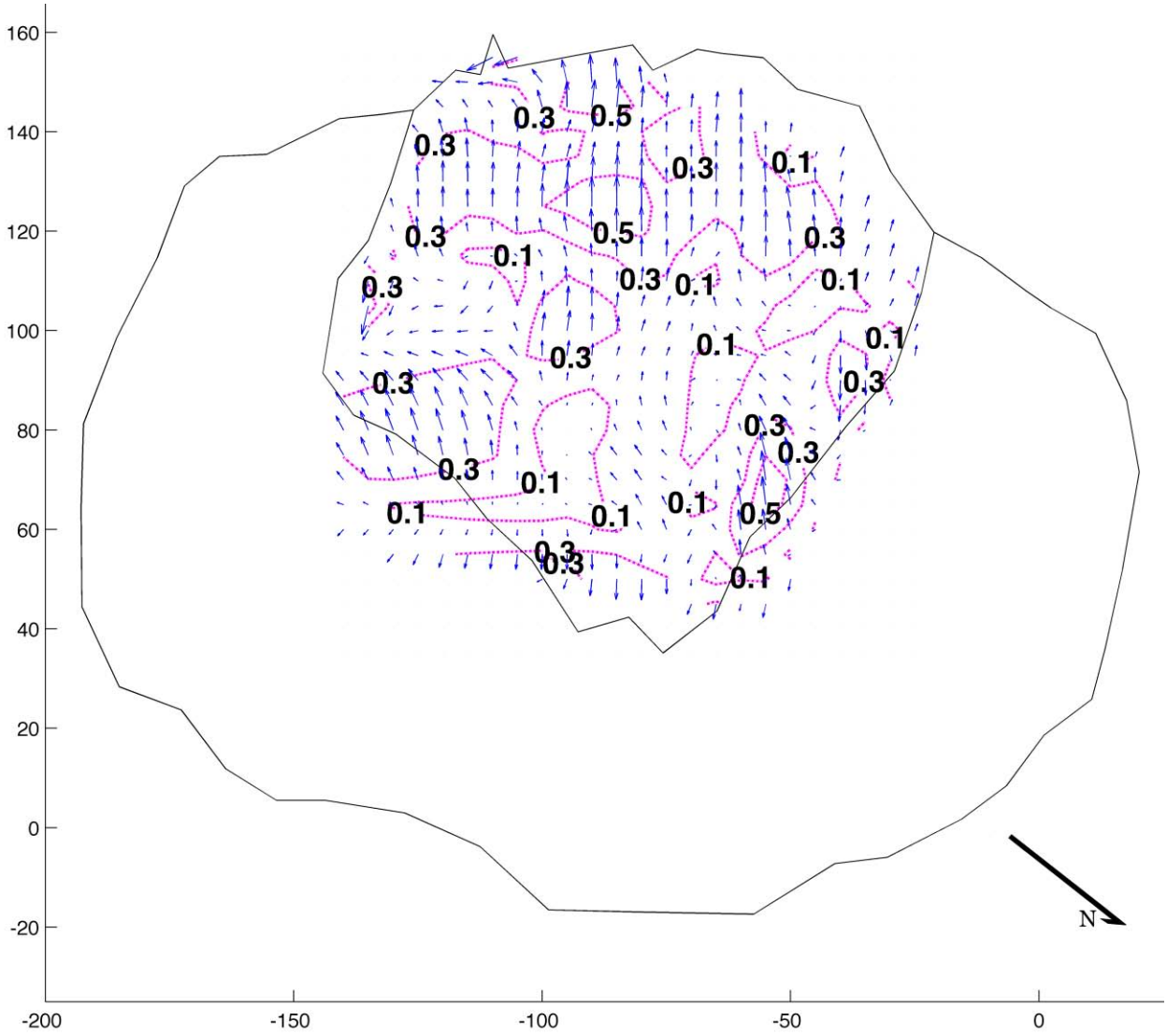


**Figure 4.18c: Interpolated block displacements from the beginning of the third explosion (14:16:30 UTC) to the end of the same explosion (14:21:19 UTC), 2 January 2009. Time elapsed was 4 m, 34 s. Camera: SGH2.**

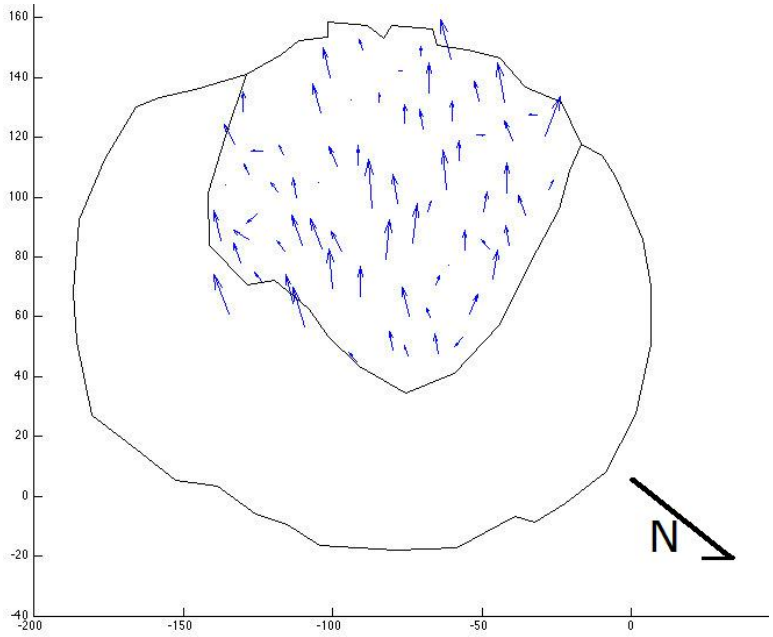


**Figure 4.19a: Block displacements from the beginning of the first explosion (14:10:16 UTC) to the end of the same explosion (14:15:43 UTC), 4 January 2009. The farthest a block travelled was 1.05 meters. Time elapsed was 5 m, 27 s. Camera: SGH2.**

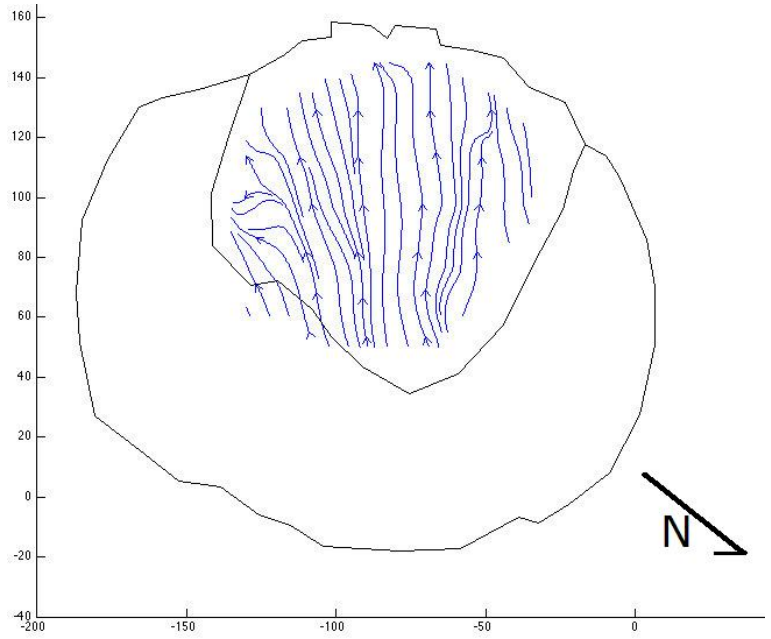


**Figure 4.19b: Streamlines from the beginning of the first explosion (14:10:16 UTC) to the end of the same explosion (14:15:43 UTC), 4 January 2009. Time elapsed was 5 m, 27 s. Camera: SGH2.**

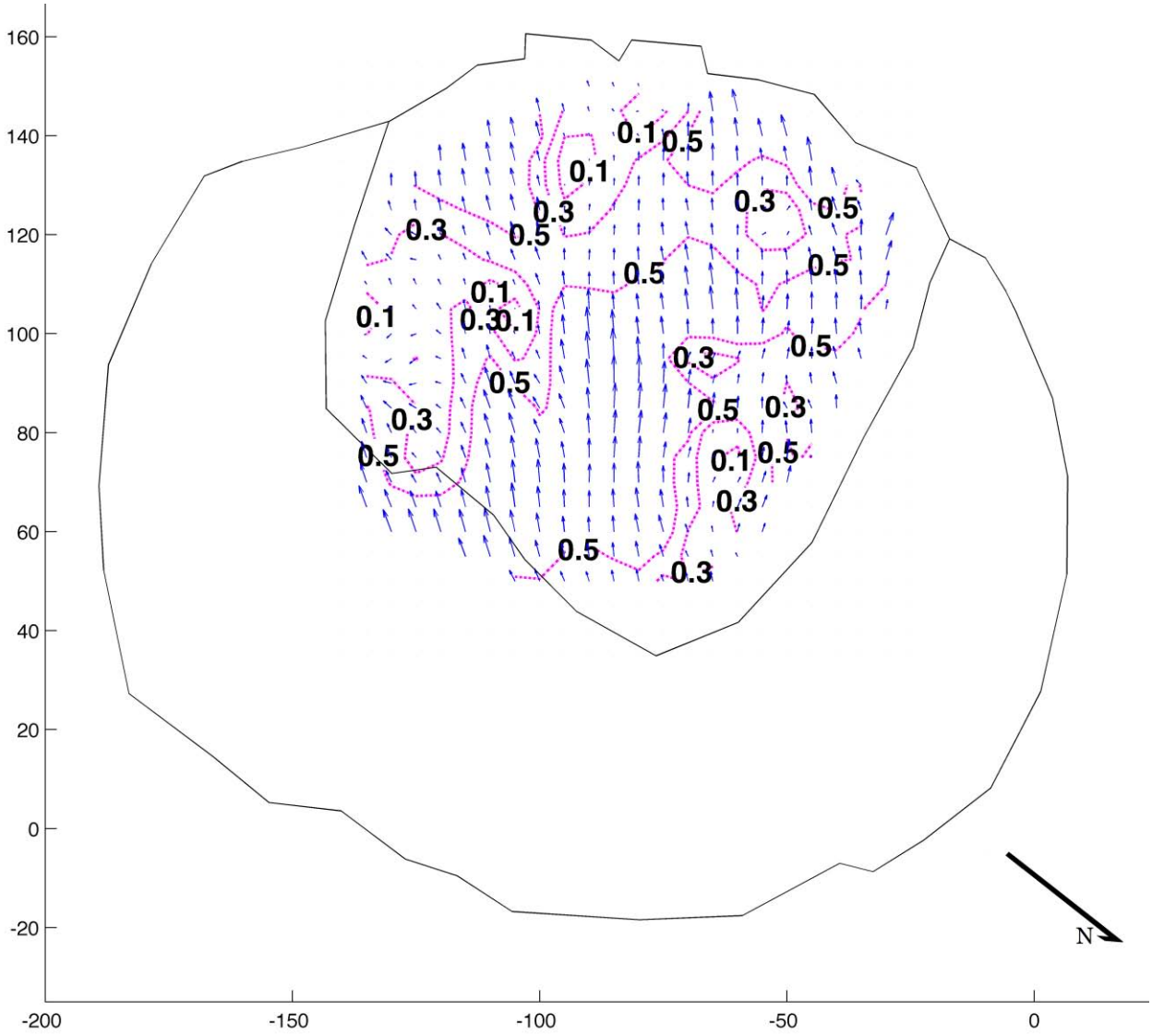


**Figure 4.19c: Interpolated block displacements from the beginning of the first explosion (14:10:16 UTC) to the end of the same explosion (14:15:43 UTC), 4 January 2009. Time elapsed was 5 m, 27 s. Camera: SGH2.**

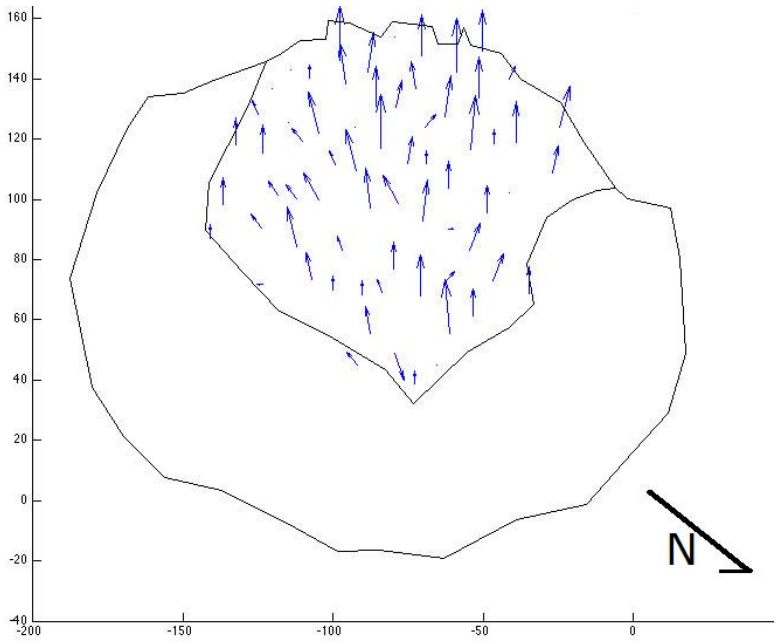


**Figure 4.20a: Block displacements from the beginning of the second explosion (15:07:05 UTC) to the end of the same explosion (15:13:43 UTC), 4 January 2009. The farthest a block travelled was 0.84 meters. Time elapsed was 6 m, 38 s. Camera: SGH2.**

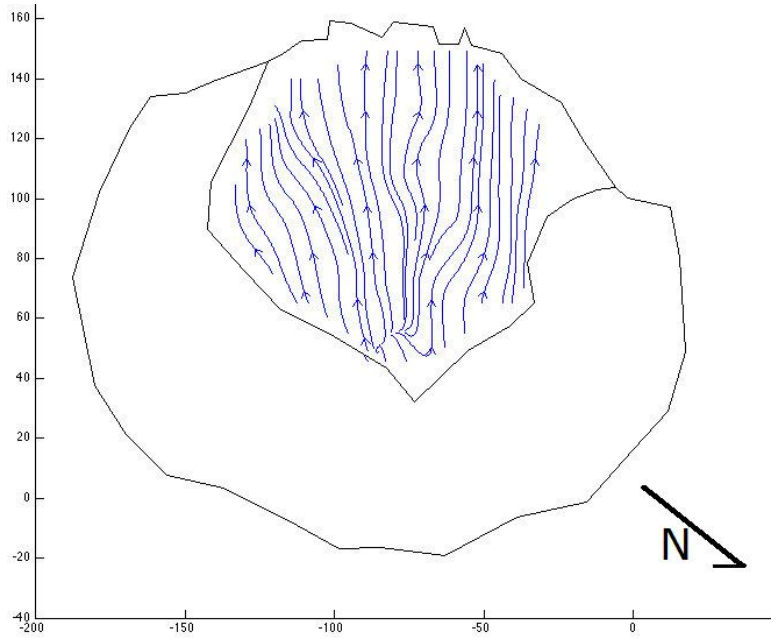


**Figure 4.20b: Streamlines from the beginning of the second explosion (15:07:05 UTC) to the end of the same explosion (15:13:43 UTC), 4 January 2009. Time elapsed was 6 m, 38 s. Camera: SGH2.**

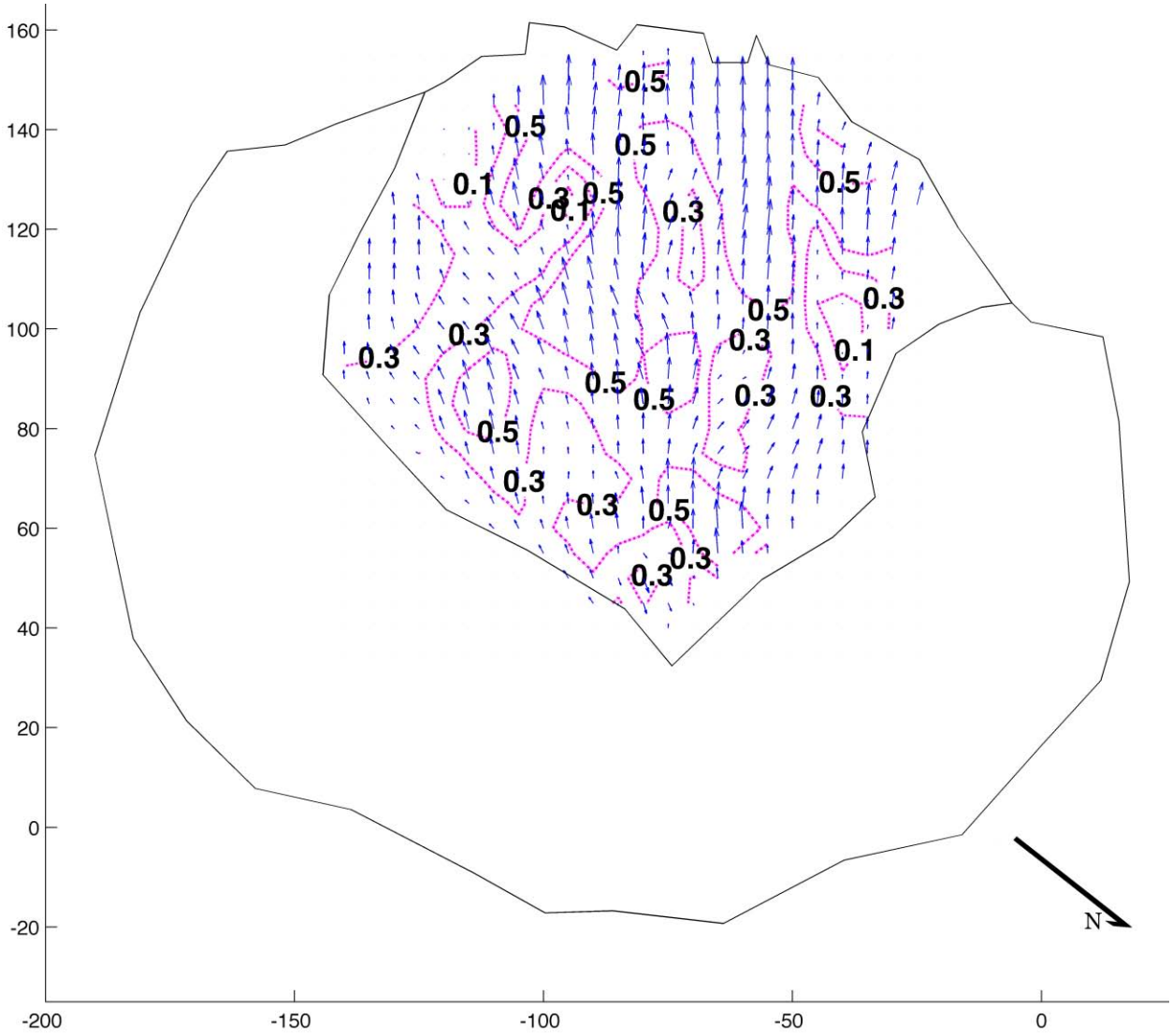


**Figure 4.20c: Interpolated block displacements from the beginning of the second explosion (15:07:05 UTC) to the end of the same explosion (15:13:43 UTC), 4 January 2009. Time elapsed was 6 m, 38 s. Camera: SGH2.**

## 4.3 1 JANUARY 2009: Between explosions and during repose

Extrusion was dramatically different on 1 January 2009 (Figures 4.21a-c; Figures 4.22a-c; Figures 4.23a-c; Figures 4.24a-c) compared with the three subsequent field days. Lava blocks flowed both west and east from a ~50 m vent, though lava only flowed over the crater rim to the southwest. The vent is oriented northwest/southeast perpendicular to the flow directions, near to the middle of the dome surface but closer to the northeast side of the dome. Four additional intervals during 1 January 2009 were investigated to evaluate the differences between times of repose and explosions: A four minute 30 second interval lasting from the beginning of the first explosion to the end of the same explosion (Figures 4.21a-c), a 50 minute 36 second interval lasting from the end of the first explosion to right before the onset of the second explosion (Figures 4.22a-c), a 25 minute interval lasting from the beginning of the second explosion to the end of the same explosion (Figures 4.23a-c), and a 21 hour, 11 minute interval lasting from the end of the second explosion to the beginning of the following day on 2 January (Figures 4.24a-c).

The first explosion displayed a medium-sized plume ring and was accompanied by loud jetting noises. The second explosion was much larger and longer in duration, and a pyroclastic flow was generated. From the beginning of the day until just before the first explosion, lava flowed both east and west. The same flow pattern is seen from just after the first explosion until just before the second explosion (Figures 4.22a-c). After the second explosion, however, lava flowed only west over the crater rim (Figures 4.24a-c).

The interval starting at the beginning of the day to the beginning of the first explosion and the interval starting at the end of the second explosion to the end of 1 January 2009 were not analyzed here because movement, though likely present, was smaller than the spatial resolution of the images.

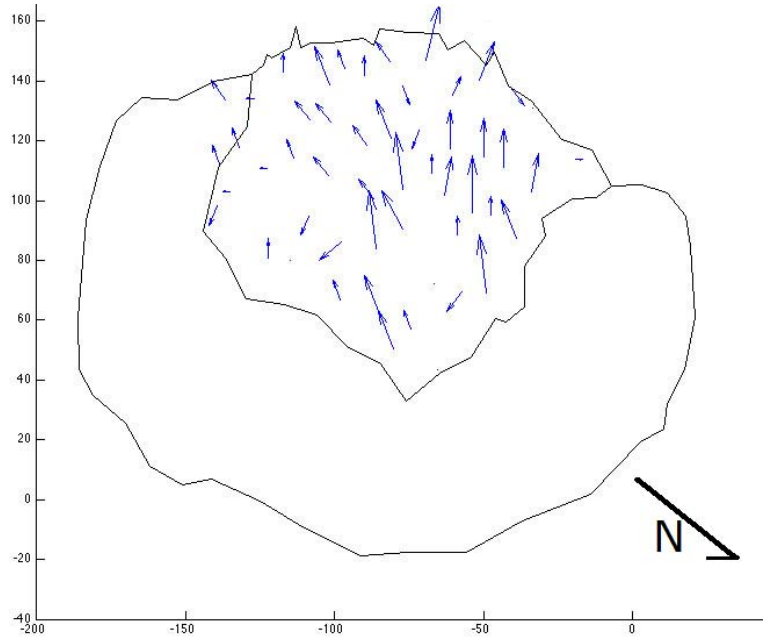


**Figure 4.21a: Block displacements from the beginning of the first explosion (14:03:38 UTC) to the end of the same explosion (14:08:11 UTC), 1 January 2009. The farthest a block travelled was 0.65 meters. Time elapsed was 4 m, 33 s. Camera: SGH2.**

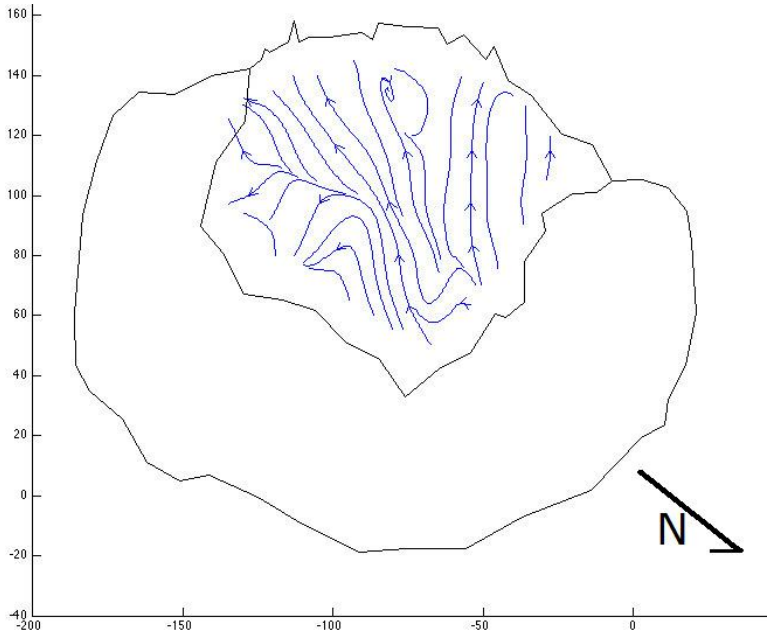


**Figure 4.21b: Streamlines from the beginning of the first explosion (14:03:38 UTC) to the end of the same explosion (14:08:11 UTC), 1 January 2009. Time elapsed was 4 m, 33 s. Camera: SGH2.**

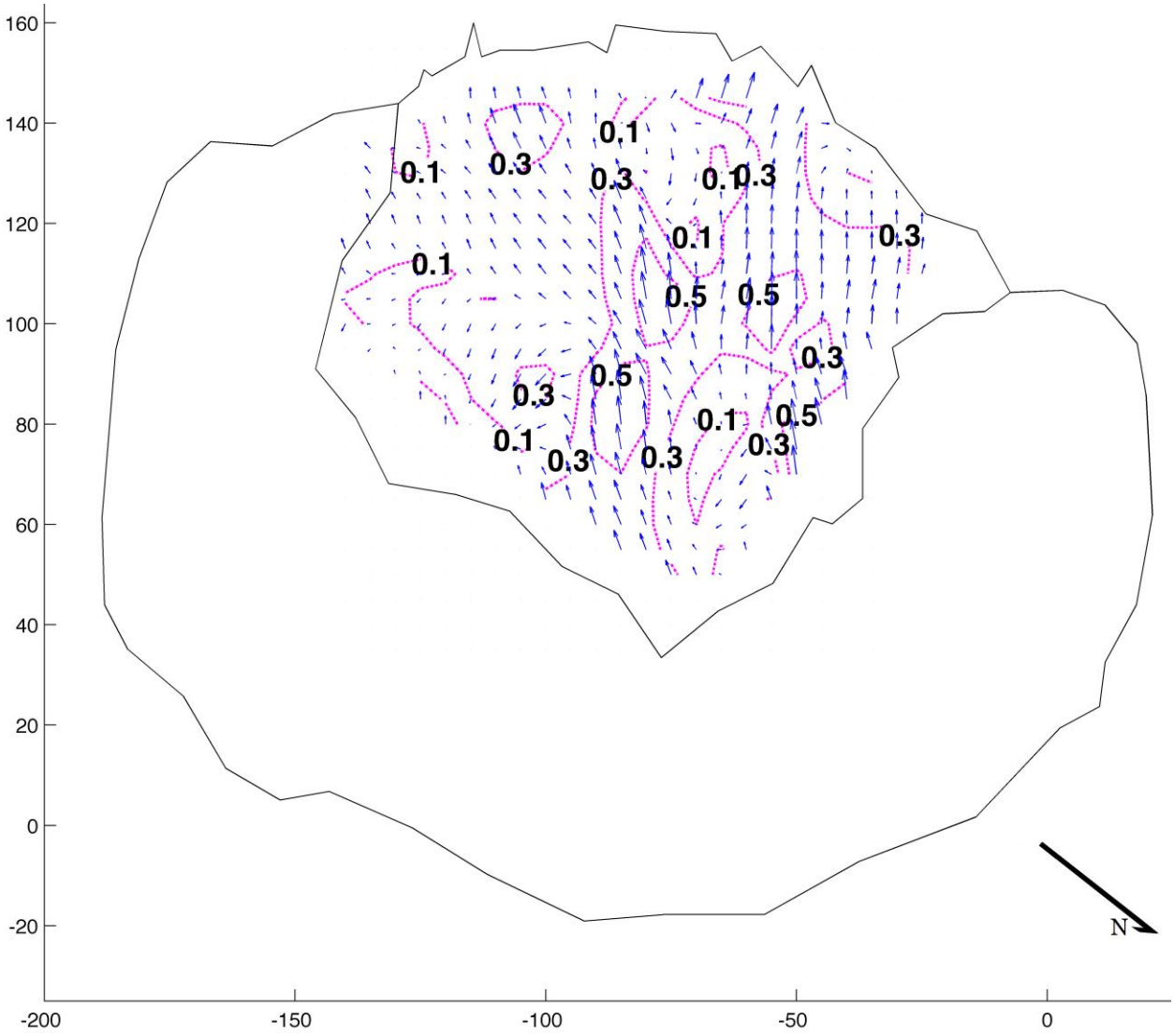


**Figure 4.21c: Interpolated block displacements from the beginning of the first explosion (14:03:38 UTC) to the end of the same explosion (14:08:11 UTC), 1 January 2009. Time elapsed was 4 m, 33 s. Camera: SGH2.**

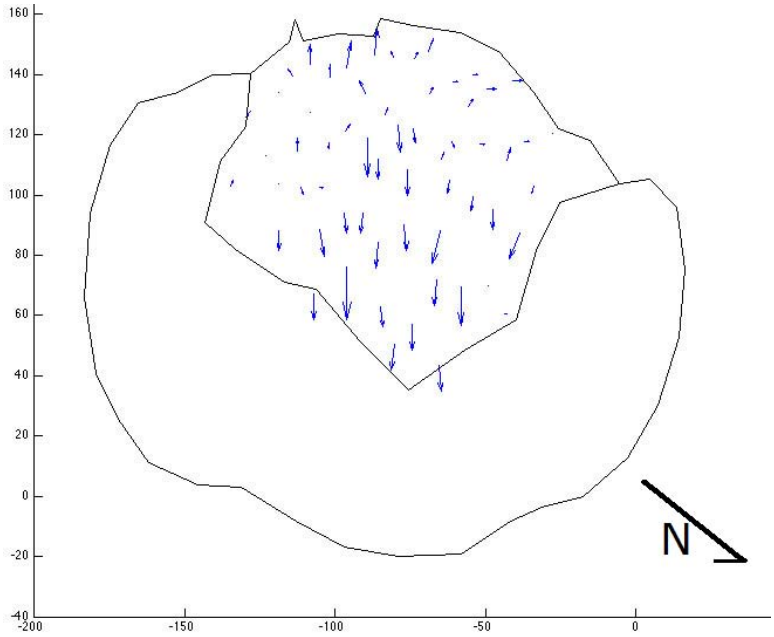


**Figure 4.22a: Block displacements from the end of the first explosion (14:08:11 UTC) to the beginning of the second explosion (14:58:47 UTC), 1 January 2009. The farthest a block travelled was 1.68 meters. Time elapsed was 50 m, 36 s. Camera: SGH2.**

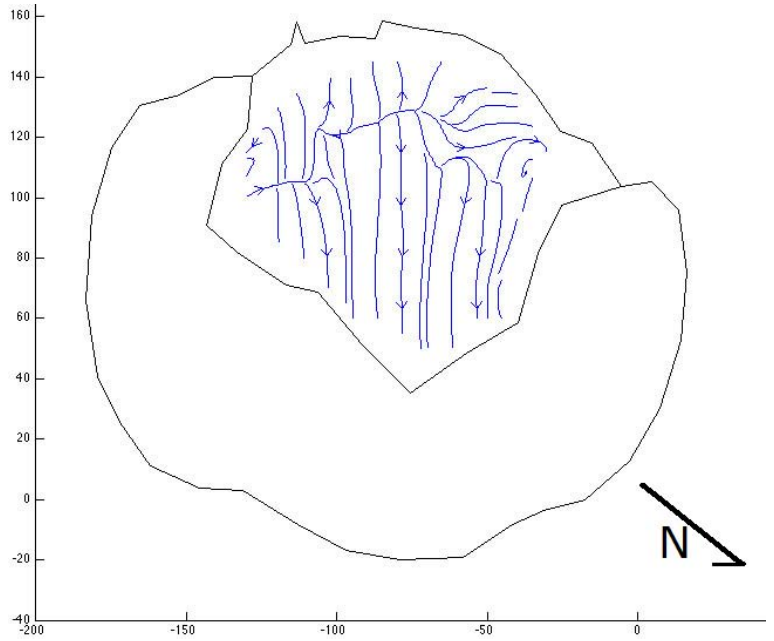


**Figure 4.22b: Streamlines from the end of the first explosion (14:08:11 UTC) to the beginning of the second explosion (14:58:47 UTC), 1 January 2009. Time elapsed was 50 m, 36 s. Camera: SGH2.**

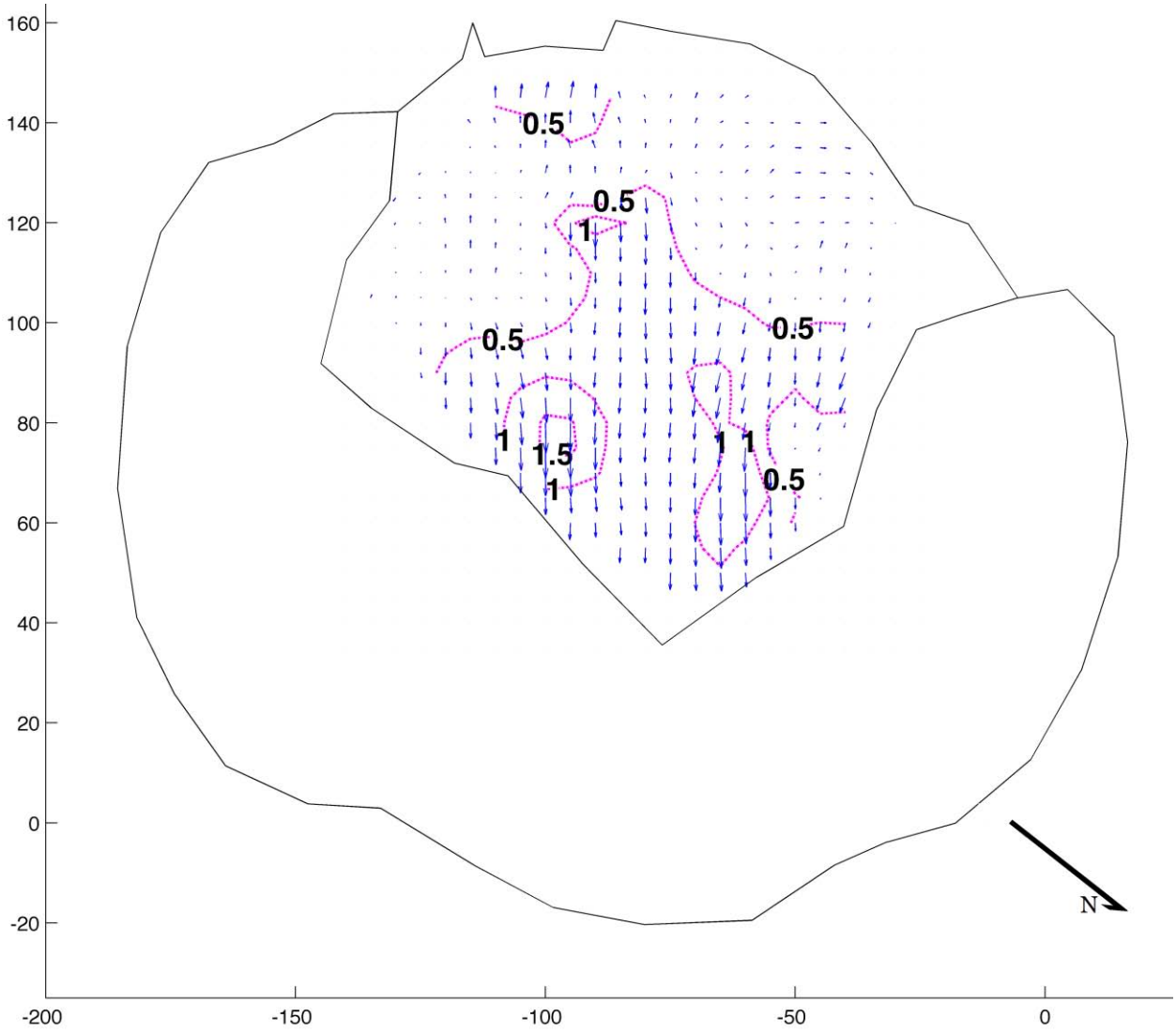


**Figure 4.22c: Interpolated block displacements from the end of the first explosion (14:08:11 UTC) to the beginning of the second explosion (14:58:47 UTC), 1 January 2009. Time elapsed was 50 m, 36 s. Camera: SGH2.**

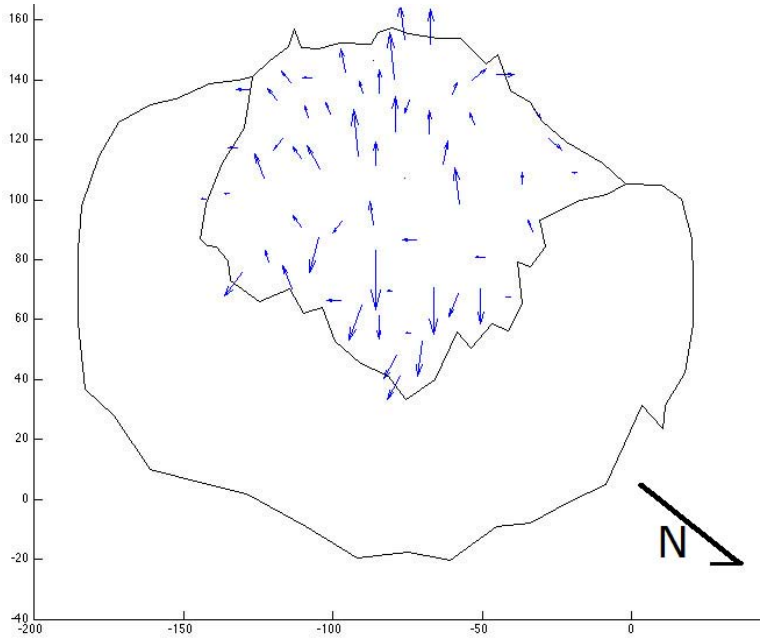


**Figure 4.23a: Block displacements from the beginning of the second explosion (14:58:47 UTC) to the end of the same explosion (15:23:44 UTC), 1 January 2009. The farthest a block travelled was 1.05 meters. Time elapsed was 24 m, 57 s. Camera: SGH2.**

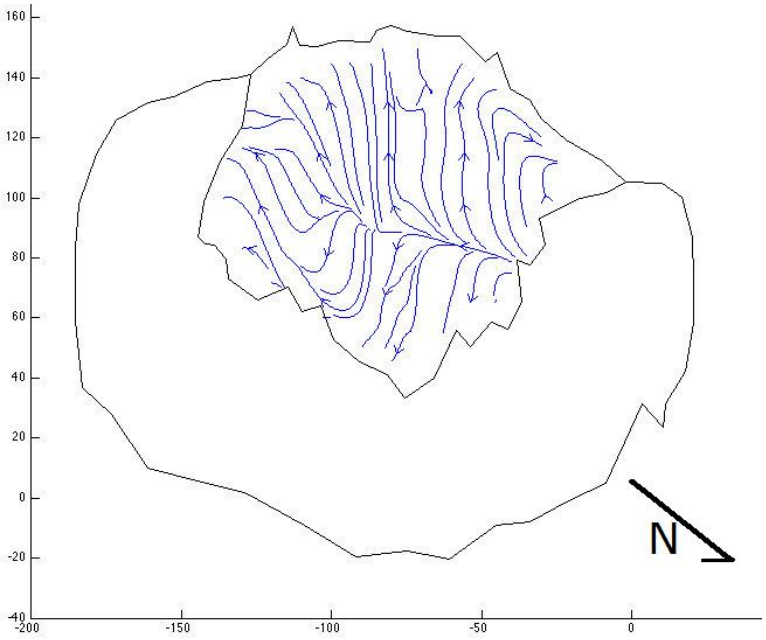


**Figure 4.23b: Streamlines from the beginning of the second explosion (14:58:47 UTC) to the end of the same explosion (15:23:44 UTC), 1 January 2009. Time elapsed was 24 m, 57 s. Camera: SGH2.**

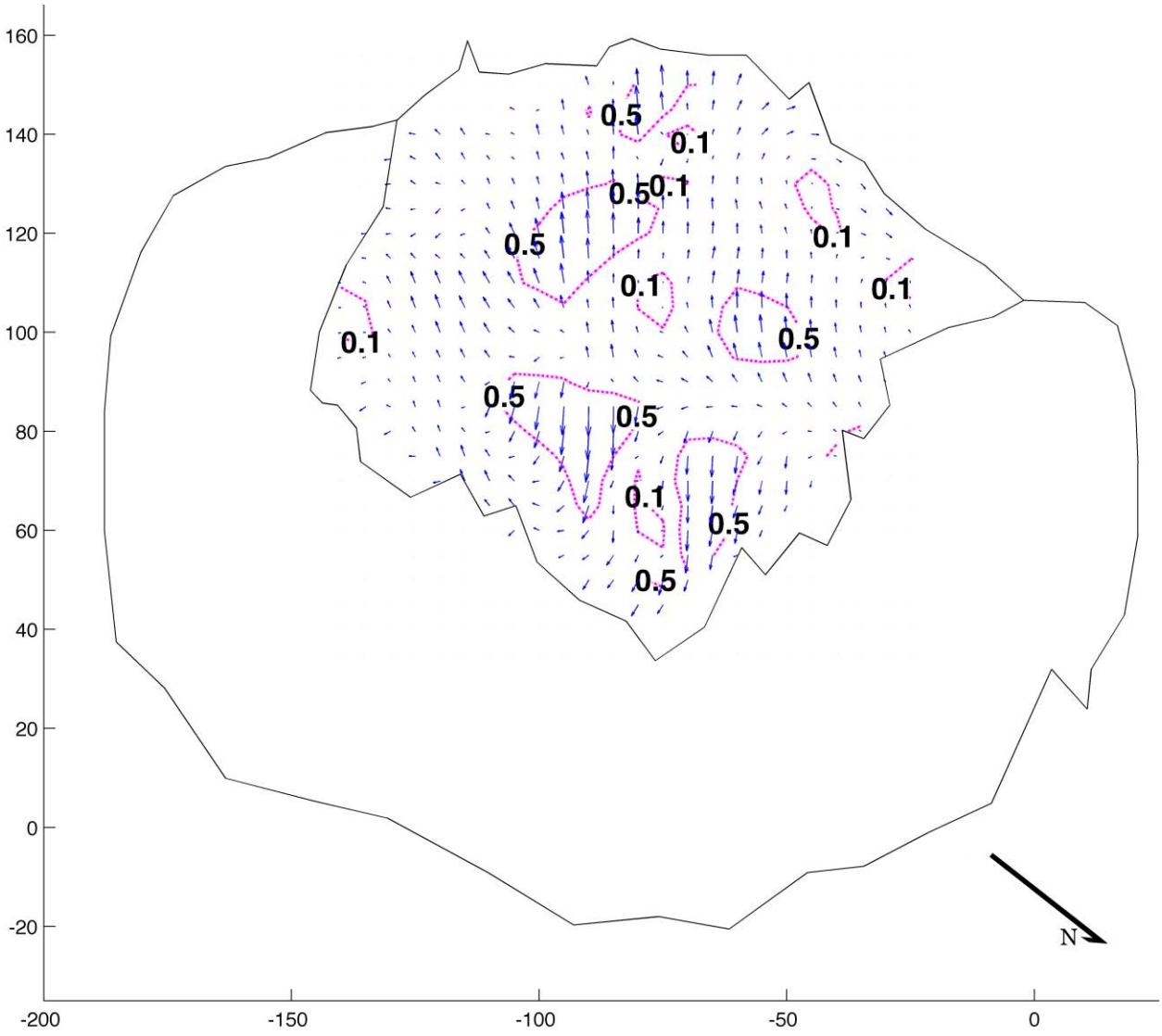


**Figure 4.23c: Interpolated block displacements from the beginning of the second explosion (14:58:47 UTC) to the end of the same explosion (15:23:44 UTC), 1 January 2009. Time elapsed was 24 m, 57 s. Camera: SGH2.**

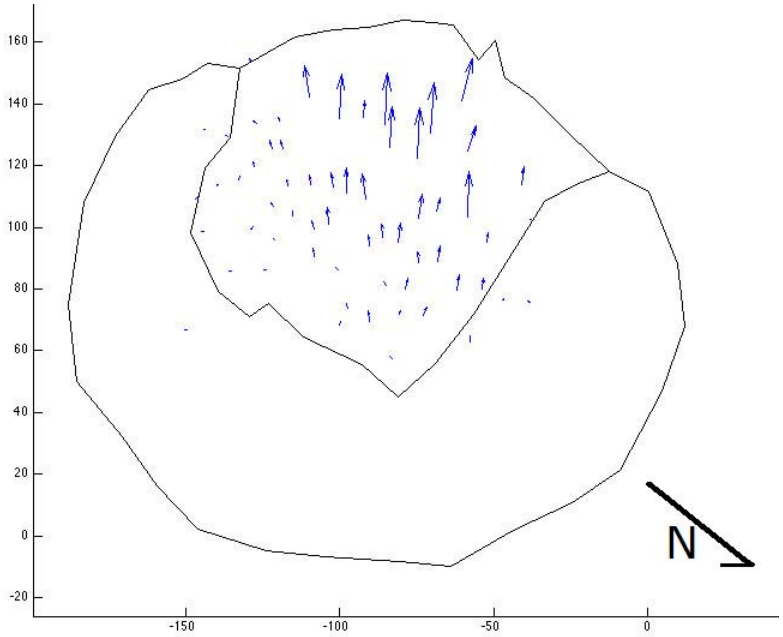


**Figure 4.24a: Block displacements from the end of the second explosion on 1 January 2009 (15:23:44 UTC) to the beginning of the next day, 2 January 2009 (12:35:11 UTC). The farthest a block travelled was 13.88 meters. Time elapsed was 21 h, 11 m, 26 s. Camera: SGH2.**

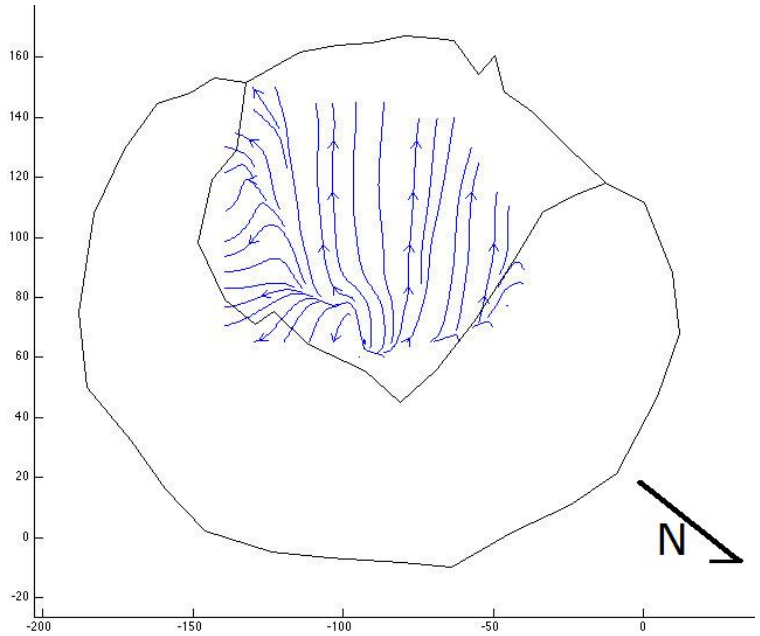


**Figure 4.24b: Streamlines from the end of the second explosion on 1 January 2009 (15:23:44 UTC) to the beginning of the next day, 2 January 2009 (12:35:11 UTC). Time elapsed was 21 h, 11 m, 26 s. Camera: SGH2.**

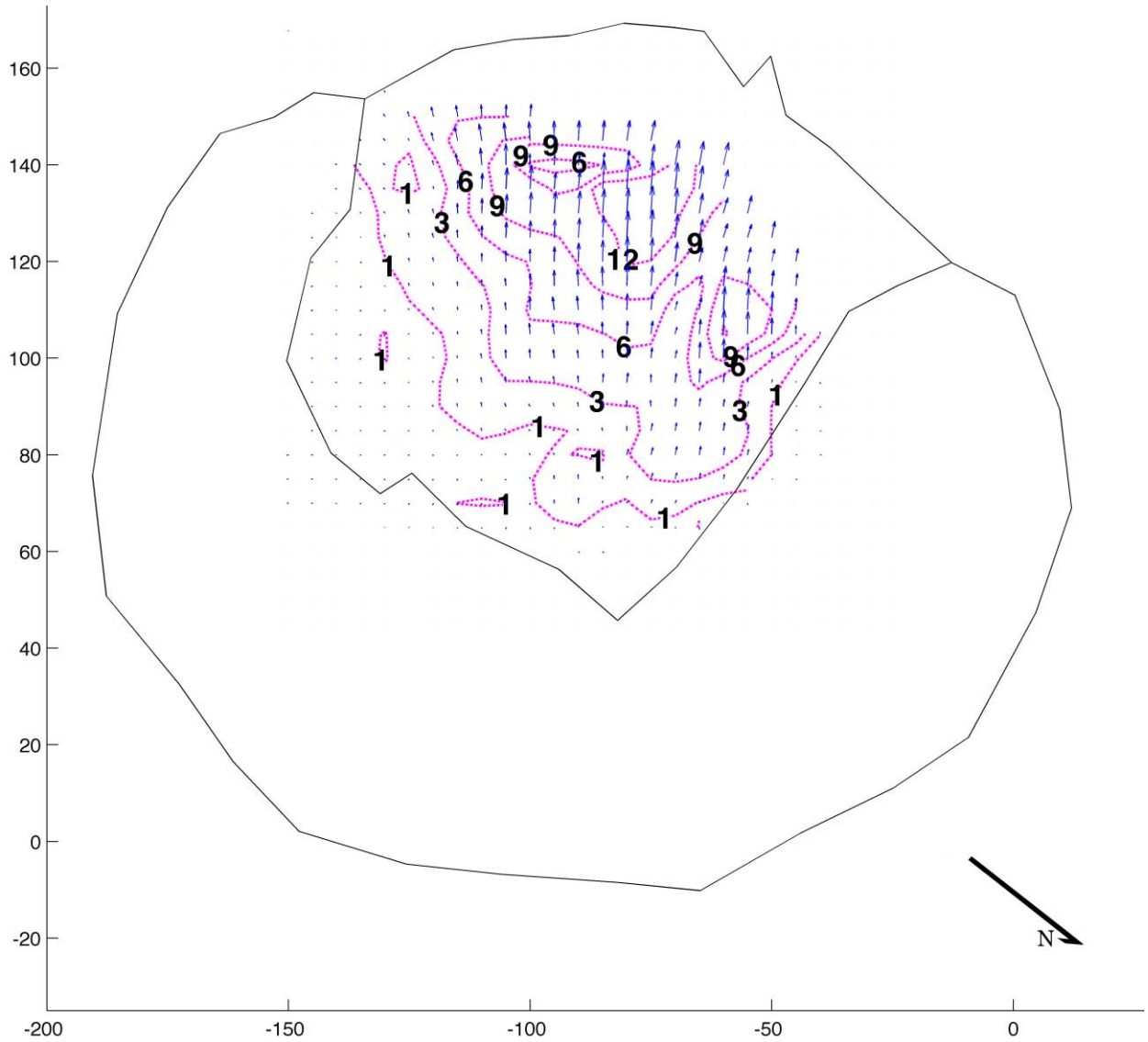


**Figure 4.24c: Interpolated block displacements from the end of the second explosion on 1 January 2009 (15:23:44 UTC) to the beginning of the next day, 2 January 2009 (12:35:11 UTC). Time elapsed was 21 h, 11 m, 26 s. Camera: SGH2.**

# 5. DISCUSSION

## 5.1 General flow-field properties from 2007 and 2009

Between 2007 and 2009, the surface of Caliente dome changed with respect to lava flow direction, flow velocity, and vent geometry. Lava in 2007 and 2009 flowed towards the southwest, though the lava in 2007 flowed to both the southwest and the south (Figure 5.1). The flow field velocity was slightly higher in 2007 than in 2009. In 2007, the flow velocity averaged from 9-10 January was 5.92 meters per day, from 10-11 January was 7.12 meters per day, and from 11-12 January was 8.08 meters per day. In 2009, the flow velocity averaged from 1-2 January was 5.20 meters per day, from 2-3 January was 5.45 meters per day, and from 3-4 January was 5.70 meters per day. The lava flow in 2007 had a distinct region of higher surface flow velocity from the vent to the west-southwest during the 24-hour periods. From 9-10 January 2007, the maximum flow velocity averaged over approximately 24 hours was 12.84 meters per day; from 10-11 January was 15.77 meters per day, and from 11-12 January was 16.98 meters per day. Residence times for blocks on the dome surface range from about nine to 13 (and more) days in 2007, and from about six to 16 days in 2009.

Individual block movements were less uniform in 2007 than those in 2009, which instead seem to move as one large mass (Figures 4.11c, 4.12c, 4.13c). Extrusion in 2007 appeared to originate from a single point location towards the center of the dome surface, closer to the northeast, from which the lava flow 'blossomed' radially and flowed towards the southwest (Figure 5.1). The lava extrusion origin in 2009 was a ~50 meter linear fissure

oriented northwest/southeast located near the center of the dome surface that directed lava perpendicularly southwest over the crater edge.

Flow direction was much different on 1 January 2009 compared with the subsequent field days. Half of the flow moved southwest from a linear division, while the other half moved northeast. During the subsequent field days, the lava flow moved in one direction to the southwest. The flow division could possibly indicate lava buildup at the vent area (noted as a 'stacking' phase by Rose, 1972b). Sometime after this period, the mass of material would eventually fail and continue to flow in the single, preferred direction (southwest) possibly at a higher velocity as the material is flushed from the crater surface. Mean velocity did gradually increase (0.23 meters per hour from 2-3 January, and 0.24 meters per hour from 3-4 January), but there is no statistical variation between these measurements.

A statistically significant daily increase in block velocity was also recorded during January 2007, beginning with 0.25 meters per hour from 9-10 January, increasing to 0.30 meters per hour from 10-11 January, and to 0.34 meters per hour from 11-12 January. No change in flow direction was observed from 9-12 January 2007.

Short-term fluctuations in lava discharge rates are not uncommon and may be related to shallow-region alternating gas pressurization and depressurization, and plug stiffening (Melnik et al., 2009). From 1980 to 1986, Mount St. Helens extruded more than 20 episodes lasting about 2-7 days each (Barmin et al., 2002). Voight et al. (1999) recognized that Soufriere Hills volcano in Montserrat, from at least 1996 to 1998, operated on repetitive, predictable cycles (hours to days each) of earthquakes, ground deformation, degassing, and explosive eruptions. Short-term cycles (hours, days, weeks) are likely related to shallow processes

(degassing, shallow pressurization, stick-slip motion of a plug), while longer-term cycles (years) are associated with deep processes related to the magma chamber.

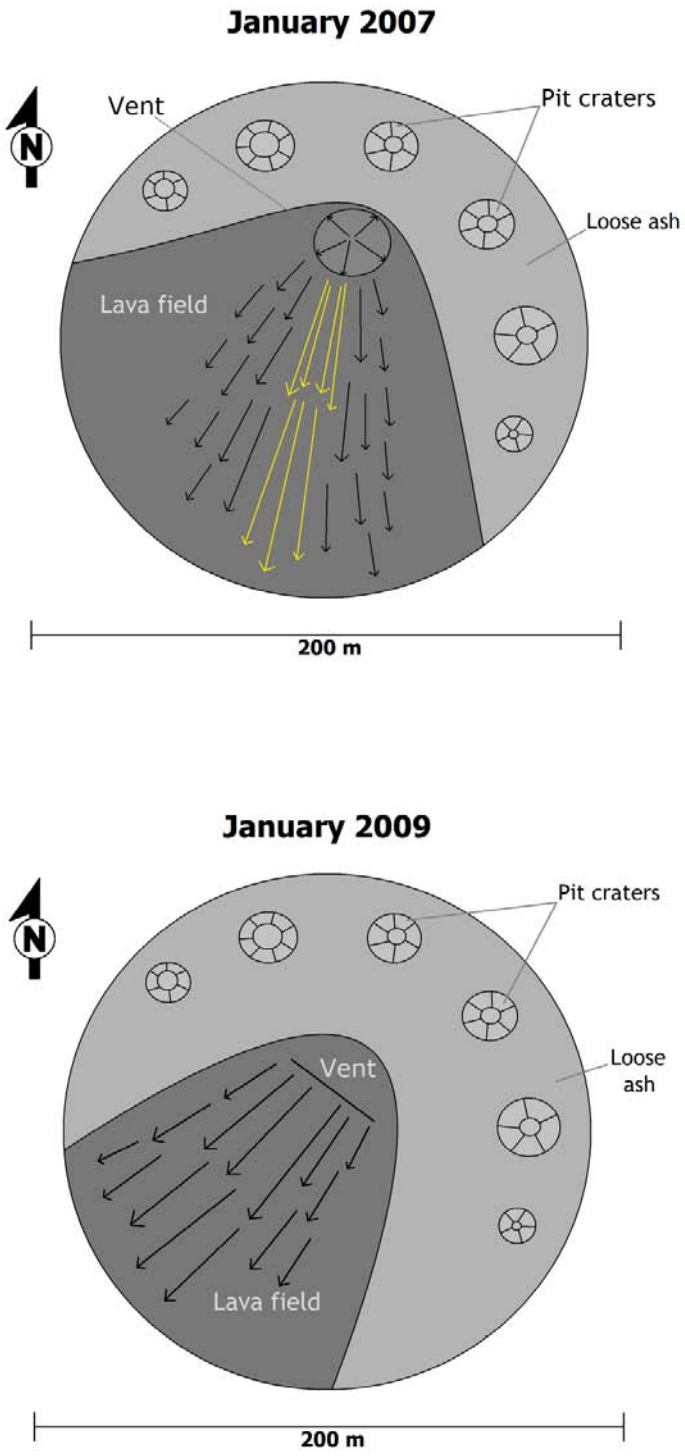


**Figure 5.1: Schematic maps of the Caliente vent surface during January 2007 and January 2009. Arrows indicate trending lava flow direction. Yellow arrows indicate a faster velocity than the black arrows. The radiating gray circle in 2007 indicates the extruding lava's origin, while the line perpendicular to the flow direction in 2009 indicates the lava extrusion origin.**

## 5.2 Short-term flow variations in response to volcanic explosions

Several intra- and inter-explosion periods were analyzed to investigate short-term (minutes to hours) variations of the lava flow field. Intra-explosion periods are defined as the time immediately before an explosion to the time when the same explosion ends. Inter-explosion periods are defined as the time after an explosion ends until the time immediately before the next explosion begins.

Surface flow velocities of intra-explosion intervals were relatively quite high (0.79 to 5.17 meters per hour). The dramatic increase in surface flow velocity seen in the short-term (<1 hour) intervals on 12 January (Figure 4.1) may be explained by the explosion that occurs from 17:27-17:34 UTC during the final interval that lasts from 17:19-17:42 UTC. Since blocks were still intact without much rotation after the explosion, lava extrusion seems to temporarily increase during an explosion.

It is notable that of the two explosions on 1 January 2009, the less vigorous event had the highest mean surface flow velocity (3.69 meters per hour) while the visually much larger event had the lowest mean velocity of all explosions investigated (0.79 meters per hour). Evacuated material in the second explosion was dominantly fractionated lava (ash, small blocks), while the less vigorous first explosion may have been a less gassy, fluid-dominated slug of lava propelled by a deeper source.

One inter-explosion interval was analyzed: Between the two explosions on 1 January 2009. The surface flow velocity averaged during this time was 0.60 meters per hour, a much higher velocity than the 24-hour intervals which range from 0.22-0.24 meters per hour. It is

possible that the increase in surface velocity due to an explosion continues beyond what is visually observed as the end of an explosion.

## 5.3 Extrusion rate calculations

Extrusion rates were extrapolated from surface flow velocities, and were estimations dependent on the lava flow thickness (Tables 5.1, 5.2, 5.3). Thickness of the lava flow on the dome surface was varied between 10 and 40 meters based on estimations from seismic measurements in Johnson et al. (2008). Two time scales were investigated. The first time scale averages the extrusion rate over approximately 24 hours (during which explosions occurred), and the second time scale covers the intra-explosion time (the time immediately before an explosion to the time at the end of the same explosion). Many variables used in estimations in this study are assumed: The thickness of the lava flow and whether it varies across the flow field, the velocity of the flow on the surface and whether it may be applied to the entire flow at depth, how the surface flow velocity changes with distance from the vent, etc. Rates from January 2007 range from 0.21 to 0.28 $m^3 s^{-1}$ daily based on an estimated surface area orthogonal to the flow surface of 2200 $m^2$ derived from an estimated lava thickness of 20 meters. This is a relatively low extrusion rate for Santiaguito, and would be expected because the low extrusion rate periods are much longer than high extrusion rate periods and therefore dominate the volcano's activity. January 2009 rates range from 0.24 to 0.26 $m^3 s^{-1}$ daily based on an estimated surface area orthogonal to the flow surface of 3000 $m^2$ using a lava thickness of 20 meters. It is important to note that extrusion rate calculations based on the dome surface are expected to differ from extrusion rate calculations based on the lava flow velocity beyond the dome's rim.

Extrusion rate calculations derived from the near-vent flow field appear to vary with time and will differ from those derived from distal parts of the lava flow. Short-term extrusion rates may also differ from long-term rates. Using longer-term (days to months) intervals is most advantageous to extrusion rate determinations. Short-term (minutes to hours) intervals display chaotic block movements that would otherwise be averaged out in longer intervals.

**Table 5.1: Extrusion rate estimates during 2007 based on lava flow thickness and mean surface flow velocity (derived from interpolated flow displacement). The periods 9-10, 10-11, and 11-12 January are approximately 24 hours each. Times are UTC.**

| Period | 10m thick ($m^3s^{-1}$) | 20m thick ($m^3s^{-1}$) | 30m thick ($m^3s^{-1}$) | 40m thick ($m^3s^{-1}$) |
|---|---|---|---|---|
| 9-10 January | 0.1 | 0.21 | 0.31 | 0.41 |
| 10-11 January | 0.12 | 0.25 | 0.37 | 0.49 |
| 11-12 January | 0.14 | 0.28 | 0.42 | 0.56 |
| 12 January: 12:53:44-13:59:51 | 0.16 | 0.32 | 0.48 | 0.64 |
| 12 January: 13:59:51-14:41:23 | 0.41 | 0.82 | 1.23 | 1.64 |
| 12 January: 14:41:23-15:08:20 | 0.39 | 0.78 | 1.17 | 1.56 |
| 12 January: 16:47:18-17:19:12 | 0.35 | 0.71 | 1.06 | 1.41 |
| 12 January: 17:19:12-17:42:55 | 0.9 | 1.79 | 2.69 | 3.58 |

**Table 5.2: Extrusion rate estimates during 2009 based on lava flow thickness and mean surface flow velocity (derived from interpolated flow displacement). The periods 1-2, 2-3, and 3-4 January are approximately 24 hours each. The periods 1, 2, 3, and 4 January are measured from the beginning of the day until the end of the morning (when meteorological conditions deteriorated). The three explosions are measured from just before the explosion's onset until just after the end of the explosion when the ash cloud clears from the dome surface.**

| Period | 10 m thick ($m^3s^{-1}$) | 20 m thick ($m^3s^{-1}$) | 30 m thick ($m^3s^{-1}$) | 40 m thick ($m^3s^{-1}$) |
|---|---|---|---|---|
| 1-2 January | 0.07 | 0.13 | 0.2 | 0.26 |
| 2-3 January | 0.07 | 0.14 | 0.21 | 0.28 |
| 3-4 January | 0.07 | 0.15 | 0.22 | 0.29 |
| 1-Jan | 0.13 | 0.26 | 0.39 | 0.52 |
| 2-Jan | 0.12 | 0.25 | 0.37 | 0.49 |
| 3-Jan | 0.12 | 0.24 | 0.36 | 0.48 |
| 4-Jan | 0.12 | 0.25 | 0.37 | 0.49 |
| 2 Jan., explosion 3 | 1 | 2 | 3.01 | 4.01 |
| 4 Jan., explosion 1 | 1.58 | 3.17 | 4.75 | 6.34 |
| 4 Jan., explosion 2 | 1.1 | 2.2 | 3.3 | 4.4 |

**Table 5.3: Extrusion rate estimates during 1 January 2009 based on lava flow thickness and mean surface flow velocity (derived from interpolated flow displacement). The explosions are measured from just before the explosion's onset until just after the end of the explosion when the ash cloud clears from the dome surface. 'After explosion 2' is measured from just after the end of the second explosion to the very beginning of the next day on 2 January.**

| Period | 10 m thick ($m^3s^{-1}$) | 20 m thick ($m^3s^{-1}$) | 30 m thick ($m^3s^{-1}$) | 40 m thick ($m^3s^{-1}$) |
|---|---|---|---|---|
| Explosion 1 | 1.13 | 2.27 | 3.4 | 4.53 |
| Between explosions | 0.18 | 0.37 | 0.55 | 0.74 |
| Explosion 2 | 0.24 | 0.48 | 0.73 | 0.97 |
| After explosion 2 | 0.06 | 0.12 | 0.18 | 0.23 |

# 6. CONCLUSIONS

We have derived surface flow velocities of a lava flow from block displacements using oblique video images during January 2007 and 2009. Santiaguito changed between these years with respect to flow velocity, flow direction, and vent geometry. While the flow in 2007 moved southwest between 5.92 and 8.08 meters per day, the flow in 2009 moved slightly more westerly at about 5.20 to 5.70 meters per day. Lava in 2007 originated from a radiating point, and lava in 2009 originated from a ~50 meter linear fissure oriented northwest-southeast.

Flow field velocities increase during explosions to 0.79 to 5.17 meters per hour from 0.22-0.34 meters per hour during 2007 and 2009 (averaged over 24 hours). One inter-explosion interval (the repose time between two explosions) was analyzed. This interval had an elevated surface flow velocity of 0.60 meters per hour, which may demonstrate that an explosion continues beyond what is visually observed.

Limited extrusion rates may be calculated from flow field velocities. These rely on assumptions such as the thickness of the flow (varied in this study from 10 and 40 meters) and the surface area of the flow orthogonal to the flow surface. Extrusion rates from January 2007 range from 0.21 to 0.28 $m^3 s^{-1}$ daily based on an estimated surface area orthogonal to the flow surface of 2200 $m^2$ derived from an estimated lava thickness of 20 meters. This is a relatively low extrusion rate for Santiaguito, and would be expected because the low extrusion rate periods are much longer than high extrusion rate periods and therefore dominate the volcano's activity. January 2009 rates range from 0.24 to 0.26 $m^3 s^{-1}$ daily based on an estimated surface area orthogonal to the flow surface of 3000 $m^2$ using a lava thickness of 20 meters. Due to the

unknown lava flow thickness, it is statistically impossible to tell if there was a difference in lava extrusion between 2007 and 2009.

A major goal of this study is to inspire future field teams at Santiaguito and similar laboratories to introduce and keep video logging as a part of their observational array. Alone, it is a fundamental, vital tool for recording behavioral trends, particularly at volcanoes such as Santiaguito where the observational setup is ideal. A few days of video reveal a wealth of information, and if every team at Santiaguito recorded video, a fairly consistent library could be developed. Combined with other methods (acoustic, seismic, thermal, etc.), it provides visual proof an event detected by other methods actually occurred. With the relatively low cost, portability, and utility of digital video equipment, visual recorded observation should be a standard addition to every applicable field operation.

# REFERENCES


Allard, P., 1997. Endogenous magma degassing and storage at Mount Etna. Geophys. Res. Lett. 24, 2219-2222.

Bailey, J. E., Harris, A.J.L., Dehn, J., Calvari, S., Rowland, S., 2006, The changing morphology of an open lava channel on Mt. Etna, Bull. Volcanol. 68, 497- 515.

Barmin, A., Melnik, O., Sparks, R.S.J., 2002. Periodic behavior in lava dome eruptions. Earth Planet. Sci. Lett. 199, 173-184.

Bluth, G.J.S., Rose, W.I., 2004. Observations of eruptive activity at Santiaguito volcano, Guatemala. J. Volcanol. Geotherm. Res. 136, 297-302.

Calvari, S., Neri, M., Pinkerton, H., 2002. Effusion rate estimations during the 1999 summit eruption on Mount Etna, and growth of two distinct lava flow fields. J. Volcanol. Geotherm. Res. 199, 107-123.

Estudio del establecimiento de los mapas básicos y mapas de amenaza para el sistema de información geográfica de la República de Guatemala. Digital elevation model. Japanese International Development Agency: Instituto Geografico Nacional, Instituto Nacional de Sismologia, Vulcanologia, Meteorolgia e Hidrologia, Secretaria de Planificacion y Programacion e la Presidencia, 2003. Digitial.

Fink, J.H., Anderson, S.W., 2000. Lava domes and coulees. Encyclopedia of Volcanoes edited by H. Sigurdson et al., 307-319, Academic, San Diego, Calif.

Fink, J.H., Griffiths, R.W., 1998. Morphology, eruption rates, and rheology of lava domes: Insights from laboratory models. J. Geophys. Res. 103, 527-545.

Francis, P., Oppenheimer, C., Stevenson, D., 1993. Endogenous growth of persistently active volcanoes. Nature 366, 554-557.

Guest, J.E., Kilburn, C.R.J., Pinkerton, H., Duncan, A.M., 1986. The evolution of lava flow-fields: observations of the 1981 and 1983 eruptions of Mount Etna, Sicily. Bull. Volc. 49, 527-540.

Hale, A.J., Wadge, G., 2008. The transition from endogenous to exogenous growth of lava domes with the development of shear bands. J. Volcanol. Geotherm. Res. 171, 237-257.

Harris, A.J.L., Dehn, J., Calvari, S., 2007. Lava effusion rate definition and measurement: A review. Bull. Volcanol. 70, 1-22.

Harris, A.J.L., Flynn, L.P., Matias, O., Rose, W.I., 2002. The thermal stealth flows of Santiaguito dome, Guatemala: Implications for the cooling and emplacement of dacitic block-lava flows. Geol. Soc. Bull. 114, 533-546.

Harris, A.J.L., Murray, J.B., Aries, S. E., Davies, M.A., Flynn, L.P., Wooster, M.J., Wright, R., Rothery, D.A., 2000. Effusion rate trends at Etna and Krafla and their implications for eruptive mechanisms. J. Volcanol. Geotherm. Res. 102, 237-270.

Harris, A.J.L., Rose, W.I., Flynn, L.P., 2003. Temporal trends in lava dome extrusion at Santiaguito 1922-2000. Bull. Volcanol. 65, 77-89.

Harris, A.J.L., Stevenson, D.S., 1997. Magma budgets and steady-state activity of Vulcano and Stromboli. Geophys. Res. Lett. 24, 1043-1046.

James, M.R., Pinkerton, H., Robson, S., 2007. Image-based measurement of flux variation in distal regions of active lava flows. Geoc. Geophys. Geosys. 8, Q03006, doi:10.1029/2006GC001448.

James, M.R., Robson, S., Pinkerton, H., Ball, M., 2006. Oblique photogrammetry with visible and thermal images of active lava flows. Bull. Volcanol. 69, 105-108.

Johnson, J.B., Harris, A.J.L., Sahetapy-Engel, S.T.M., Wolf, R., Rose, W.I., 2004. Explosion dynamics of pyroclastic eruptions at Santiaguito Volcano. Geophys. Res. Lett. 31, L06610, doi:10.1029/2003GL019079.

Johnson, J.B., Lees, J.M., Gerst, A., Sahagian, D., Varley, N., 2008. Long-period earthquakes and co-eruptive dome inflation seen with particle image velocimetry. Nature 456, 377-381.

Lautze, N.C., Harris, A.J.L., Bailey, J.E., Ripepe, M., Calvari, S., Dehn, J., Rowland, S.K., Evans-Jones, K., 2004. Pulsed lava effusion at Mount Etna during 2001. J. Volcanol. Geotherm. Res. 137, 231-246.

Lipman, P.W., Banks, N.G., 1987. Aa flow dynamics, Mauna Loa 1984. U.S. Geol. Surv. Prof. Pap. 1350, 1527-1567.

Lyman, A.W., Koenig, E., Fink, J.H., 2004. Predicting yield strengths and effusion rates of lava domes from morphology and underlying topography. J. Volcanol. Geotherm. Res. 129, 125-138.

Melnik, O., Sparks, R.S.J., Costa, A., Barmin, A.A., 2009. Volcanic eruptions: Cyclicity during lava

dome growth. In: Encyclopedia of Complexity and Systems Science. Springer, p. 9763-9784.

Oppenheimer, C., Francis, P., 1998. Implications of longeval lava lakes for geomorphological and plutonic processes at Erta 'Ale volcano, Afar. J. Volcanol. Geotherm. Res. 80, 101-111.

Oppenheimer, C., Lomakima, A.S., Kyle, P.R., Kingsbury, N.G., Boichu, M., 2009. Pulsatory magma supply to a phonolite lava lake. Earth Planet. Sci. Lett. 284, 392-398.

Rose, W.I., 1972a. Notes on the 1902 eruption of Santa María volcano, Guatemala. Bull. Volcanol. 36, 29-45.

Rose, W.I., 1972b. Santiaguito volcanic dome, Guatemala. Geol. Soc. Bull. 83, 1413-1433.

Rose, W.I., 1972c. Pattern and mechanism of volcanic activity at the Santiaguito volcanic dome, Guatemala. Bull. Volc. 37, 73.

Rose, W.I., 1987. Volcanic activity at Santiaguito volcano, 1976-1984. Geol. Soc. Amer. Spec. Pap. 212, 17-27.

Rose, W.I., Grant, N.K., Hahn, G.A., Lange, I.M., Powell, J.L., Easter, J., Degraff, J.M., 1977. The evolution of Santa María volcano, Guatemala. J. Geol. 85, 63-87.

Rose, W.I., Stoiber, R.E., Bonis, S.B., 1970. Volcanic activity at Santiaguito volcano, Guatemala June 1968 – August 1969. Bull. Volcanol. 40, 23-38.

Sahetapy-Engel, S.T., Harris, A.J.L., Marchetti, E., 2008. Thermal, seismic and infrasound observations of persistent explosive activity and conduit dynamics at Santiaguito lava dome, Guatemala. J. Volcanol. Geotherm. Res. 173, 1-14.

Sapper, K., Termer, F., 1930. Der Ausbruch des Vulkans Santa María in Guatemala. Zeitschrift fur Vulkanologie, 13, 156.

Simpkin, T., Siebert, L., 2000. Appendix 2: Catalog of historically active volcanoes on Earth. Encyclopedia of Volcanoes edited by H. Sigurdson et al., 1365-1383, Academic, San Diego, Calif.

Spampinato, L., Oppenheimer, C., Calvari, S., Cannata, A., Montalto, P., 2008. Lava lake surface characterization by thermal imaging: Erta 'Ale volcano (Ethiopia). Geoc. Geophys. Geosys. 9, Q12008, doi:10.1029/2008GC002164.

Stoiber, R.E., Rose, W.I., 1969. Recent volcanic and fumarolic activity at Santiaguito volcano, Guatemala. Bull. Volcanol. 33, 475-502.

Tanguy, J.C., Kieffer, G., Patane, G., 1996. Dynamics, lava volume and effusion rate during the 1991–1993 eruption of Mount Etna. J. Volc. Geotherm. 71, 259-265.

Thompson, R.A., Schilling, S.P., 2007. Photogrammetry, *in* Dzurisin, Daniel, Volcano deformation - Geodetic monitoring techniques. Berlin, Springer-Verlag, 195-221.

Voight, B., Sparks, R.S.J., Miller, D., Stewart, R.C., Hoblitt, R.P., Clarke, A., Ewart, J., Aspinall, W.P., Baptie, B., Calder, E.S., Cole, P., Druitt, T.H., Hartford, C., Herd, R.A., Jackson, P., Lejeune, A.M., Lockhart, A.B., Loughlin, S.C., Luckett, R., Lynch, L., Norton, G.E., Robertson, R., Watson, I.M., Watts, R., Young, S.R., 1999. Magma flow instability and cyclic activity at Soufriere Hills volcano, Montserrat, British West Indies. Science 283, 1138-1142.

Walker, G.P.L., 1973. Lengths of lava flows Phil. Trans. Roy. Soc. Lond. A274, 107-118.

Wright, R., Blake, S., Harris, A.J.L., Rothery, D.A., 2001. A simple explanation for the space-based calculation of lava eruption rates. Earth Planet. Sci. Lett. 192 223-233.

Yamashina, K., Matsushima, T., Ohmi, S., 1999. Volcanic deformation at Unzen, Japan, visualized by a time-differential stereoscopy. J. Volcanol. Geotherm. Res. 89, 73-80.

# Appendix A:

List of videos taken during January 2009 season

All files recorded by camera SGH1. 'File start time,' 'File end time,' and 'Start real time' are UTC. 'Start time difference' is the difference between 'File' and 'Real' start times, included for error.

| FILE NAME | DATE | FILE START TIME | FILE END TIME | START REAL TIME | START TIME DIFFERENCE | TOTAL MOVIE TIME | NOTES |
|---|---|---|---|---|---|---|---|
| CIMG0399 | 1-Jan-09 | 12:01:51.62 | 12:24:55.00 | 12:01:51.66 | 00:00:00.04 | 00:23:03.38 | |
| CIMG0401 | 1-Jan-09 | 12:25:32.20 | 13:01:14.00 | - | - | 00:35:41.80 | |
| CIMG0402 | 1-Jan-09 | 13:01:21.95 | 13:41:14.00 | - | - | 00:39:52.05 | |
| CIMG0403 | 1-Jan-09 | 13:42:45.95 | 14:22:38.00 | 13:42:44.17 | -00:00:01.78 | 00:39:52.05 | |
| CIMG0404 | 1-Jan-09 | 14:23:30.97 | 14:35:14.00 | 14:23:29.11 | -00:00:01.86 | 00:11:43.03 | |
| CIMG0405 | 1-Jan-09 | 14:35:18.34 | 14:35:20.00 | - | - | 00:00:01.66 | |
| CIMG0406 | 1-Jan-09 | 14:36:07.78 | 15:07:44.00 | 14:36:06.49 | -00:00:01.29 | 00:31:36.22 | |
| CIMG0407 | 1-Jan-09 | 15:19:15.95 | 15:59:08.00 | 15:19:13.12 | -00:00:02.83 | 00:39:52.05 | |
| CIMG0408 | 1-Jan-09 | 15:59:25.88 | 16:07:00.00 | - | - | 00:07:34.12 | |
| CIMG0409 | 2-Jan-09 | 12:07:12.43 | 12:22:24.00 | 12:07:10.68 | -00:00:01.75 | 00:15:11.57 | |
| CIMG0410 | 2-Jan-09 | 12:22:40.32 | 12:56:24.00 | 12:22:38.72 | -00:00:01.60 | 00:33:43.68 | |
| CIMG0411 | 2-Jan-09 | 12:56:26.50 | 13:16:00.00 | - | - | 00:19:33.50 | |
| CIMG0412 | 2-Jan-09 | 13:16:27.35 | 13:49:38.00 | - | - | 00:33:10.65 | |
| CIMG0413 | 2-Jan-09 | 13:49:40.78 | 14:26:44.00 | 13:49:38.80 | -00:00:01.98 | 00:37:03.22 | |
| CIMG0414 | 2-Jan-09 | 14:26:51.95 | 15:06:44.00 | 14:26:50.18 | -00:00:01.77 | 00:39:52.05 | |
| CIMG0415 | 2-Jan-09 | 15:11:10.14 | 15:47:52.00 | 15:11:07.37 | -00:00:02.77 | 00:36:41.86 | |
| CIMG0416 | 2-Jan-09 | 15:47:54.67 | 15:47:58.00 | - | - | 00:00:03.33 | |
| CIMG0417 | 2-Jan-09 | 15:48:05.31 | 15:48:16.00 | - | - | 00:00:10.69 | |
| CIMG0418 | 2-Jan-09 | 15:48:23.62 | 15:49:08.00 | - | - | 00:00:44.38 | |
| CIMG0419 | 2-Jan-09 | 15:49:21.80 | 15:52:48.00 | - | - | 00:03:26.20 | |
| CIMG0420 | 2-Jan-09 | 15:53:55.27 | 16:11:42.00 | 15:52:52.83 | -00:01:02.44 | 00:17:46.73 | |
| CIMG0421 | 2-Jan-09 | 16:15:46.99 | 16:15:58.00 | - | - | 00:00:11.01 | |
| CIMG0422 | 2-Jan-09 | 16:28:45.99 | 16:28:52.00 | - | - | 00:00:06.01 | |
| CIMG0423 | 2-Jan-09 | 16:28:54.98 | 16:29:04.00 | - | - | 00:00:09.02 | |
| CIMG0424 | 3-Jan-09 | 11:24:31.95 | 12:04:24.00 | - | - | 00:39:52.05 | Night of 2 Jan 09 (local time) |
| CIMG0425 | 3-Jan-09 | 12:04:30.34 | 12:04:32.00 | - | - | 00:00:01.66 | |
| CIMG0426 | 3-Jan-09 | 12:04:36.04 | 12:15:00.00 | 12:04:35.03 | -00:00:01.01 | 00:10:23.96 | |
| CIMG0427 | 3-Jan-09 | 12:15:19.17 | 12:18:08.00 | 12:15:18.76 | -00:00:00.41 | 00:02:48.83 | Clouded (gas) - explosion breaks through |
| CIMG0428 | 3-Jan-09 | 12:18:17.61 | 12:24:54.00 | - | - | 00:06:36.39 | Clouded |

| | | | | | | | (gas) |
|---|---|---|---|---|---|---|---|
| CIMG0429 | 3-Jan-09 | 15:43:07.24 | 15:44:42.00 | 15:42:05.25 | -00:01:01.99 | 00:01:34.76 | |
| CIMG0430 | 3-Jan-09 | 15:45:04.95 | 15:45:56.00 | - | - | 00:00:51.05 | |
| CIMG0431 | 4-Jan-09 | 12:14:24.63 | 12:48:28.00 | - | - | 00:34:03.37 | |
| CIMG0432 | 4-Jan-09 | 12:48:31.80 | 12:51:44.00 | - | - | 00:03:12.20 | |
| CIMG0433 | 4-Jan-09 | 12:51:52.53 | 13:22:00.00 | - | - | 00:30:07.47 | |
| CIMG0434 | 4-Jan-09 | 13:23:44.21 | 13:59:14.00 | 13:23:43.68 | -00:00:00.53 | 00:35:29.79 | |
| CIMG0435 | 4-Jan-09 | 13:59:19.71 | 14:37:36.00 | 13:59:18.97 | -00:00:00.74 | 00:38:16.29 | |
| CIMG0436 | 4-Jan-09 | 14:37:41.71 | 15:16:02.00 | 14:37:41.50 | -00:00:00.21 | 00:38:20.29 | |
| CIMG0437 | 4-Jan-09 | 15:16:14.30 | 15:50:16.00 | - | - | 00:34:01.70 | |
| CIMG0438 | 4-Jan-09 | 15:50:22.65 | 15:50:30.00 | - | - | 00:00:07.35 | |
| CIMG0439 | 4-Jan-09 | 15:52:47.27 | 16:21:44.00 | 15:52:44.51 | -00:00:02.76 | 00:28:56.73 | |
| CIMG0440 | 4-Jan-09 | 16:23:40.66 | 16:23:50.00 | - | - | 00:00:09.34 | |

All files recorded by camera SGH2. 'File start time,' 'File end time,' and 'Start real time' are UTC. 'Start time difference' is the difference between 'File' and 'Real' start times, included for error.

| FILE NAME | DATE | FILE START TIME | FILE END TIME | START REAL TIME | START TIME DIFFERENCE | TOTAL MOVIE TIME |
|---|---|---|---|---|---|---|
| CIMG0008 | 1-Jan-09 | 13:56:19.98 | 13:56:24.00 | - | - | 00:00:04.02 |
| CIMG0009 | 1-Jan-09 | 13:56:35.95 | 14:36:28.00 | 13:56:36.47 | 00:00:00.52 | 00:39:52.05 |
| CIMG0010 | 1-Jan-09 | 14:47:58.13 | 14:56:48.00 | - | - | 00:08:49.87 |
| CIMG0011 | 1-Jan-09 | 14:56:52.43 | 15:34:18.00 | 14:56:52.31 | -00:00:00.12 | 00:37:25.57 |
| **CIMG0012** | 1-Jan-09 | 15:34:21.95 | 16:14:14.00 | 15:34:23.09 | 00:00:01.14 | 00:39:52.05 |
| CIMG0014 | 2-Jan-09 | 12:31:50.95 | 12:55:00.00 | - | - | 00:23:09.05 |
| CIMG0015 | 2-Jan-09 | 12:55:31.11 | 13:32:38.00 | 12:55:30.19 | -00:00:00.92 | 00:37:06.89 |
| **CIMG0016** | 2-Jan-09 | 13:32:42.75 | 14:10:16.00 | 13:32:44.07 | 00:00:01.32 | 00:37:33.25 |
| **CIMG0017** | 2-Jan-09 | 14:10:20.16 | 14:46:40.00 | 14:10:21.04 | 00:00:00.88 | 00:36:19.84 |
| CIMG0018 | 2-Jan-09 | 10:35:00.23 | 15:14:52.00 | - | - | 04:39:51.77 |
| **CIMG0019** | 2-Jan-09 | 15:15:11.84 | 15:34:40.00 | 15:15:12.91 | 00:00:01.07 | 00:19:28.16 |
| CIMG0020 | 2-Jan-09 | 15:35:24.30 | 16:15:00.00 | - | - | 00:39:35.70 |
| **CIMG0021** | 2-Jan-09 | 16:15:05.51 | 16:34:28.00 | 16:15:07.33 | 00:00:01.82 | 00:19:22.49 |
| **CIMG0022** | 3-Jan-09 | 12:58:21.92 | 13:33:08.00 | 12:58:22.13 | 00:00:00.21 | 00:34:46.08 |
| **CIMG0023** | 3-Jan-09 | 13:33:11.95 | 14:13:04.00 | 13:33:11.48 | -00:00:00.47 | 00:39:52.05 |
| CIMG0024 | 3-Jan-09 | 14:13:09.73 | 14:34:30.00 | - | - | 00:21:20.27 |
| CIMG0025 | 3-Jan-09 | 14:35:09.66 | 14:52:02.00 | - | - | 00:16:52.34 |
| **CIMG0026** | 3-Jan-09 | 15:05:44.72 | 15:43:48.00 | 15:05:45.61 | 00:00:00.89 | 00:38:03.28 |
| CIMG0027 | 3-Jan-09 | 15:43:49.52 | 16:03:02.00 | 15:43:51.91 | 00:00:02.39 | 00:19:12.48 |
| CIMG0028 | 3-Jan-09 | 16:06:17.74 | 16:33:00.00 | - | - | 00:26:42.26 |
| CIMG0029 | 3-Jan-09 | 16:43:35.79 | 16:47:14.00 | - | - | 00:03:38.21 |
| CIMG0030 | 4-Jan-09 | 12:42:34.00 | 13:16:04.00 | - | - | 00:33:30.00 |
| CIMG0031 | 4-Jan-09 | 13:16:07.70 | 13:26:44.00 | - | - | 00:10:36.30 |
| CIMG0032 | 4-Jan-09 | 13:27:15.56 | 13:56:54.00 | - | - | 00:29:38.44 |
| **CIMG0033** | 4-Jan-09 | 13:56:59.10 | 14:23:10.00 | 13:56:58.94 | -00:00:00.16 | 00:26:10.90 |
| CIMG0034 | 4-Jan-09 | 14:23:11.95 | 15:03:04.00 | - | - | 00:39:52.05 |
| CIMG0035 | 4-Jan-09 | 15:06:30.96 | 15:18:26.00 | 15:06:33.07 | 00:00:02.11 | 00:11:55.04 |
| CIMG0036 | 4-Jan-09 | 15:18:30.37 | 15:56:58.00 | 15:18:30.73 | 00:00:00.36 | 00:38:27.63 |
| CIMG0037 | 4-Jan-09 | 15:56:59.86 | 15:59:10.00 | - | - | 00:02:10.14 |
| CIMG0038 | 4-Jan-09 | 15:59:48.60 | 16:34:24.00 | - | - | 00:34:35.40 |
| CIMG0039 | 4-Jan-09 | 16:34:27.82 | 16:48:38.00 | - | - | 00:14:10.18 |

# Appendix B:

List of events recorded during January 2009

All events from 1 January to 4 January 2009 taken by camera SGH1. 'Real time' is UTC; 'Movie time' is the time the event occurred within the file.

| FILE NAME | DATE | REAL TIME | MOVIE TIME | EVENT NOTES |
|---|---|---|---|---|
| CIMG0399 | 1-Jan-09 | 12:01:51.66 | 00:00:00.00 | |
| CIMG0399 | 1-Jan-09 | **12:09:08.00** | 00:07:16.34 | GPS synch; audio only (JBJ GPS) |
| CIMG0399 | 1-Jan-09 | **12:10:16.00** | 00:23:03.38 | GPS synch; visual only (JBJ GPS) |
| CiMG0401 | 1-Jan-09 | | 00:03:49.00 | Rockfalls (nearly cont. indiv. plumes) |
| CIMG0402 | 1-Jan-09 | | 00:02:30.69 | Rockfalls (nearly cont. indiv. plumes) |
| CIMG0402 | 1-Jan-09 | | 00:27:11.81 | Rockfall |
| CIMG0402 | 1-Jan-09 | | 00:28:18.68 | Rockfall |
| CIMG0402 | 1-Jan-09 | | 00:28:43.00 | Rockfall |
| CIMG0402 | 1-Jan-09 | | 00:29:29.64 | Rockfall |
| CiMG0402 | 1-Jan-09 | | 00:29:45.42 | Rockfall |
| CIMG0402 | 1-Jan-09 | | 00:31:03.22 | Rockfall |
| CIMG0403 | 1-Jan-09 | 13:42:44.17 | 00:00:00.00 | |
| CIMG0403 | 1-Jan-09 | 13:43:16.41 | 00:00:32.24 | Rockfall |
| CIMG0403 | 1-Jan-09 | 13:47:16.27 | 00:04:32.10 | Rockfall (small) |
| CIMG0403 | 1-Jan-09 | 13:49:17.22 | 00:06:33.05 | Rockfall |
| CIMG0403 | 1-Jan-09 | 13:52:48.48 | 00:10:04.31 | Rockfall |
| CIMG0403 | 1-Jan-09 | 13:55:24.81 | 00:12:40.64 | Rockfall |
| CIMG0403 | 1-Jan-09 | 14:01:10.95 | 00:18:26.78 | Rockfall |
| CIMG0403 | 1-Jan-09 | 14:03:40.14 | 00:20:55.97 | Explosion (starts at center point, then large ring) |
| CIMG0403 | 1-Jan-09 | **14:10:32.00** | 00:27:48.73 | GPS synch; audio and visual (time marked here by audio) (CCF GPS) |
| CIMG0403 | 1-Jan-09 | 14:15:56.54 | 00:33:13.27 | Rockfall (small) |
| CIMG0403 | 1-Jan-09 | 14:16:53.63 | 00:34:10.36 | Rockfall |
| CIMG0403 | 1-Jan-09 | 14:17:22.27 | 00:34:39.00 | Rockfall (large) |
| CIMG0403 | 1-Jan-09 | 14:18:42.62 | 00:35:59.35 | Rockfall |
| CIMG0404 | 1-Jan-09 | 14:23:29.11 | 00:00:00.00 | |
| CIMG0404 | 1-Jan-09 | 14:23:54.67 | 00:00:25.56 | Rockfall |
| CIMG0404 | 1-Jan-09 | 14:27:19.86 | 00:03:50.75 | Rockfall (and degassing in center crater) |
| CIMG0404 | 1-Jan-09 | 14:27:58.01 | 00:04:28.90 | Degassing (larger half-ring) |
| CIMG0404 | 1-Jan-09 | 14:28:43.62 | 00:05:14.51 | Rockfall |
| CIMG0404 | 1-Jan-09 | 14:29:19.89 | 00:05:50.78 | Degasing (center left) |
| CIMG0404 | 1-Jan-09 | 14:29:56.25 | 00:06:27.14 | Rockfall |
| CIMG0404 | 1-Jan-09 | 14:32:34.06 | 00:09:04.95 | Rockfall |
| CIMG0404 | 1-Jan-09 | **14:33:27.00** | 00:09:57.89 | GPS synch; audio and visual (time marked here |

| | | | | |
|---|---|---|---|---|
| | | | | by audio) (CCF GPS) |
| CIMG0404 | 1-Jan-09 | 14:34:45.64 | 00:11:16.53 | Rockfall (large) |
| CIMG0406 | 1-Jan-09 | 14:36:06.49 | 00:00:00.00 | |
| CIMG0406 | 1-Jan-09 | **14:36:15.00** | 00:00:08.49 | GPS synch; audio and visual (time marked here by audio) (CCF GPS) |
| CIMG0406 | 1-Jan-09 | 14:37:22.66 | 00:01:16.17 | Rockfall |
| CIMG0406 | 1-Jan-09 | 14:38:02.75 | 00:01:56.26 | Rockfall |
| CIMG0406 | 1-Jan-09 | 14:41:03.59 | 00:04:57.10 | Rockfall |
| CIMG0406 | 1-Jan-09 | 14:43:35.82 | 00:07:29.33 | Rockfall |
| CIMG0406 | 1-Jan-09 | 14:45:17.47 | 00:09:10.98 | Rockfall |
| CIMG0406 | 1-Jan-09 | 14:46:14.73 | 00:10:08.24 | Degassing |
| CIMG0406 | 1-Jan-09 | 14:46:32.58 | 00:10:26.09 | Rockfall |
| CIMG0406 | 1-Jan-09 | 14:51:47.61 | 00:15:41.12 | Rockfall |
| CIMG0406 | 1-Jan-09 | 14:55:41.71 | 00:19:35.22 | Rockfall |
| CIMG0406 | 1-Jan-09 | 14:58:51.06 | 00:22:44.57 | Explosion (large ring, very large explosion…jetting on left, pyroclastic flow) |
| CiMG0406 | 1-Jan-09 | **15:04:57.00** | 00:28:50.51 | GPS synch; audio and visual (time marked here by audio) (CCF GPS) |
| CIMG0407 | 1-Jan-09 | 15:19:13.12 | 00:00:00:00 | |
| CIMG0407 | 1-Jan-09 | **15:19:30.00** | 00:00:16.88 | GPS synch; audio and visual (time marked here by audio) (CCF GPS) |
| CIMG0407 | 1-Jan-09 | 15:24:19.77 | 00:05:06.65 | Rockfall |
| CIMG0407 | 1-Jan-09 | 15:26:33.34 | 00:07:20.22 | Rockfall |
| CIMG0407 | 1-Jan-09 | 15:29:01.34 | 00:09:48.22 | Rockfall |
| CIMG0408 | 1-Jan-09 | | 00:00:53.16 | GPS synch; audio and visual (time inaudible? Marked by CCF GPS) |
| CIMG0409 | 2-Jan-09 | 12:07:10.68 | 00:00:00:00 | |
| CIMG0409 | 2-Jan-09 | **12:07:47.00** | 00:00:36.32 | GPS synch; audio and visual (time marked here by audio) (CCF GPS) |
| CIMG0410 | 2-Jan-09 | 12:22:38.72 | 00:00:00:00 | |
| CIMG0410 | 2-Jan-09 | **12:23:13.00** | 00:00:34.28 | GPS synch; audio and visual (time marked here by audio) (CCF GPS) |
| CIMG0410 | 2-Jan-09 | 12:21:32.63 | 00:02:14.65 | Rockfall |
| CIMG0410 | 2-Jan-09 | 12:30:58.14 | 00:11:40.16 | Rockfall |
| CIMG0410 | 2-Jan-09 | 12:31:42.26 | 00:12:24.28 | Rockfall |
| CIMG0410 | 2-Jan-09 | 12:34:02.37 | 00:14:44.39 | Rockfall (very large, long duration?) |
| CIMG0410 | 2-Jan-09 | 12:48:53.83 | 00:29:35.85 | Rockfall |
| CIMG0410 | 2-Jan-09 | 12:52:01.58 | 00:32:43.60 | Degassing (lower crater) |
| CIMG0411 | 2-Jan-09 | | 00:01:32.28 | Rockfall (large, long duration) |
| CIMG0411 | 2-Jan-09 | | 00:04:30.18 | Rockfall (small) |
| CIMG0411 | 2-Jan-09 | | 00:07:54.02 | Rockfall |
| CIMG0411 | 2-Jan-09 | | 00:11:16.33 | Rockfall |
| CIMG0411 | 2-Jan-09 | | 00:14:15.46 | Rockfall |
| CIMG0411 | 2-Jan-09 | | 00:17:06.25 | Rockfall |
| CIMG0411 | 2-Jan-09 | | 00:17:56.10 | Rockfall |
| CIMG0412 | 2-Jan-09 | | 00:00:28.05 | Rockfall |
| CIMG0412 | 2-Jan-09 | | 00:14:13.12 | Rockfall |
| CIMG0412 | 2-Jan-09 | | 00:23:29.98 | Rockfall |
| CIMG0412 | 2-Jan-09 | | 00:25:09.10 | Rockfall (small) |

| | | | | |
|---|---|---|---|---|
| CIMG0412 | 2-Jan-09 | | 00:29:31.08 | Rockfall (small) |
| CIMG0412 | 2-Jan-09 | | 00:30:52.53 | Rockfall |
| **CIMG0413** | 2-Jan-09 | 13:49:38.80 | 00:00:00:00 | |
| **CIMG0413** | 2-Jan-09 | 13:51:26.65 | 00:01:47.85 | Rockfall |
| **CIMG0413** | 2-Jan-09 | 13:54:02.06 | 00:04:23.26 | Explosion (medium ring) |
| **CIMG0413** | 2-Jan-09 | **13:58:05.00** | 00:09:17.28 | GPS synch; audio and visual (time marked here by audio) (CCF GPS) DOES NOT SYNCH WITH SGH2 |
| **CIMG0413** | 2-Jan-09 | 14:02:40.01 | 00:13:01.21 | Explosion (small half ring, long duration) |
| **CIMG0413** | 2-Jan-09 | **14:05:03.00** | 00:16:25.10 | GPS synch; audio and visual (time marked here by audio) (CCF GPS) DOES NOT SYNCH WITH SGH2 |
| **CIMG0413** | 2-Jan-09 | 14:06:36.04 | 00:16:57.24 | Rockfall (two separate plumes) |
| **CIMG0413** | 2-Jan-09 | 14:09:04.16 | 00:19:25.36 | Rockfall |
| **CIMG0413** | 2-Jan-09 | 14:12:03.06 | 00:22:24.26 | Rockfall |
| **CIMG0413** | 2-Jan-09 | 14:15:04.00 | 00:25:25.20 | Rockfall |
| **CIMG0413** | 2-Jan-09 | 14:16:48.34 | 00:27:09.54 | Explosion (large ring) |
| **CIMG0413** | 2-Jan-09 | **14:20:09.00** | 00:30:30.54 | GPS synch; audio and visual (time unreadable? Marked by CCF GPS) |
| **CIMG0413** | 2-Jan-09 | 14:21:59.80 | 00:32:21.34 | Rockfall |
| **CIMG0413** | 2-Jan-09 | 14:25:42.90 | 00:36:04.44 | Degassing |
| CIMG0414 | 2-Jan-09 | 14:26:50.18 | 00:00:00:00 | |
| CIMG0414 | 2-Jan-09 | **14:27:15.00** | 00:00:24.82 | GPS synch; audio and visual (time marked here by audio) (CCF GPS) |
| CIMG0414 | 2-Jan-09 | 14:27:37.92 | 00:00:47.74 | Rockfall |
| CIMG0414 | 2-Jan-09 | 14:34:27.11 | 00:07:36.93 | Rockfall |
| CIMG0414 | 2-Jan-09 | 14:38:19.45 | 00:11:29.27 | Rockfall |
| CIMG0414 | 2-Jan-09 | 14:45:52.40 | 00:19:02.22 | Rockfall (small) |
| CIMG0414 | 2-Jan-09 | 14:48:16.99 | 00:21:26.81 | Rockfall |
| CIMG0414 | 2-Jan-09 | 14:51:29.29 | 00:24:39.11 | Rockfall |
| CIMG0414 | 2-Jan-09 | 14:54:18.36 | 00:27:28.18 | Rockfall (large) |
| CIMG0414 | 2-Jan-09 | 15:02:27.51 | 00:35:37.33 | Rockfall |
| CIMG0415 | 2-Jan-09 | 15:11:07.37 | 00:00:00:00 | Explosion (starts in middle of event) |
| CIMG0415 | 2-Jan-09 | **15:15:23.00** | 00:04:15.63 | GPS synch; audio and visual (time marked here by audio) (CCF GPS) |
| CIMG0415 | 2-Jan-09 | 15:20:35.46 | 00:09:28.09 | Rockfall |
| CIMG0415 | 2-Jan-09 | 15:31:17.01 | 00:20:09.64 | Rockfall (large) |
| CIMG0415 | 2-Jan-09 | 15:39:14.73 | 00:28:07.36 | Rockfall |
| CIMG0415 | 2-Jan-09 | 15:42:18.77 | 00:31:11.40 | Rockfall |
| CimG0420 | 2-Jan-09 | 15:52:52.83 | 00:00:00:00 | |
| CIMG0420 | 2-Jan-09 | **15:54:50.00** | 00:01:57.17 | GPS synch; audio and visual (time unreadable? Marked by CCF GPS) |
| CIMG0421 | 2-Jan-09 | | 00:00:00:00 | Explosion in clouds |
| CIMG0424 | 3-Jan-09 | | | |
| CIMG0424 | 3-Jan-09 | **23:25:16.00** | 00:00:44.46 | GPS synch; audio and visual (time unreadable? Marked by CCF GPS) |
| CIMG0424 | 3-Jan-09 | | 00:15:24.00 | Rockfall |
| CIMG0424 | 3-Jan-09 | | 00:20:13.06 | Rockfall |
| CIMG0424 | 3-Jan-09 | | 00:21:04.16 | Rockfall |
| CIMG0426 | 3-Jan-09 | 12:04:35.03 | 00:00:00:00 | |
| CIMG0426 | 3-Jan-09 | 12:09:22.48 | 00:04:47.45 | Explosion (video is very dark…only see plume) |

| | | | | |
|---|---|---|---|---|
| CIMG0426 | 3-Jan-09 | **12:14:40.00** | 00:10:04.97 | GPS synch; audio and visual (time unreadable? Marked by CCF GPS) |
| CIMG0427 | 3-Jan-09 | 12:15:18.76 | 00:00:00:00 | |
| CIMG0427 | 3-Jan-09 | **12:15:47.00** | 00:00:28.24 | GPS synch; audio and visual (time unreadable?). Small explosion…unnoticed |
| CIMG0429 | 3-Jan-09 | 15:42:05.25 | 00:00:00:00 | |
| CIMG0429 | 3-Jan-09 | **15:42:48.00** | 00:00:42.75 | GPS synch; audio and visual (time marked by audio) |
| CIMG0431 | 4-Jan-09 | | 00:03:09.11 | Rockfall |
| CIMG0431 | 4-Jan-09 | | 00:29:05.12 | Rockfall |
| CIMG0431 | 4-Jan-09 | | 00:32:11.28 | Rockfall? |
| CIMG0433 | 4-Jan-09 | | 00:19:42.19 | Rockfall |
| CIMG0433 | 4-Jan-09 | | 00:23:26.06 | Rockfall |
| CIMG0434 | 4-Jan-09 | 13:23:43.68 | 00:00:00:00 | |
| CIMG0434 | 4-Jan-09 | **13:24:26.00** | 00:00:42.32 | GPS synch; audio and visual (time marked here by audio) |
| CIMG0434 | 4-Jan-09 | 13:35:57.62 | 00:12:13.94 | Rockfall |
| CIMG0434 | 4-Jan-09 | 13:39:44.73 | 00:16:01.05 | Rockfall |
| CIMG0434 | 4-Jan-09 | 13:46:08.78 | 00:22:25.10 | Rockfall |
| CIMG0434 | 4-Jan-09 | 13:48:50.83 | 00:25:07.15 | Rockfall |
| CIMG0434 | 4-Jan-09 | 13:53:14.71 | 00:29:31.03 | Rockfall |
| CIMG0434 | 4-Jan-09 | 13:56:30.77 | 00:32:47.09 | Rockfall (small) |
| CIMG0435 | 4-Jan-09 | 13:59:18.97 | 00:00:00:00 | |
| CIMG0435 | 4-Jan-09 | 14:01:02.85 | 00:01:43.88 | Rockfall |
| CIMG0435 | 4-Jan-09 | 14:02:26.12 | 00:03:07.15 | Rockfall |
| CIMG0435 | 4-Jan-09 | 14:03:10.05 | 00:03:51.08 | Rockfall |
| CIMG0435 | 4-Jan-09 | 14:04:10.04 | 00:04:51.07 | Rockfall |
| CIMG0435 | 4-Jan-09 | 14:05:05.12 | 00:05:46.15 | Rockfall (two separate plumes, very large) |
| CIMG0435 | 4-Jan-09 | 14:10:24.21 | 00:11:05.24 | Explosion (center point, then large ring, very large explosion, jetting in foreground) |
| CIMG0435 | 4-Jan-09 | 14:17:32.70 | 00:18:13.73 | Rockfall |
| CIMG0435 | 4-Jan-09 | **14:20:53.00** | 00:21:34.03 | GPS synch; audio and visual (time marked here by audio) |
| CIMG0435 | 4-Jan-09 | 14:23:37.97 | 00:24:19.00 | Degassing (small plume) |
| CIMG0435 | 4-Jan-09 | 14:25:37.81 | 00:26:18.84 | Rockfall |
| CIMG0435 | 4-Jan-09 | 14:26:09.26 | 00:26:50.29 | Rockfall |
| CIMG0435 | 4-Jan-09 | 14:33:06.17 | 00:33:47.20 | Rockfall |
| CIMG0435 | 4-Jan-09 | 14:36:05.38 | 00:36:46.41 | Rockfall |
| CIMG0436 | 4-Jan-09 | 14:37:41.50 | 00:00:00:00 | |
| CIMG0436 | 4-Jan-09 | 14:41:09.19 | 00:03:27.69 | Rockfall |
| CIMG0436 | 4-Jan-09 | 14:49:59.47 | 00:12:17.97 | Rockfall |
| CIMG0436 | 4-Jan-09 | 14:55:11.56 | 00:17:30.06 | Rockfall |
| CiMG0436 | 4-Jan-09 | 14:56:01.65 | 00:18:20.15 | Rockfall |
| CIMG0436 | 4-Jan-09 | 15:07:11.41 | 00:29:29.91 | Explosion (small) |
| CIMG0436 | 4-Jan-09 | **15:15:44.00** | 00:38:02.50 | GPS synch; audio and visual (time marked here by audio) |
| CIMG0437 | 4-Jan-09 | | 00:07:45.95 | Rockfall |
| CIMG0437 | 4-Jan-09 | | 00:10:20.31 | Rockfall |
| CIMG0437 | 4-Jan-09 | | 00:11:21.06 | Rockfall (large) |
| CiMG0437 | 4-Jan-09 | | 00:14:48.59 | Rockfall |
| CIMG0437 | 4-Jan-09 | | 00:17:28.43 | Rockfall |

| | | | | |
|---|---|---|---|---|
| CIMG0437 | 4-Jan-09 | | 00:28:31.02 | Degassing (lower crater) |
| CIMG0437 | 4-Jan-09 | | 00:33:10.00 | Rockfall |
| CIMG0439 | 4-Jan-09 | 15:52:44.51 | 00:00:00:00 | |
| CIMG0439 | 4-Jan-09 | 15:52:46.79 | 00:00:02.28 | Explosion (catches onset but is zoomed out. Very noisy - jet sounds) |
| CIMG0439 | 4-Jan-09 | 15:52:51.51 | 00:00:07.00 | GPS synch (visual only) |
| CIMG0439 | 4-Jan-09 | **16:02:39.00** | 00:09:54.49 | GPS synch; audio and visual (time marked by audio) |
| CIMG0439 | 4-Jan-09 | 16:06:15.40 | 00:13:30.89 | Rockfall |
| CIMG0439 | 4-Jan-09 | 16:08:26.83 | 00:15:42.32 | Rockfall |
| CIMG0439 | 4-Jan-09 | 16:10:18.65 | 00:17:34.14 | Rockfall |
| CIMG0439 | 4-Jan-09 | 16:11:35.52 | 00:18:51.01 | Rockfall |
| CIMG0439 | 4-Jan-09 | 16:15:45.74 | 00:23:01.23 | Rockfall |
| CIMG0439 | 4-Jan-09 | 16:18:15.86 | 00:25:31.35 | Rockfall |

All events from 1 January to 4 January 2009 taken by camera SGH2. 'Real time' is UTC; 'Movie time' is the time the event occurred within the file.

| FILE NAME | DATE | REAL TIME | MOVIE TIME | EVENT NOTES |
|---|---|---|---|---|
| CIMG0009 | 1-Jan-09 | 13:56:36.47 | 00:00:00.00 | |
| CIMG0009 | 1-Jan-09 | 13:57:59.49 | 00:01:23.02 | Rockfall |
| CIMG0009 | 1-Jan-09 | 14:01:09.59 | 00:04:33.12 | Rockfall (small) |
| CIMG0009 | 1-Jan-09 | 14:03:40.14 | 00:07:03.67 | Explosion (medium-large ring; loud jet noises) |
| CIMG0009 | 1-Jan-09 | **14:08:19.00** | 00:11:42.53 | GPS synch (audio; UTC time) |
| CIMG0009 | 1-Jan-09 | 14:09:34.30 | 00:12:57.83 | Rockfall?; GPS synch (visual; possibly unreadable) |
| CIMG0009 | 1-Jan-09 | 14:15:57.64 | 00:19:21.17 | Rockfall |
| CIMG0009 | 1-Jan-09 | 14:16:55.50 | 00:20:19.03 | Rockfall (large, prolonged) |
| CIMG0009 | 1-Jan-09 | 14:18:43.87 | 00:22:07.40 | Rockfall (prolonged) |
| CiMG0009 | 1-Jan-09 | 14:27:27.57 | 00:30:51.10 | Degassing (center right crater) |
| CIMG0009 | 1-Jan-09 | 14:27:31.82 | 00:30:55.35 | Rockfall |
| CIMG0009 | 1-Jan-09 | 14:30:01.00 | 00:33:24.53 | Rockfall ('migrates' to left; large & prolonged) |
| CIMG0009 | 1-Jan-09 | 14:32:37.22 | 00:36:00.75 | Rockfall |
| CIMG0009 | 1-Jan-09 | 14:34:47.69 | 00:38:11.22 | Rockfall (large) |
| CIMG0010 | 1-Jan-09 | | 00:03:49.01 | Rockfall |
| CIMG0010 | 1-Jan-09 | | 00:07:44.19 | Rockfall |
| CIMG0011 | 1-Jan-09 | 14:56:52.31 | 00:00:00.00 | |
| CIMG0011 | 1-Jan-09 | 14:58:51.21 | 00:01:58.90 | Explosion (large; plumes emerge from outside crater rim. Plume hangs over crater for long after event) |
| CIMG0011 | 1-Jan-09 | **15:05:24.00** | 00:08:31.69 | GPS synch (audio; UTC time) |
| CIMG0011 | 1-Jan-09 | 15:06:15.29 | 00:09:22.98 | GPS synch (visual; probably unreadable) |
| CIMG0011 | 1-Jan-09 | 15:24:20.65 | 00:27:28.34 | Rockfall |
| CIMG0011 | 1-Jan-09 | 15:26:33.92 | 00:29:41.61 | Rockfall |
| CIMG0011 | 1-Jan-09 | 15:29:03.38 | 00:32:11.07 | Rockfall |
| **CIMG0012** | 1-Jan-09 | 15:34:23.09 | 00:00:00.00 | |
| **CIMG0012** | 1-Jan-09 | 15:41:46.26 | 00:07:23.17 | Rockfall (large; clouds over afterwards) |
| **CIMG0012** | 1-Jan-09 | 16:08:23.09 | 00:34:00.00 | Not exact time; loud jet sound heard but crater is obscured by clouds |
| **CIMG0012** | 1-Jan-09 | **16:13:47.00** | 00:39:23.91 | GPS synch (visual; this time is well-synched) |
| **CIMG0012** | 1-Jan-09 | **16:14:12.00** | 00:39:50.83 | GPS synch (audio; cut off at end) |
| CIMG0014 | 2-Jan-09 | | 00:02:26.72 | Rockfall |
| CIMG0014 | 2-Jan-09 | | 00:03:11.11 | Rockfall (very large, prolonged) |
| CIMG0014 | 2-Jan-09 | | 00:05:29.67 | Rockfall (very large; prolonged) |
| CIMG0014 | 2-Jan-09 | | 00:20:23.23 | Rockfall |
| CIMG0015 | 2-Jan-09 | 12:55:30.19 | 00:00:00.00 | |
| CIMG0015 | 2-Jan-09 | 12:57:57.61 | 00:02:27.42 | Rockfall (large; 'migrates' left) |
| CIMG0015 | 2-Jan-09 | **12:59:58.00** | 00:04:27.81 | GPS synch (audio only; UTC time - 7am local time) |
| CIMG0015 | 2-Jan-09 | 13:04:18.24 | 00:08:48.05 | Rockfall |
| CIMG0015 | 2-Jan-09 | 13:10:41.25 | 00:15:11.06 | Rockfall |
| CIMG0015 | 2-Jan-09 | 13:13:29.50 | 00:17:59.31 | Rockfall (small) |
| CIMG0015 | 2-Jan-09 | 13:16:08.01 | 00:20:37.82 | Rockfall |
| CIMG0015 | 2-Jan-09 | 13:16:52.56 | 00:21:22.37 | Rockfall |

| | | | | |
|---|---|---|---|---|
| CIMG0015 | 2-Jan-09 | 13:30:39.11 | 00:35:08.92 | Rockfall |
| **CIMG0016** | 2-Jan-09 | 13:32:44.07 | 00:00:00.00 | |
| **CIMG0016** | 2-Jan-09 | 13:47:18.20 | 00:14:34.13 | Rockfall (small) |
| **CIMG0016** | 2-Jan-09 | 13:51:42.99 | 00:18:58.92 | Rockfall |
| **CIMG0016** | 2-Jan-09 | 13:54:02.06 | 00:21:17.99 | Explosion (starts with small ring, expands slightly, jetting, some light whoosing and rumbling |
| **CIMG0016** | 2-Jan-09 | **14:00:51.00** | 00:28:06.55 | GPS synch (audio only - UTC time; visual may be unreadable) |
| **CIMG0016** | 2-Jan-09 | **14:02:14.00** | 00:29:29.81 | GPS synch (audio only - UTC time) |
| **CIMG0016** | 2-Jan-09 | 14:02:40.01 | 00:29:55.97 | Explosion (small, starts as half-circle on left side, expands to right side) |
| **CIMG0016** | 2-Jan-09 | 14:06:37.58 | 00:33:53.54 | Rockfall |
| **CIMG0016** | 2-Jan-09 | **14:07:46.00** | 00:35:01.70 | GPS synch (audio only - UTC time; visual possibly unreadable) |
| **CIMG0016** | 2-Jan-09 | 14:09:04.06 | 00:36:20.02 | Rockfall (large) |
| **CIMG0017** | 2-Jan-09 | 14:10:21.04 | 00:00:00.00 | |
| **CIMG0017** | 2-Jan-09 | 14:12:01.67 | 00:01:40.63 | Rockfall |
| **CIMG0017** | 2-Jan-09 | 14:15:04.11 | 00:04:43.07 | Rockfall (small) |
| **CIMG0017** | 2-Jan-09 | 14:16:33.46 | 00:06:12.42 | Rockfall (small) |
| **CIMG0017** | 2-Jan-09 | 14:16:48.34 | 00:06:27.30 | Explosion (large ring) |
| **CIMG0017** | 2-Jan-09 | 14:22:02.22 | 00:11:41.18 | Rockfall |
| **CIMG0017** | 2-Jan-09 | **14:23:56.00** | 00:13:35.42 | GPS synch (audio only - UTC time) |
| **CIMG0017** | 2-Jan-09 | **14:24:26.00** | 00:14:04.96 | GPS synch (visual; this time is well-synched with many (10+) seconds visible) |
| **CIMG0017** | 2-Jan-09 | 14:25:42.64 | 00:15:21.60 | Degassing (center left crater) |
| **CIMG0017** | 2-Jan-09 | 14:27:40.84 | 00:17:19.80 | Rockfall |
| **CIMG0017** | 2-Jan-09 | 14:34:29.12 | 00:24:08.08 | Rockfall |
| **CIMG0017** | 2-Jan-09 | 14:38:28.21 | 00:28:07.17 | Rockfall |
| CiMG0018 | 2-Jan-09 | | | Poor res, very long (>60 fps), no audio, and no readable GPS frames. One explosion towards end. |
| **CIMG0019** | 2-Jan-09 | 15:15:12.91 | 00:00:00.00 | |
| **CIMG0019** | 2-Jan-09 | **15:15:58.00** | 00:00:45.09 | GPS synch (visual; this time is well-synched with many seconds visible) |
| **CIMG0019** | 2-Jan-09 | 15:31:19.04 | 00:16:06.13 | Rockfall |
| CIMG0020 | 2-Jan-09 | | 00:03:45.48 | Rockfall |
| CIMG0020 | 2-Jan-09 | | 00:06:55.03 | Rockfall (clouds over) |
| **CIMG0021** | 2-Jan-09 | 16:15:07.33 | 00:00:00.00 | |
| **CIMG0021** | 2-Jan-09 | 16:15:40.33 | 00:00:33.00 | Loud, short boom (clouded over, no visual. Cam zooms out and can see plume rising from clouds) |
| **CIMG0021** | 2-Jan-09 | **16:16:59.00** | 00:01:51.98 | GPS synch (audio only - UTC time) |
| **CIMG0021** | 2-Jan-09 | **16:17:47.00** | 00:02:39.67 | GPS synch (visual; this time is well-synched with many seconds visible) |
| **CIMG0021** | 2-Jan-09 | **16:32:00.00** | 00:16:53.06 | GPS synch (visual; this time is well-synched with many seconds visible) |
| **CIMG0021** | 2-Jan-09 | **16:32:17.00** | 00:17:10.07 | GPS synch (audio only - UTC time) |
| **CIMG0022** | 3-Jan-09 | 12:58:22.13 | 00:00:00.00 | |
| **CIMG0022** | 3-Jan-09 | **12:58:50.00** | 00:00:27.87 | GPS synch (audio and visual; time fairly well-synched by visual. Hard to read) |
| **CIMG0023** | 3-Jan-09 | 13:33:11.48 | 00:00:00.00 | |

| | | | | |
|---|---|---|---|---|
| **CIMG0023** | 3-Jan-09 | 13:49:24.28 | 00:16:12.80 | Explosion; with PF down east (obscured by clouds) |
| **CIMG0023** | 3-Jan-09 | **14:01:10.00** | 00:27:58.52 | GPS synch (audio and visual; time fairly well-synched by visual. Hard to read) |
| **CIMG0026** | 3-Jan-09 | 15:05:45.61 | 00:00:00.00 | |
| **CIMG0026** | 3-Jan-09 | 15:06:44.92 | 00:00:59.31 | Rockfall (two plumes) |
| **CIMG0026** | 3-Jan-09 | 15:16:24.33 | 00:10:38.72 | Explosion (gas obscures crater; time may be off by up to 1 second. Onset is visible in outside crater flow. Excellent jetting in foreground) |
| **CIMG0026** | 3-Jan-09 | 15:21:04.77 | 00:15:19.16 | Explosion (small, gas obscures onset; time may be up to 1 second late. Jetting, slowly increases in size) |
| **CIMG0026** | 3-Jan-09 | **15:28:50.00** | 00:23:04.39 | GPS synch (audio and visual; time well-synched by visual. Multiple seconds visible) |
| CIMG0027 | 3-Jan-09 | 15:43:51.91 | 00:00:00.00 | |
| CIMG0027 | 3-Jan-09 | 15:48:46.93 | 00:04:55.02 | Rockfall |
| CIMG0027 | 3-Jan-09 | 15:51:26.75 | 00:07:34.84 | Explosion (small; unsure of onset due to gassy crater. Long degassing period follows) |
| CIMG0027 | 3-Jan-09 | **15:57:30.00** | 00:13:38.09 | GPS synch (audio only - UTC time) |
| CIMG0030 | 4-Jan-09 | | 00:00:46.73 | Rockfall (large) |
| CIMG0030 | 4-Jan-09 | | 00:04:00.90 | Rockfall? |
| CIMG0030 | 4-Jan-09 | | 00:06:46.22 | Rockfall? |
| CIMG0030 | 4-Jan-09 | | 00:18:37.13 | Rockfall? |
| CIMG0030 | 4-Jan-09 | | 00:29:00.03 | Rockfall |
| CIMG0030 | 4-Jan-09 | | 00:32:44.23 | Rockfall |
| CIMG0031 | 4-Jan-09 | | 00:08:12.18 | Rockfall |
| CIMG0032 | 4-Jan-09 | | 00:05:35.38 | Degassing (small, crater floor) |
| CIMG0032 | 4-Jan-09 | | 00:06:40.32 | Rockfall |
| CIMG0032 | 4-Jan-09 | | 00:07:12.96 | Rockfall |
| CIMG0032 | 4-Jan-09 | | 00:08:40.90 | Rockfall |
| CIMG0032 | 4-Jan-09 | | 00:12:28.68 | Rockfall |
| CIMG0032 | 4-Jan-09 | | 00:17:54.34 | Rockfall |
| CIMG0032 | 4-Jan-09 | | 00:18:49.69 | Rockfall |
| CIMG0032 | 4-Jan-09 | | 00:19:56.10 | Rockfall |
| CIMG0032 | 4-Jan-09 | | 00:21:34.13 | Rockfall |
| CIMG0032 | 4-Jan-09 | | 00:24:28.26 | Rockfall |
| CIMG0032 | 4-Jan-09 | | 00:25:57.34 | Rockfall |
| CIMG0032 | 4-Jan-09 | | 00:29:13.14 | Rockfall |
| **CIMG0033** | 4-Jan-09 | 13:56:58.94 | 00:00:00.00 | |
| **CIMG0033** | 4-Jan-09 | 13:58:57.48 | 00:01:58.54 | Rockfall |
| **CIMG0033** | 4-Jan-09 | 14:02:27.03 | 00:05:28.09 | Rockfall |
| **CIMG0033** | 4-Jan-09 | 14:03:09.85 | 00:06:10.91 | Rockfall |
| **CIMG0033** | 4-Jan-09 | 14:04:10.07 | 00:07:11.13 | Rockfall |
| **CIMG0033** | 4-Jan-09 | 14:05:06.14 | 00:08:07.20 | Rockfall (two plumes; very large) |
| **CIMG0033** | 4-Jan-09 | 14:10:24.56 | 00:13:25.62 | Explosion (large) |
| **CIMG0033** | 4-Jan-09 | 14:17:33.05 | 00:20:34.11 | Rockfall |
| **CIMG0033** | 4-Jan-09 | **14:19:58.00** | 00:22:59.06 | GPS synch (audio and visual; time fairly well-synched. Hard to read) |
| CIMG0034 | 4-Jan-09 | | 00:00:25.47 | Degassing |
| CIMG0034 | 4-Jan-09 | | 00:07:48.32 | Rockfall |

| | | | | |
|---|---|---|---|---|
| CIMG0034 | 4-Jan-09 | | 00:10:19.83 | Rockfall |
| CIMG0034 | 4-Jan-09 | | 00:13:12.80 | Rockfall |
| CIMG0034 | 4-Jan-09 | | 00:17:58.01 | Rockfall |
| CIMG0034 | 4-Jan-09 | | 00:32:49.20 | Rockfall |
| CIMG0035 | 4-Jan-09 | 15:06:33.07 | 00:00:00.00 | |
| CIMG0035 | 4-Jan-09 | 15:07:11.32 | 00:00:38.25 | Explosion |
| CIMG0035 | 4-Jan-09 | **15:13:20.00** | 00:06:46.93 | GPS synch (audio; UTC time) |
| CIMG0036 | 4-Jan-09 | 15:18:30.73 | 00:00:00.00 | |
| CIMG0036 | 4-Jan-09 | 15:24:01.11 | 00:05:30.38 | Rockfall |
| CIMG0036 | 4-Jan-09 | 15:25:08.14 | 00:06:37.41 | Degassing |
| CIMG0036 | 4-Jan-09 | 15:26:35.80 | 00:08:05.07 | Rockfall |
| CIMG0036 | 4-Jan-09 | 15:27:35.93 | 00:09:05.20 | Rockfall (large) |
| CIMG0036 | 4-Jan-09 | 15:44:45.31 | 00:26:14.58 | Degassing |
| CIMG0036 | 4-Jan-09 | 15:49:10.77 | 00:30:40.04 | Rockfall |
| CIMG0036 | 4-Jan-09 | 15:51:10.81 | 00:32:40.08 | Degassing |
| CIMG0036 | 4-Jan-09 | 15:52:34.80 | 00:34:04.07 | Rockfall |
| CIMG0036 | 4-Jan-09 | 15:52:46.70 | 00:34:15.97 | Explosion |
| CIMG0036 | 4-Jan-09 | **15:56:48.00** | 00:38:17.27 | GPS synch (audio; UTC, hard to read) |
| CIMG0038 | 4-Jan-09 | | 00:06:25.25 | Rockfall |
| CIMG0038 | 4-Jan-09 | | 00:08:37.06 | Rockfall |
| CIMG0038 | 4-Jan-09 | | 00:10:28.48 | Rockfall |
| CIMG0038 | 4-Jan-09 | | 00:11:47.17 | Rockfall |
| CIMG0038 | 4-Jan-09 | | 00:15:55.81 | Rockfall |
| CIMG0038 | 4-Jan-09 | | 00:18:26.99 | Rockfall |
| CIMG0038 | 4-Jan-09 | | 00:29:00.86 | Rockfall |
| CIMG0038 | 4-Jan-09 | | 00:33:51.22 | Rockfall |
| CIMG0039 | 4-Jan-09 | | 00:00:23.29 | Rockfall |
| CIMG0039 | 4-Jan-09 | | 00:08:53.29 | Explosion (jetting in foreground) |

# Appendix C:

MATLAB script for displacement map generation

**MATLAB script written by Dr. Jeffrey Johnson (New Mexico Institute of Mining and Technology). Edits and additions by Christina Forbes, Alex Rinehart, and David Wooten. Example numbers are from 19:12 to 17:42:55 (UTC) on 12 January 2007.**

```
%Coordinates of the dome outline relative to the reference
%origin on the image.  The 'x' value in 'ones' corresponds to
%the number of x,y)dome outline coordinates.  The value both
%'ones' are multiplied by corresponds to the origin of the
%reference point.

dome1 = [ones(51,1)*(-2373),ones(51,1)*(-351)] + [
1954 830
2090 790
2194 708
2290 608
2294 506
2244 418
2166 320
2052 286
1918 232
1782 194
1620 160
1476 164
1388 154
1206 160
984  162
770  172
630  190
464  254
306  372
248  476
198  592
244  696
352  774
500  850
648  912
848  946
1058 966
1226 984
1388 982
1532 950
1716 910
1954 830
1824 794
```

```
1686 788
1570 760
1544 728
1630 644
1744 622
1862 538
1842 456
1766 396
1662 354
1540 348
1396 382
1190 426
1038 414
888  412
742  364
624  334
536  280
464  254];

%%
%Coordinates of the block vectors.  The two columns on the left
%are the (x,y) locations of the block of interest at the start
%of the time period, relative to the reference point.  The two
%columns on the right are the (x,y) locations of the block of
%interest at the end of the time period, relative to the
%reference point.

expl2 = [
-1793     -100 -1796     -105
-1854     15   -1862     4
-1704     106  -1712     104
-1572     107  -1578     105
-1586     15   -1592     12
-2074     256  -2088     258
-1897     265  -1904     260
-1819     393  -1825     394
-1839     188  -1833     193
-1720     194  -1726     193
-1699     283  -1709     282
-1717     355  -1726     354
-1647     431  -1654     431
-1603     492  -1607     492
-1469     514  -1477     518
-1511     396  -1518     393
-1550     336  -1558     335
-1490     380  -1496     378
```

```
-1447     330  -1453     332
-1385     444  -1389     444
-1341     583  -1349     585
-1306     523  -1314     520
-1312     424  -1318     424
-1584     282  -1588     281
-1562     186  -1569     184
-1423     242  -1428     243
-1367     156  -1372     158
-1372     298  -1378     301
-1028     544  -1027     546
-1185     532  -1189     533
-1144     471  -1147     473
-1213     393  -1218     394
-1061     395  -1068     396
-1149     340  -1154     346
-1293     276  -1298     276
-1245     208  -1249     210
-1175     211  -1178     215
-1122     266  -1125     269
-1052     240  -1053     247
-989      305  -997      307
-907      305  -910      305
-1096     108  -1098     113
-1044     168  -1048     171
-977      152  -982      152
-994      88   -997      88
-958      255  -959      261
-926      49   -929      49
-917      125  -922      125
-898      186  -903      191
-854      169  -856      172
-833      79   -839      80
-813      232  -817      236
-797      145  -802      147
-760      189  -764      189
-708      217  -711      220
-715      115  -719      119
-709      60   -711      60
-608      116  -608      120
-618      153  -618      154];

%%

hold off
hold on
```

```
dome = dome1;

clear u1s v1s x1s y1s
for jday = 1:1
    switch jday
        case 1
            Jdiff = expl2; figure(1); clf
    end

%Change pixels to meters
m_per_pixel_x = 0.10;
m_per_pixel_y = 0.10;

%Calculate block origins and correct the y-direction for
%viewing distortion
x = (Jdiff(:,1))*m_per_pixel_x;
y = (Jdiff(:,2))*m_per_pixel_y/0.42; % meters/sin(Θ)
u = (Jdiff(:,3)-Jdiff(:,1))*m_per_pixel_x;
v = (Jdiff(:,4)-Jdiff(:,2))*m_per_pixel_y/0.42; % meters/sin(Θ)

dome_x = dome(:,1)*m_per_pixel_x;
dome_y = dome(:,2)*m_per_pixel_y/0.42; % meters/sin(Θ)

%Interpolate motions to a gridded space
increment = 5;
xrange = [-220 -10]
yrange = [-50 155]
newx = [min(xrange):increment:max(xrange)];
newy = [min(yrange):increment:max(yrange)]
[x1,y1] = meshgrid(newx,newy);
u1 = griddata(x,y,u,newx,newy','cubic');
v1 = griddata(x,y,v,newx,newy','cubic');

%Plot the vector data
quiver(x,y,u,v)
daspect([1 1 1])
xlims = xlim;
ylims = ylim;
xlims = [-235 5]
ylims = [-70 145]
hold on
plot(dome_x,dome_y,'k-');
hold off
xlim(xlims)
ylim(ylims)
```

```
axis([-230 85 -60 160])

xstart = 20; %x-position of the legend
xend = 70; %Far right side of the legend (larger = wider line)
ylegend = 20; %y-position of the legend
ytick = 2; %Size of tick marks at end of legend

line([xstart xend], [ylegend ylegend]); %Horizontal line scale
line([xstart xstart], [ylegend-ytick ylegend+ytick]); %Left tick
line([xend xend], [ylegend-ytick ylegend+ytick]); %Right tick
text(xstart+3, ylegend+8, '50 meters', 'FontSize',16); %Legend
description

figure

%Plot the interpolated data at specific grid increments

[C,h] = contour(newx,newy,sqrt(u1.^2 + v1.^2),'m');
clabel(C,h,'FontSize',15,'Color','k');

hold on
quiver(x1,y1,u1,v1)
daspect([1 1 1])
hold off

hold on
plot(dome_x,dome_y,'k-');
hold off
xlim(xlims)
ylim(ylims)
axis([-230 85 -60 160])

xstart = 20; %x-position of the legend
xend = 70; %Far right side of the legend (larger = wider line)
ylegend = 30; %y-position of the legend
ytick = 2; %Size of tick marks at end of legend

line([xstart xend], [ylegend ylegend]); %Horizontal line scale
line([xstart xstart], [ylegend-ytick ylegend+ytick]); %Left tick
line([xend xend], [ylegend-ytick ylegend+ytick]); %Right tick
text(xstart+3, ylegend+8, '50 meters', 'FontSize',16); %Legend
description

figure

%Plot streamlines
```

```
streamslice(x1,y1,u1,v1)
daspect([1 1 1])
hold on
plot(dome_x,dome_y,'k-');
hold off
xlim(xlims)
ylim(ylims)
axis([-230 85 -60 160])

x1s(:,:,jday) = x1;
y1s(:,:,jday) = y1;
u1s(:,:,jday) = u1;
v1s(:,:,jday) = v1;

xstart = 20; %x-position of the legend
xend = 70; %Far right side of the legend (larger = wider line)
ylegend = 30; %y-position of the legend
ytick = 2; %Size of tick marks at end of legend

line([xstart xend], [ylegend ylegend]); %Horizontal line scale
line([xstart xstart], [ylegend-ytick ylegend+ytick]); %Left tick
line([xend xend], [ylegend-ytick ylegend+ytick]); %Right tick
text(xstart+3, ylegend+8, '50 meters', 'FontSize',16); %Legend
description

figure

end
```